Modeling and simulation of radio signals in confined environments using a software defined radio

Hussein Zeaiter

THÈSE DE DOCTORAT

DE L'ÉTABLISSEMENT UNIVERSITÉ BOURGOGNE-FRANCHE-COMTÉ

PRÉPARÉE À L'UNIVERSITÉ DE FRANCHE-COMTÉ

École doctorale n°37

Sciences Pour l'Ingénieur et Microtechniques

Doctorat d'Informatique

par

HUSSEIN ZEAITER

Modeling and Simulation of radio signals in confined environments using a software defined radio

Modélisation et Simulation de signaux radioélectriques dans des environnements confinés à l'aide d'une radio logicielle

Thèse présentée et soutenue à Montbéliard, le 30 mai 2023

Composition du Jury :

PAILLASSA BÉATRICE	Professeur à l'ENSEEIHT de Toulouse	Président
MAKHOUL ABDALLAH	Professeur à l'Université de Franche-comté	Examinateur
GENON-CATALOT DENIS	MCF HDR à l'Université de Grenoble Alpes	Examinateur
HILT BENOIT	MCF HDR à l'Université de Haute-Alsace	Rapporteur
MOREIRA ADRIANO	Professeur à l'Université de Minho, Portugal	Rapporteur
SPIES FRANÇOIS	Professeur à l'Université de Franche-comté	Directeur de thèse
BAALA OUMAYA	MCF HDR à l'UTBM	Co-directeur de thèse
VAL THIERRY	Professeur à l'Université de Toulouse 2	Co-encadrant de thèse

N° | X | X | X |

ABSTRACT

Nowadays, the Internet of Things (IoT) is growing rapidly. A large number of everyday applications such as hospitals, universities, airports, smart cities, industrial fields, use IoT for data exchange and communication. One of the main purposes of IoT is to track and trace users. Tracking an end user or a connected object is a very important aspect in many fields such as transportation and navigation. The most known outdoors navigation system is the Global Positioning System (GPS). The operation is based on the unidirectional transmission of a satellite signal located at an altitude of over 20,000 km. GPS provides accurate positioning results outdoors. However, GPS signal suffers from low availability in difficult environments, such as the indoor positioning area. Many IoT applications require tracking continuity in the indoor domain. To make this possible, it is necessary to build an indoor tracking system for emergency applications.

Radio frequency engineering has attracted the attention of the research community in both scientific and industrial fields. Software Defined Radio (SDR) is a well known concept in the field of radio frequency tracking, bringing new possibilities, and allow us to study and investigate existing radio frequency technologies such as LoRa (Long-Range Low-Power). The objective of this thesis is to propose an indoor tracking solution that exploits the radio signals emitted from indoors in order to build a radio architecture composed of fixed elements (Anchor nodes) whose coordinates are known and mobile terminals whose coordinates are to be determined.

To achieve the objective, an approach was considered during this thesis: In a first step, a state of the art study has been performed on the existing research works that study wireless technologies in the field of indoor tracking. These works present an overview of the most promising technological solutions and techniques for indoor tracking. In addition, this step involves a general study of Software Defined Radio technology, which consists of two parts, a software part that includes the GNU Radio and a hardware part that includes the USRP (Universal Software Radio Peripheral).

The second step consists of designing and developing embedded software that organizes wireless radio communications between elements communicating with the LoRa wireless technology. The LoRa signals were processed and simulated using a SDR platform. Using the SDR allows for easy visualization and analysis of the LoRa signal profiles. Processing, demodulating, and decoding the LoRa signal were also part of my assignments. The demodulation and decoding process was performed using the gr-lora library

integrated into GNU Radio, as well as a USRP-based SDR.

In the third step, an Angle of Arrival based localisation system was proposed and implemented on a SDR platform. The proposed system measures the phase difference between the two antennas of an SDR in GNU Radio. The algorithm consists of detecting the presence of the LoRa signal in the channel, computing the phase of the signal for each antenna of the receiver, and measuring the AoA and the location coordinates of a moving transmitter using trigonometric functions. In addition, detecting and tracking a weak LoRa signal was implemented via dual antenna SDR. Due to its CSS (Chirp Spread Spectrum) modulation, LoRa can demodulate a signal down to -20 dB below the noise level. The objective of detecting signals below the noise level is as follows: First, it will increase the battery lifetime of the LoRa device. Secondly, it extends the communication distance between devices. Finally, it secures our communication and data exchange by preventing third party devices from gaining access to our location coordinates.

The localization system consisted of a Adafruit Feather M0 containing a RFM95 LoRa transceiver, and the USRP B210 SDR receiver with dual omnidirectional antennas. The software was implemented on a personal computer and is compatible with the latest GNU Radio libraries. The experimentation was done in the indoor and outdoor domains. As a results of this research, it was shown that the AoA could be used to successfully localize a LoRa transmitter with high accuracy. The presented thesis is proposed as a new LoRa/SDR approach for indoor localization and for future research.

Keywords: Internet of Things, Software Defined Radio, Indoor localization, Long-Range, Low-Power, GNU Radio, AoA.

RÉSUMÉ

De nos jours, l'Internet des objets (IoT) connaît une croissance rapide. Un grand nombre d'applications quotidiennes telles que les hôpitaux, les universités, les aéroports, les villes intelligentes, les domaines industriels, utilisent l'IoT pour l'échange de données et la communication. L'un des principaux objectifs de l'IoT est le suivi et la localisation des utilisateurs. Le suivi d'un utilisateur final ou d'un objet connecté est un aspect très important dans de nombreux domaines tels que le transport et la navigation. Le système de navigation externe le plus connu est le système de positionnement global (GPS). Son fonctionnement est basé sur la transmission unidirectionnelle d'un signal satellite situé à une altitude de plus de 20 000 km. Le GPS fournit des résultats de positionnement précis en extérieur. Cependant, le signal GPS souffre d'une faible disponibilité dans les environnements difficiles, tels que la zone de positionnement intérieure. De nombreuses applications IoT nécessitent une continuité de suivi dans le domaine intérieur. Pour que cela soit possible, il est nécessaire de construire un système de suivi en intérieur pour les applications d'urgence.

L'ingénierie des radiofréquences a attiré l'attention de la communauté des chercheurs dans les domaines scientifiques et industriels. La radio définie par logiciel (SDR) est un concept bien connu dans le domaine du suivi par radiofréquence, apportant de nouvelles possibilités, et nous permettant d'étudier et d'investiguer les technologies de radiofréquence existantes telles que LoRa (Long-Range Low-Power). L'objectif de cette thèse est de proposer une solution de tracking indoor qui exploite les signaux radio émis depuis l'intérieur des bâtiments afin de construire une architecture radio composée d'éléments fixes (nœuds d'ancrage) dont les coordonnées sont connues et de terminaux mobiles dont les coordonnées sont à déterminer.

Pour atteindre cet objectif, une approche a été envisagée au cours de cette thèse : Dans un premier temps, un état de l'art a été réalisé sur les travaux de recherche existants qui étudient les technologies sans fil dans le domaine du tracking indoor. Ces travaux présentent une vue d'ensemble des solutions technologiques et des techniques les plus prometteuses pour le suivi en intérieur. En outre, cette étape comprend une étude générale de la technologie de la radio logicielle, qui se compose de deux parties, une partie logicielle qui comprend la radio GNU et une partie matérielle qui comprend l'USRP (Universal Software Radio Peripheral).

La deuxième étape consiste à concevoir et à développer un logiciel embarqué qui organ-

ise les communications radio sans fil entre les éléments communiquant avec la technologie sans fil LoRa. Les signaux LoRa ont été traités et simulés à l'aide d'une plateforme SDR. L'utilisation de la SDR permet de visualiser et d'analyser facilement les profils des signaux LoRa. Le traitement, la démodulation et le décodage du signal LoRa faisaient également partie de mes tâches. Le processus de démodulation et de décodage a été réalisé à l'aide de la bibliothèque gr-lora intégrée à GNU Radio, ainsi que d'un SDR basé sur l'USRP.

Dans la troisième étape, un système de localisation basé sur l'AoA a été proposé et mis en œuvre sur une plateforme SDR. Le système proposé mesure la différence de phase entre les deux antennes d'un SDR dans GNU Radio. L'algorithme consiste à détecter la présence du signal LoRa dans le canal, à calculer la phase du signal pour chaque antenne du récepteur, et à mesurer l'AoA et les coordonnées de localisation d'un émetteur mobile à l'aide de fonctions trigonométriques. En outre, la détection et le suivi d'un faible signal LoRa ont été mis en œuvre à l'aide d'une SDR à double antenne. Grâce à sa modulation CSS (Chirp Spread Spectrum), LoRa peut démoduler un signal jusqu'à -20 dB sous le niveau de bruit. L'objectif de la détection des signaux en dessous du niveau de bruit est le suivant : Premièrement, elle permet d'augmenter la durée de vie de la batterie du dispositif LoRa. Ensuite, elle permet d'étendre la distance de communication entre les dispositifs. Enfin, elle sécurise notre communication et l'échange de données en empêchant les dispositifs tiers d'accéder à nos coordonnées de localisation.

Le système de localisation était composé d'un Adafruit Feather M0 contenant un émetteur-récepteur RFM95 LoRa, et du récepteur USRP B210 SDR avec deux antennes omnidirectionnelles. Le logiciel a été implémenté sur un ordinateur personnel et est compatible avec les dernières bibliothèques GNU Radio. L'expérimentation a été faite dans le domaine intérieur et extérieur. Les résultats de cette recherche ont montré que l'AoA pouvait être utilisé pour localiser avec succès un émetteur LoRa avec une grande précision. La thèse présentée est proposée comme une nouvelle approche LoRa/SDR pour la localisation en intérieur et pour les recherches futures.

Mots clés: Internet des objets, Radio Définie par Logiciel, Localisation intérieur, Longue-portée, Faible puissance, GNU Radio, AoA.

DEDICATION

This thesis work is dedicated to my beloved family. My parents, ALi and Set Albanat, who raised me, love me, educated me, supported me, and encouraged me to pursue my dreams and my doctoral degree. I am truly grateful for having you in my life. My sister Marianna, and my brother Hadi who have never left my side and support me thoughout this journey. Your are very special to me.

I also dedicate this thesis to my supervisor Professor François SPIES, Professor Oumaya BAALA and Professor Thierry VAL who have helped and guided me during this process. As well as enriching me on scientific matters, they also provided me valuable advice whenever i needed it.

Lastly, i give special thanks to the Femto-st staff, colleagues and friends who have supported me during this process. My gratitude goes out to them for all they have done.

ACKNOWLEDGEMENTS

This dissertation is a part of the SYLOIN project (Système de Localisation en Intérieur), a collaboration effort between Femto-st institute and Jolliet-Innovation company. This research work was done at the research laboratory Femto-st (Franche-Comté Électronique Mécanique Thermique et Optique - Sciences et Technologies), Numerica, France, of Franche-Comté University.

First, i would like to sincerely and warmly thank my thesis supervisor, Professor François SPIES, for having proposed me this interesting and exciting thesis subject, and for having welcomed me during these three years in his research laboratory. Professor SPIES has guided me very well throughout this journey with his wide experience and his scientific and technical expertise in his field. He has been an excellent director and mentor. I wish also to express my deepest and most sincere gratitude to my other co-directors, Professor Oumaya BAALA, and Professor Thierry VAL. My two co-directors gave me the best scientific and technical advice, and provided invaluable guidance and knowledge. It has been a pleasure working in their laboratory to accomplish my research and experiments. I am very grateful for this opportunity. I would also like to warmly thank Mr. Stephane GIVRON (Specialized teacher at IUT Belfort-Montbéliard - Univeristy of Franche-Comté) for his highly valuable contribution

I would like to pay my special thanks to the entire Femto-st laboratory, professional and administrative team for their warm welcome, help, guidance and generosity. I would also like to thank the companies Jolliet-Innovation and Seca headed by Mr. Jean Michel PFISTER and Mr. Olivier GRAND for their collaboration and their help which allowed me to conduct experiments in their local.

I am extremely grateful for the financial support provided by the Region of Bourgogne Franche-Comté and the European Union for making this project possible. The funding has been instrumental in allowing me to pursue my research and bring my ideas to fruition.

I would like to express my gratitude to the members of the jury for the time they took to evaluate my work.

Finally, this three-year journey would not have succeeded without the love, sacrifice, education, and support of my family. My sister and brother, Marianna and Hadi, thank you for your love and support. My father and mother, Ali and Set Albanat, thank you for being there for me and helping me to overcome the difficult moments.

CONTENTS

1

INTRODUCTION

1

INTRODUCTION

This dissertation presents an advanced approach to indoor tracking in the logistics domain, with a particular interest on investigating the Long-Range (LoRa) technology and the Sotfware Defined Radio (SDR) platform. The research work was conducted in the department of computer science and complex systems of the Femto-st institute (FEMTO-ST/DISC) in collaboration with the Jolliet-Innovation company. This chapter introduces the research work conducted for this thesis. Section 1.1 introduces the general context of the dissertation. Section 1.2 discusses indoor tracking's problems, limitations, and challenges. As a result of this information, Section 1.3 presents a novel tracking approach. The dissertation's outlines are summarized in Section 1.4.

1.1/ GENERAL INTRODUCTION

In recent years, wireless communication technologies have become an integral part of modern society. The rapid growth of the Internet of Things (IoT) technology has encouraged researchers and developers to engage more with this technology. According to statista [1], the total number of IoT devices connected to the internet will reach up to 13 billion in 2022 and 29 billion in 2030. According to IEEE [2], IoT is a network of connected devices that enables connectivity and data exchanges for applications such as smart cities, healthcare, industrial and commerical fields, transportation, and asset tracking. The total number of IoT devices across all industries will reach more that 8 billion by 2030. Among consumer IoT devices, asset tracking is one of the most important use cases for IoT in the consumer segment. Asset tracking is a method for tracking physical assets including the tracking or locating of persons or objects in indoor environment using sensor tags. Tracking system refers to technology used to determine the geo-location of users.

The tracking system technologies can be classified into two categories: outdoor and indoor tracking. The Global Navigation Satellite System (GNSS) [2] is the most com-

monly used positioning system (PS) in outdoor areas. There is now GNSS using multi-constellation system such as GPS, Glonass, Beidou and Galileo. GNSS radio systems use satellites to determine the location of the users. Nowadays, GNSS is the most effective PS in outdoor, providing precise location information of mobile devices with worldwide coverage. However, GNSS has its weaknesses and is not available to operate location for indoor areas. This is due to the inability of the signal to penetrate walls and most building materials. These limitations led the research community to deepen their research in the field of indoor tracking. Many scientific studies [3,4] propose solutions to the indoor tracking problem, such as radio waves, sound waves, camera and image analysis. However, the difficulty of installing an indoor tracking system lies mainly in the financial cost and the expected accuracy.

Nowadays, radio frequency (RF) engineering has attracted the attention of the research community. A new technology called Software Defined Radio (SDR) has been emerged. SDR refers to a technological revolution in wireless communication and signal processing, bringing new possibilities, and allowing to study existing radio technologies such as the Long-Range Low-Power (LoRa) wireless radio technology.

This thesis focuses on indoor tracking, in which we utilize RF signals emitted indoors to create radio architecture consisting of fixed elements (Anchor nodes) whose coordinates are known and mobile terminals whose coordinates are to be determined.

1.2/ Problem Statement

As described in the previous section, there is many of research work devoted to the problem of indoor localization, but implementations with low cost, low energy consumption and high localization accuracy are very rare. The are numerous techniques for localizing signals using signals properties such as fingerprinting, Time of Arrival (ToA), Time Differential of Arrival (TDoA), and Received Signal Strength Indicator (RSSI). The fingerprinting method requires a laborious time to record RSSI values and process the location coordinates, not to mention that this method is not suitable for infrastructures whose layout is updated frequently. RSSI-based localization solutions cannot provide high localization accuracy. The quality of RSS can be affected by channel fading and multipath effects, making RSSI-based localization solutions unreliable. Time-based localization methods such as ToA and TDoA require large bandwidth and high timestamp precision of the received signal at the receiver. Additionally, when using the ToA method, it is essential that the clocks and time of the transmitter and the receiver are synchronized. Despite the fact that TDoA method does not require synchronization between transmitter and receiver, it does require highly accurate synchronization between all the receivers. Addressing these limitations can be done using the Angle of Arrival (AoA) localization technique.

There are numerous benefits to using an AoA-based localization solution. In contrast to the ToA and TDoA technique, the AoA technique does not require a large signal bandwidth or high timestamp precision at the receiver. Additionally, AoA-based localization systems measure the received angle between the transmitter and the receiver by measuring the phase difference at the receiver's antennas. Consequently, LoRa RF technology uses a narrow bandwidth, which allows us to obtain accurate phase and AoA location coordinates regardless of the bandwidth size. Finally, our localization system is more immune to multipath and channel fading by using AoA rather than relying on RSSI.

For this purpose, the objective of this thesis is to propose a solution for indoor localization system based on the AoA approach over a LoRa wireless communication system implemented on SDR platform which is the USRP B210. The localization system is illustrated in Figure 1.1.

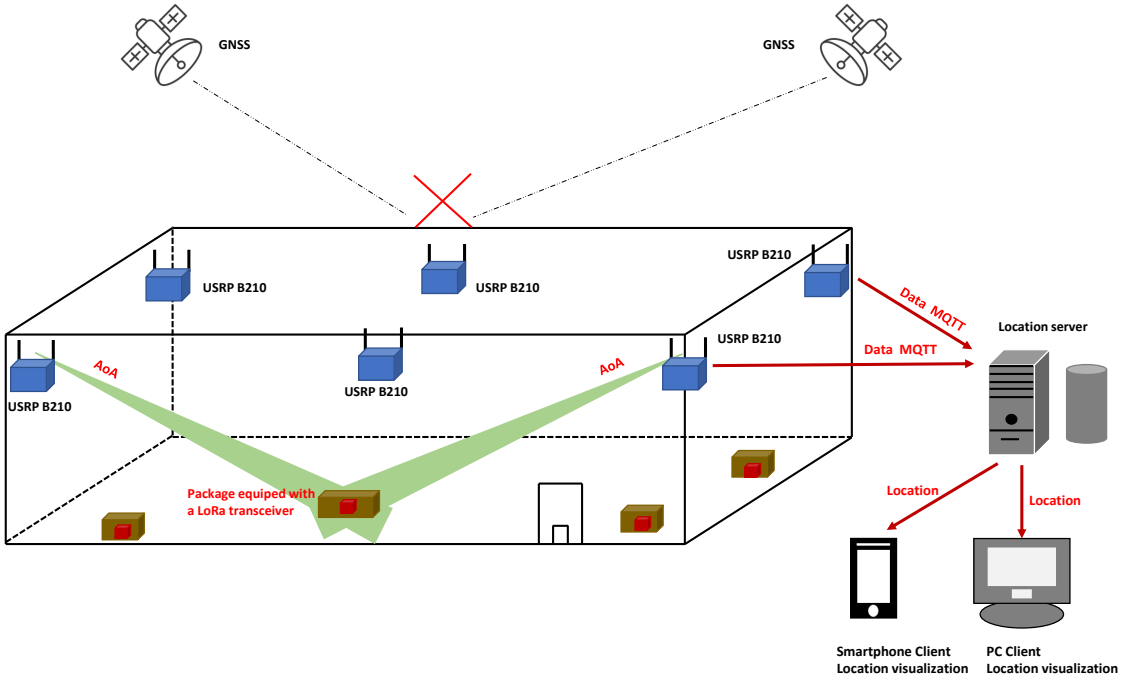

Figure 1.1: Indoor localization system based on AoA and USRP B210

Using the AoA method as shown in Figure 1.1, the location of the LoRa sensor node can be estimated. In order to determine the location of the LoRa transmitter, a mathematical triangulation algorithm is used along with the measured AoA and the known location coordinates of the USRP B210. The LoRa signal is transmitted from a single antenna, and is received by at least two USRP B210 equipped with multiple-antenna, in order to process the triangulation process. The triangulation process is shown in Figure 1.2.

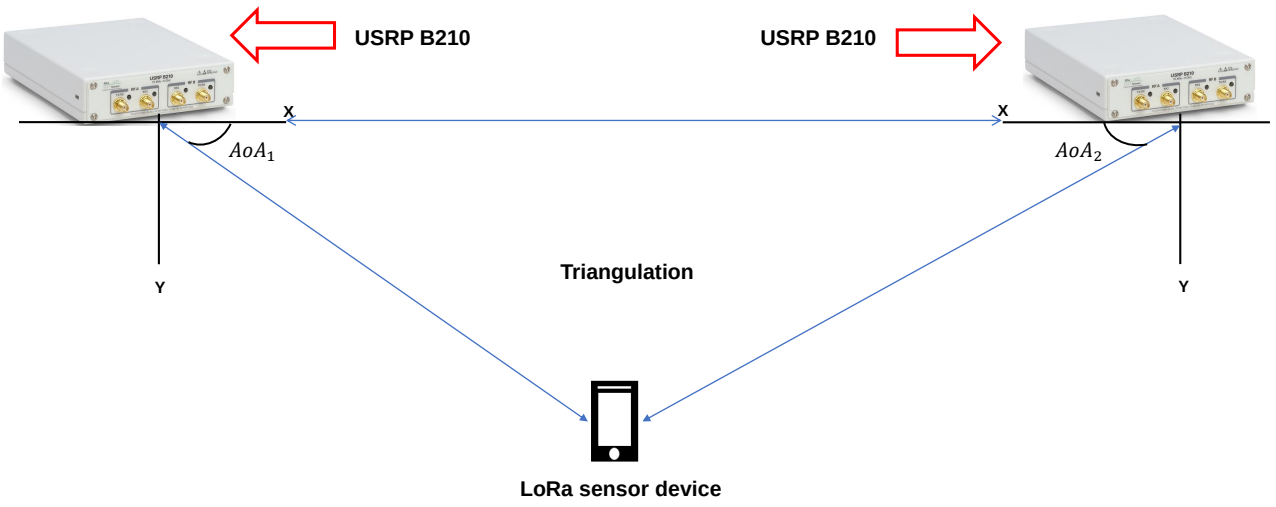

Figure 1.2: Localization system with two USRP B210 and a LoRa sensor

Figure 1.2 demonstrates the use of triangulation to determine the location of the target. Two measured AoA values from the USRP B210 receivers are necessary to perform this technique. The point of intersection of the two lines corresponding to the measured AoA values represents the location of the LoRa target.

The proposed system in this thesis is also designed to deploy an indoor localization system with the following characteristics:

- Install connected sensors on packages that transmit the signal at very low transmission power.
- Locate the connected sensors using the LoRa radio communication technology.
- Detecting and locating weak LoRa signals that operate at very low transmission power, thereby reducing power consumption and extending the battery life of the LoRa sensors.
- Improving detection accuracy by improving the signal-to-noise ratio (SNR).
- Keeping our location coordinates secure by preventing third party devices from accessing them.
- Implementing of user tools such as location server, user location information, smartphone application and web application.

1.3/ CONTRIBUTIONS OF THE THESIS

The main objective of this thesis it to develop an indoor localization and tracking system based on the AoA technique that is high accurate, low-cost and easy-to-deploy by using the LoRa radio technology implemented as an SDR platform. Our research's main contributions are presented as follows:

1. The first contribution of this thesis involves the development of an embedded software to organize wireless radio communication between elements using LoRa wireless technology. LoRa is one of the promising technologies to develop an indoor localization system. Because of its Chirp Spread Spectrum modulation (CSS), LoRa is more resistant to interference, multipath and Doppler effects than other wireless radio technologies. These characteristics make LoRa a good candidate for indoor localization. Through the use of a SDR, the LoRa signal was processed, simulated, demodulated and decoded using the *gr-lora* library in Gnu Radio. *gr-lora* is a reverse engineering open source software implementation of the LoRa physical layer, composed of a set of Gnu radio blocks for implementing LoRa transmitters and receivers.

2. Following our first contribution, the second contribution of this thesis will focus on addressing the calculation of the Angle of Arrival (AoA) and location coordinates, which can be achieved through a three-step process. The first step involves detect the presence of a LoRa signal in the channel. The second step requires measuring the phase of the received signal for each antenna of the SDR receiver. Finally, in the thirst step, the phase difference among the antennas is computed, and the AoA is measured. It is important to highlight that this methodology has been implemented and tested in real-time using real LoRa transceivers.

3. Third, our research contributes to the development of signal processing approaches for detecting and measuring the AoA of weak LoRa signals below the noise level. Specifically, when signals operate below the noise floor, the detection performance decreases, making it impossible to track them using AoA techniques. To overcome this problem, we developed a signal processing approaches based on the Fast Fourier Transform (FFT) and the autocorrelation function (ACF). Our new approach, called dual-antenna fast autocorrelation localization system, measures the ACF of the LoRa signal in the frequency domain using FFT. Performing the ACF combined with FFT increase the detection accuracy and the SNR level. With the proposed method, we demonstrated that weak LoRa signals can be detected up to -20 dB below the noise level while maintaining good AoA accuracy, and so location coordinates. In addition, the ACF allows us to gain in terms of link budget, since

the reception threshold can reach -140 dBm with a transmission power of +20 dBm, resulting in a superior communication distance to Wi-Fi.

1.4/ PUBLICATIONS

1.4.1/ CONFERENCE PAPER

- **Hussein ZEAITER**, Francois SPIES, Oumaya BAALA, and Thierry VAL, "Measuring accurate Angle of Arrival of weak LoRa signals for Indoor Positionning," 2022 IEEE 12th International Conference on Indoor Positioning and Indoor Navigation (IPIN), 2022, pp. 1-8, doi: 10.1109/IPIN54987.2022.9918114, Beijing, China
- **Hussein ZEAITER**, Francois SPIES, Oumaya BAALA, and Thierry VAL, "Performance Evaluation of the Angle of Arrival of LoRa Signals under Interference," 2022 IEEE Ninth International Conference on Communications and Electronics (ICCE), 2022, pp. 31-36, doi: 10.1109/ICCE55644.2022.9852102, Nha Trang, Vietnam
- **Hussein ZEAITER**, Francois SPIES, Oumaya BAALA, and Thierry VAL, "SYLOIN: Measuring Angle of Arrival of LoRa signals using Software Defined Radio," 2021 International Conference on Indoor Positioning and Indoor Navigation (IPIN), 2021, pp. 1-8, doi: 10.1109/IPIN51156.2021.9662518, Lloret de mar, Spain
- **Hussein ZEAITER**, Francois SPIES, Oumaya BAALA, and Thierry VAL, "Modeling and simulation of radio signals in confined environments for indoor tracking using software defined radio", Journées LPWAN2021, Clermont Ferrand-France.
- **Hussein ZEAITER**, Francois SPIES, Oumaya BAALA, and Thierry VAL, "Owlp-s/LoRa: un système de localization intérieure pour suivre un groupe de personnes en intervention", FUTURMOB'18 Conference, Nevers-France.

1.4.2/ JOURNAL PAPER

- **Hussein ZEAITER**, Francois SPIES, Oumaya BAALA, and Thierry VAL, "Measuring AoA of LoRa chirp signal in real-time using SDR/GNU Radio," to be submitted in the Journal of IoT.

1.5/ STRUCTURE OF THE DISSERTATION

The rest of this dissertation is organized as follows:

- **Chapter 2:** Chapter 2 of this dissertation provides a comprehensive review of the current state of the art in wireless communication technologies and localization techniques. This chapter presents an overview of the various localization technologies that have been developed over the years including radio frequency technologies such as Wi-Fi, BLE, UWB, RFID, LPWAN, and others. In addition, this chapter also delves into the various techniques used for localization of wireless devices, including triangulation, multilateration, fingerprinting, and others. The strengths and weakness of each technique are evaluated.

- **Chapter 3:** Chapter 3 examines the Software Defined Radio (SDR) technology, which is a revolutionary technology that enables for the exploitation of wireless communication technologies. This chapter presents a detailed examination of the hardware and software components that constitute an SDR system. The hardware section discusses the Universal Software Radio Peripheral (USRP) based SDR platform, especially the USRP B210 receiver. On the software side, this chapter provides an overview of the GNU Radio software framework, libraries, and programming languages used in SDR system.

- **Chapter 4:** Chapter 4 presents the first major contribution of this dissertation. In this chapter, we introduce a novel *LoRa/SDR AoA-based tracking system* . Our system is designed to accurately measure the AoA of objects within indoor spaces, using a dual antenna SDR receiver and a phase difference approach, which has proven to be an effective and reliable method. The use of SDR technology allows for greater capability to study the LoRa's signal profile, while the phase difference approach offers a highly accurate method for determining the AoA.

- **Chapter 5:** This chapter provides the second major contribution of this thesis, introducing a new approach in the filed of weak LoRa signal detection and AoA measurement. Our approach named as *Fast autocorrelation signal detection and AoA measurement*, leverages the autcorrelation function of the LoRa signal using a dual antenna SDR receiver. By utilizing this unique approach, our system is able to accurately detect and measure weak LoRa signals, which is particularly important for tracking applications where transmission power must be kept to a minimum in order to save energy. To evaluate the feasibility of this approach, experiments were conducted both in indoor and outdoor environments, demonstrating its effectiveness in a real world scenario.

- **Chapter 6:** Chapter 6 presents the summary and conclusion of this dissertation efforts, presenting the conclusions from the previous chapters, providing the potential perspectives and future directions in the field of LoRa signal detection and AoA measurement. In this chapter, we provide a road-map for researchers who wish to expand on the contributions and advancements presented in this dissertation.

II

BACKGROUND

2

INDOOR LOCALIZATION TECHNOLOGIES AND TECHNIQUES

2.1/ INTRODUCTION

As described in chapter 1, the rapid evolution of wireless communication technologies an smart phones has resulted in a high demand for indoor localization solutions in emergency situations. Indoor localization can be referred as a system that provides a known location of a sensor node in indoor environment such as airports, hospitals, railway stations, universities, etc [3]. Generally, an indoor localization system consists of a specific number of access points (anchor nodes) of known locations and mobile nodes (non-anchor nodes) of unknown locations, to be determined [4]. The key objective of any indoor localization system is to determine the location of the mobile node based on measurements exchanged with the anchor nodes. However, the main challenge is to find the best localization solution in terms of technology and localization technique. This chapter provides an overview of the technologies and techniques used for indoor localization, as shown in Figure 2.1.

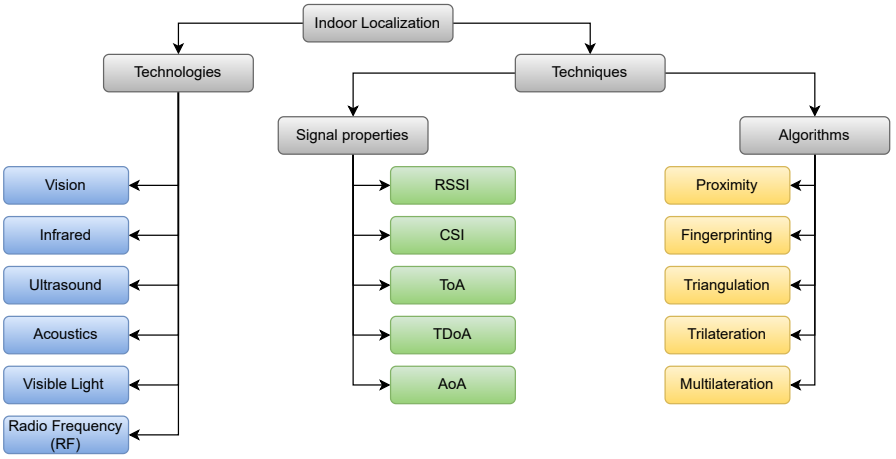

Figure 2.1: Classification of indoor localization technologies and techniques

2.2/ LOCALIZATION TECHNOLOGIES

The section presents the most promising technology options and techniques for indoor localization that have been used alternative to GPS. A detailed description of these technologies is presented in the following:

2.2.1/ COMPUTER VISION

Computer vision based indoor localization systems use information (e.g images or video) collected from cameras and images processing algorithms to locate a mobile target . These systems use the existing infrastructure of fixed cameras or mobile cameras attached to the target entity [5, 6].We identify two type of computer vision indoor localization systems:

- **Static camera-based systems**: Static camera or fixed camera computer vision localization systems use one or several cameras fixed at known locations in the building in order to capture images and locate the moving target or entity (e.g human, animal or robot) [7, 8].
- **Mobile camera-based systems**: Mobile camera computer vision localization system use a mobile camera carried by the user or the target. During the localization process, there are typically two phases: The offline phase where the user starts to capture images or video of its environment at predetermined locations, followed by an online phase in which the captured images are compared to images stored in the database with location information to track and estimate the location of the user or the camera [9, 10].

An example of mobile camera localization system is presented in [10]. The proposed system determines the target's location by using images captured by a smartphone camera. The captured images are periodically transferred to a web server where the location is processed. According to the authors, room-level accuracy exceeds 90% and at the corner level exceeds 80%.

Another localization system that uses computer vision method and a smartphone camera is implemented in [11]. The localization process involves two phases: the offline (calibration) phase and the online (localization) phase. During the offline phase, a database is built with images including their corresponding location, viewing direction, scale and rotation invariant description. During the online phase, the smartphone starts to capture images and computes SURF (Speeded Up Robust Features) transformation algorithm, uploading them to the server where a comparison and a location are determined.

2.2.2/ INFRARED

Infrared indoor localization systems use infrared transmitters and receivers to locate sensors. The target or sensor equipped with an infrared light transmitter diode transmits an infrared radiation or signal that contains an ID (Unique Identifier code). Infrared receivers equipped with a photodetector detect incoming infrared signals (e.g sensor ID) and estimate distances and localize the target using a trilateration algorithm [12].

The are many benefits to using IR systems, such as centimeter-level localization accuracy, immunity to radio interference, and simplicity of deployment. However, it is important to note that most of IR systems require a line-of-sight (LoS) condition for a better performance and localization accuracy, and of-course they are susceptible to multipath effects and environmental changes [13].

2.2.3/ ULTRASOUND

Ultrasound based localization systems use ultrasonic signal with a frequency higher than 20 KHz to estimate the distance and the location of a target by measuring the time it takes a sound signal to travel from a transmitter to a receiver. Ultrasonic signals are transmitted along with RF pulses to facilitate synchronization among all receivers. In most ultrasound systems, the existing mobile devices can be used for localization and can provide centimeter-level localization accuracy in indoors [14].

This technology is advantageous due to its low cost components and deployment, and being able to penetrate though walls and materials in indoors, and, as mentioned before, can handle existing mobile devices. However, it can be affected by multipath, which can cause distance measurements to be degraded and localization to be incorrect. Furthermore, the speed or velocity of the sound signal can be affected by the environment and the temperature changes [15]. Finally, Ultrasound systems require complex signal processing algorithms to remove the noise components from the signal of interest, which can degrade localization accuracy .

2.2.4/ ACOUSTIC

The acoustic based localization systems utilize the build-in microphone sensors in smartphones to detect acoustic signal. The user or target node transmits a sound modulated signal including a time stamp information that is used by receivers microphones to estimate the ToF, and therefore locate the target with multilateration [16, 17].

Acoustic localization can be used in a wide range of fields such as airports, hospitals, shopping mall, and universities, providing accurate localization measurement. However,

the sound signal should me modulated at a frequency less than 20 KHz and at a low transmission power in order to avoid unwanted effects on human health (the sound signal should be undetectable by humans). The detection of low power transmitted signals requires complex signal processing algorithms at the receiver side, making this technology unpopular for indoor localization.

2.2.5/ Visible Light

Visible Light Communication (VLC) is a widely used localization technology in emergency places such as hospitals where RF technologies cannot be used due to their implications for human health. VLC technology uses visible light that is modulated/coded and transmitted by a light emitting diode (LED) lamp to estimate the location [18]. The receiver/sensor carried out by the user detect the light and compares it to the corresponding coded light stored in the database, and estimate the sensor location using AoA [19].

The advantage of VLC based localization is its high-level of localization accuracy, its wide range of developments compared to other systems such as Wi-Fi, as well as cost-effectiveness, low energy consumption, and high-speed data transfer. However, a major disadvantage of this technology is that both the LEDs and sensors must meet LoS conditions to ensure accurate localization.

2.2.6/ Radio Frequency RF localization

This subsection discusses radio frequency (RF) based systems for indoor localization. Examples of RF based localization systems such as Frequency Modulation (FM), cellular technology, Wi-Fi, Bluetooth, Zigbee, Ultra-Wideband (UWB) and Radio Frequency Identification (RFID) will be presented First. Secondly, emerging technologies such Sigfox and Long-Range (LoRa) will be discussed in detail.

2.2.6.1/ Wi-Fi

Wi-Fi is a wireless communication technology that uses the Wireless Local Area Network (WLAN) to estimate the location of a target node. Wi-Fi technology operates in the Industrial, Scientific, and Medical (ISM) spectrum with the following frequencies: 2.5 GHz for IEEE 802.11b, IEEE 802.11g, and IEEE 802.11n, and 5 GHz for IEEE 802.11a, with a medium coverage range of about 100 meters and can now reach 1 km in IEEE 802.11ah [20]. Originally, Wi-Fi was used to network and connect devices such as smartphones, laptops, tablets, and other portable user devices to the internet. Today, Wi-Fi is one the most popular wireless technologies [21, 22] used in indoor areas such as universities

and office buildings since all these places are equipped with Wi-Fi access points (APs) that provide coverage for the entire building without the need for additional hardware or infrastructure.

A variety of signal parameters and techniques can be used in Wi-Fi localization. These techniques include AoA-based triangulation [23], CSI-based fingerprinting [24], and RSSI-based fingerprinting [25]. Among these localization algorithms, RSS-based fingerprinting localization is the most commonly used and highly efficient technique for Wi-Fi localization since LoS is not required. One of the main benefits of using Wi-Fi over other technologies is its low-cost and simplicity since the layout cost and the user cost are low. Despite this, it was shown that Wi-Fi based localization systems are susceptible to environmental changes such as temperature, humidity and human mobility [26]. Furthermore, materials, walls and furniture can attenuate wireless signal (RSSI) that influence the accuracy of the Wi-Fi location.

2.2.6.2/ BLUETOOTH

Bluetooth is a wireless technology that uses the Wireless Personal Area Network (WPANs) to enable communication between moving or fixed smart devices . Bluetooth signal also known as IEEE 802.15.1 operates in the range from 2.4 GHz to 2.4835 GHz in ISM band and enables a short communication range. Now there is new version of smart Bluetooth known as Bluetooth Low Energy (BLE) which provides a data rate up to 24 Mbps and a covering range of 70-100m. BLE was first introduced to the industry in 2010 [27] featuring low cost, low power consumption, secure communication and easy access. These benefits make BLE a good candidate for indoor localization. BLE-based localization systems using iBeacon technology was presented by Apple in 2013 [28]. This solution allows the localization of smartphones in public spaces including airports, shopping centers and train stations. The protocol consists of sending periodic signal (beacons) containing a Universally Unique Identifier (UUID). Once the beacon is received by a BLE enable smart device, a proximity RSS localization algorithm can locate the smart device. Google launched another protocol named Eddystone in 2015 [29]. Eddystone is an open source communication protocol based on beacon protocol developed for both IOS and Android operating systems and can be used for tracking people.

All these benefits make Bluetooth a competitive technology for indoor localization. However, the following drawbacks of BLE must be considered : First, this system is sensitive to collisions and interferences with Wi-Fi technology since both technologies operate in the same frequency range. Second, BLE in susceptible to signal attenuation and reflection due to obstacles and Walls. Finally, due to its limited communication range, BLE in not a suitable solution for large-scale localization.

2.2.6.3/ ULTRA-WIDEBAND (UWB)

Ultra-Wideband is a RF communication technology based on the transmission of electromagnetic waves that uses a large bandwidth (>500 MHz) and a frequency range from 3.1 to 10.6 GHz [28]. UWB communication uses ultra-short pulses with high time resolution which results in low power consumption,high data rate communication and short signal wavelengths. With its large bandwidth, UWB provides more resistance to interference [30]. Moreover, UWB signals are known for their ability to penetrate through walls, obstacles,and building materials due to their low frequency components. Additionally, it has a less detrimental effect on human health because it operates at a low transmission power [3]. Finally, UWB is less susceptible to multipath effects, since the UWB pulses are highly time-resolved so we can determine the main path of the signal of interest. As a result of all those characteristics, UWB technology has been significantly investigated as an advanced indoor localization technology.

ToA and TDoA are the most widely used UWB localization techniques because the time resolution of UWB signals and they have shown to achieve sub-meters and centimeters level accuracy in indoor environments [31, 32]. RSS in rarely used in UWB-based localization system because of its lower accuracy compared to ToA and TDoA. The main drawback of UWB is that it only offers the best performance over short ranges. Thus, in large infrastructures, more nodes must be deployed to achieve the best accuracy, which impacts the system's cost. In addition to its drawbacks, UWB is also challenged by NLOS effects on the accuracy of its localization [33].

2.2.6.4/ RADIO FREQUENCY IDENTIFICATION (RFID)

Radio Frequency Identification (RFID) is a wireless communication technology that uses electromagnetic waves between a transmitter and any RF compatible circuit. The RFID system consists of an RFID reader and an RFID tag. There two types of RFID systems are active tags system and passive tags system [34]. In active RFID system, the user holds an active tag that is powered by its integrated battery and sends periodic signals containing a specific ID number. Active tags operate on ULtra High Frequency (UHF) [35] to achieve a larger communication distance (up to 100 m) and can provide long-range localization. However, active RFID systems consume more power and are more expensive, and can not provide sub-meter localization accuracy. In contrast, passive tags do not have built-in batteries and simply respond to signals received from the readers. A Passive RFID tag can operate in low and UHF frequency ranges. Its benefits include low cost, small size, and easy of fabricating since it only consists of a small microchip and printed circuit board (PCB) that serves as an antenna. As passive tags have a short communication range (2 m), they are not suitable for indoor localization, but can be attributed

for proximity localization. Another limitation of passive tags is their inability to support complex cryptography algorithms for data protection due to their limited computational capacity [33].

2.3/ LPWAN LOCALIZATION SOLUTIONS

In this section, we provide an overview of two major LPWAN technologies, SigFox and LoRa dedicated to IoT communication, which can be attributed for indoor localization.

2.3.1/ SIGFOX

Sigfox [36] network operator is the first LPWAN proprietary technology dedicated to the IoT and M2M communication, founded in 2010 by the start-up company named Sigfox in Toulouse France. Sigfox use the Ultra Narrow Band (UNB) (100 Hz) radio technology and operates in the unlicensed ISM frequency bands: 868 MHz in Europe and Middle East, 915 MHz in the United States, and 433 MHz in Asia. Due to its UNB technology, Sigfox can only use a very small part of the spectrum, which results in very low noise levels, high receiver sensitivity, and minimal power consumption. Sigfox network operator consists of a number of sensors and a proprietary base stations equipped with software defined radio (SDR) platform. Initially, the sensors use a Binary Phase Shift Keying (BPSK) modulation to transmit a signal and connect to the base station (uplink communication) which in turn sends the data to a server using IP protocol. Later on, Sigfox supports bidirectional communication, where Gaussian Frequency Shift Keying (GFSK) modulation is used to transmit a signal (downlink) from the base station to the sensors. Due to its UNB bandwidth, Sigfox can support numerous devices to communicate with a communication range up to 10 km in urban areas and up to 50 km in rural areas [37].

However, the UNB of Sigfox signals makes it unsuitable for indoor localization. Localization methods based on timing (e.g ToA and TDoA) are not suitable due to its UNB modulation [38]. As a result, other approaches have been proposed. A Sigfox Geolocation approach based on RSS measurement and trilateration has been implemented. The trilateration use a minimum of three Sigfox base stations to estimate the sensor location. This method developed by Sigfox is not a standalone approach and has to be used combined with other localization systems such as Wi-Fi or GPS [38]. Another approach is investigated in [39]. The authors proposed an RSSI and fingerprinting approach to locate Sigfox's sensor nodes. The base stations are equipped with GPS modules to minimize the distance measurement error. However, the approach would require many GPS modules, which could impact the system cost.

2.3.2/ LoRa

Long-Range (LoRa) is the leader of LPWAN technologies designed for long-range and low-power and low bit-rate communication and developed by Semtech [40]. LoRa [41, 42, 43] is a physical layer (PHY) technology that uses a proprietary modulation technique named Chirp Spread Spectrum (CSS), operating in the ISM bands (169 MHz, 433 MHz, 868 MHZ, 915 MHz and 2.4 GHz). The CSS modulation scheme consists of modulating and encoding the LoRa symbols into multiple signals of increasing frequencies (up-chirp) as shown in Figure 2.2 (a) and decreasing frequencies (down-chirp) as shown in Figure 2.2 (b). Due to its CSS modulation, LoRa is robust to channel noise and more resilient to interference and multipath. Moreover, CSS technique offers high communication range with low power consumption and high receiver's sensitivity.

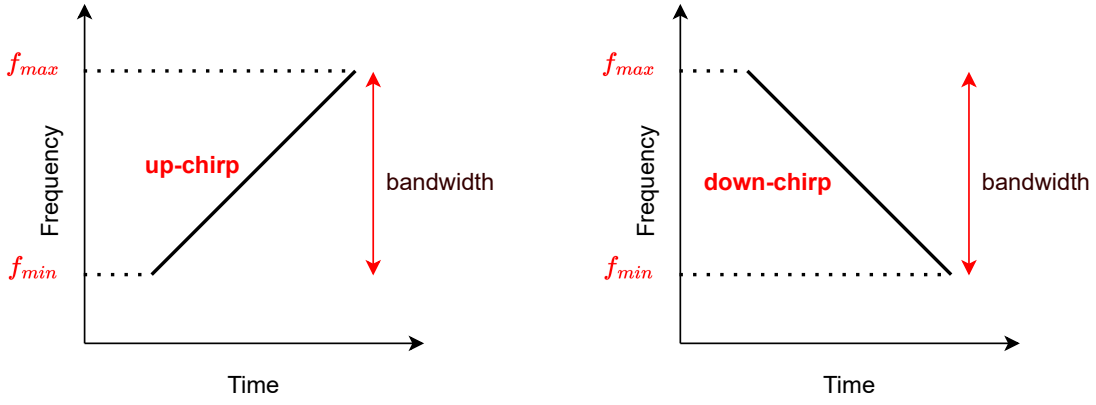

(a) LoRa up-chirp (b) LoRa down-chirp

Figure 2.2: An example of LoRa chirps

LoRa physical layer frame format:

LoRa technology offers a maximum frame size of 256 bytes. The frame structure contains the followings fields and is illustrated in Figure 2.3:

- **Preamble:** Each LoRa frame begins with a preamble, which is used to synchronize the receiver with the transmitter and to detect the frame as shown in Figure 2.3. The preamble involves a serie of unmodulated up-chirp symbols ($n_{up-chirps} <= 8$) and a predetermined 4.25 chirp symbols for frame and frequency synchronization (2 up-chirp symbols for frame synchronization and 2.25 down-chirp symbols for frequency synchronization). Therefore, the preamble length is equal to 12.25 symbols.
- **Header:** It is an optional field. The header is sent after the preamble and it specifies the length of the payload, the header Cyclic Redundancy Check (CRC) to allow the receiver the reject frames with incorrect header, and the Forward Error Correction

(FEC) code rate (CR).

- **Payload:** The payload is sent after the header and it contains the actual transmitted data with a maximum size of 255 bytes, and an optional payload CRC.

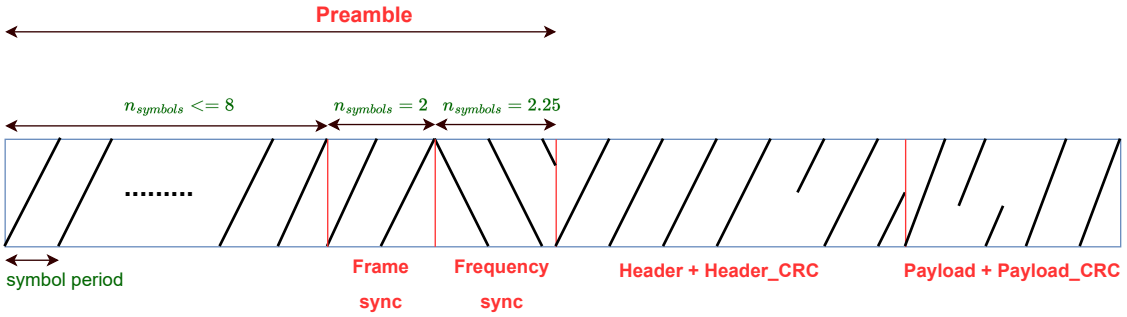

Figure 2.3: LoRa frame structure

LoRa transmission parameters:

To ensure the best performance in term of power consumption and communication range, LoRa offers the following parameters: Transmission Power (TP), Carrier Frequency (CF), Spreading Factor (SF), Bandwidth (BW), and Coding Rate (CR).

- **Transmission Power:** A LoRa end-device can transmit a signal with a TP ranging from -4 dBm to 20 dBm with a step of 1 dB [44]. The transmission power is set to 14 dBm by default (25 mW) [45]. Increasing the TP improves the communication range and the signal-to-noise ratio, but at the expense of battery lifetime of the end-device.
- **Carrier Frequency:** The CF is the center transmission frequency that uses a LoRa end-device to transmits a signal. LoRa operates in the ISM licence-free sub-GHz bands (169 and 433 MHz in Asia, 868 MHz in Europe, 915 MHz in North America and now it also operates at 2.4 GHz). There are typically several channels within a LoRa frequency band [46].
- **Spreading Factor:** As described earlier, LoRa modulation uses chirp spread spectrum technology (CSS) for encoding. The CSS uses chirps which are signals with a increasing frequency (up-chirp) or decreasing frequency (down-chirp). The Spreading Factor determines the speed at which the chirp changes across the bandwidth of a channel. In another word, SF refers to the number of bits encoded by a symbol and can be calculated as follows:

$$SF = \log_2(\frac{R_c}{R_s}) \tag{2.1}$$

Where R_c is the chip rate and R_s is the symbol rate. The SF of a LoRa chirp can range from 7 to 12. Each LoRa chirp can contains 2^{SF} chips. For example, with SF = 7, there are 2^{SF} = 128 chips used per symbol. Using a large SF improves the communication range and the receiver sensitivity (SNR), at the expense of the transmission duration. During a transmission, the time that takes a chirp to be transmitted is related to the SF and the BW. Therefore, the time of a chirp can be defined as follows [47, 48]:

$$T_{chirp} = \frac{2^{SF}}{BW} \tag{2.2}$$

As described in Figure 2.3, the LoRa PHY frame format consists of a preamble, an optional header, and a payload. Thus, if we exclude the header, the time that takes a LoRa frame to be transmitted from a transmitter to a receiver is:

$$T_{frame} = T_{preamble} + T_{payload} \tag{2.3}$$

where

$$T_{preamble} = n_{preamble\_chirp} * T_{chirp} \tag{2.4}$$

and

$$T_{payload} = n_{payload\_chirp} * T_{chirp} \tag{2.5}$$

From Equation 2.4, 2.5, and 2.3, we can conclude that T_{frame} depends on T_{chirp}, thus, higher SF increases the transmission time of a LoRa PHY frame. Moreover, increasing the SF has a negative impact on the energy consumption of a LoRa end-device.

- **Bandwidth:** BW is the difference between the maximum frequency (f_{max}) and the minimum frequency (f_{min}). It is also known as the width of frequencies in the transmission band. Increasing the BW leads to high data rate, thus short transmission time and less sensitivity (due to high noise components). On the other hand, decreasing the BW gives low data rate, but higher sensitivity (due to less noise components). The BW can be set from 7.8 kHz to 500 kHz. Typically, a LoRa network operates at either 125 kHz, 250 kHz or 500 kHz.

- **Coding Rate:** The CR refers to the error correction bits added to the actual transmitted bits. CR is set to 4/(4 + n)) with $n \in [1;4]$. Increasing the CR offers more protection against interference, but increases time on air.

LoRa for indoor localization:

Recently, LoRa technology is being investigated as a new solution for indoor localization by the research community. LoRa is capable of providing localization solutions based on RSSI and the TDoA techniques. A comparison study of LoRa, Wi-Fi, and BLE localization accuracy was investigated in [49]. The authors deploy their localization solution in indoor environments including open spaces, corridors, and spaces with walls and furniture. They compared the three technologies in terms of signals attenuation and stability, power consumption, and localization accuracy. As a result, they showed that LoRa achieved the best localization accuracy (0.76 m-3.72 m) than WiFi (0.52 m-4.06 m) and BLE (1.53 m-26.46 m). Therefore, they concluded that LoRa is the best candidate for indoor localization due to its sub-1 GHz frequency band.

Another exploration study of LoRa (915 MHz), Wi-Fi, BLE, and ZigBee technology was explored in [50]. A localization solution using Received Signal Strength Indicator (RSSI) measurements and trilateration was used to estimate the user location for each technology. The results showed that LoRa has the highest transmission range and very low power consumption. However, LoRa does not provide the best localization accuracy compared to the other technologies.

RSSI-based indoor localization solution with LoRa (868 MHz) and BLE (2.4 GHz) was introduced in [51]. Four Different RSSI localization algorithms were conducted in a large indoor environment (69m x 69m open industrial hall) with Line of Sight (LOS) condition. The results showed that LoRa gives better performance and localization accuracy than BLE.

Another research that studies the Feasibility of LoRa (915 MHz) for indoor localization applications was presented in [52]. The authors conduct a LoRa localization experiments in a furnished apartment with an area of 114.4 m^2 with both LOS and NLOS conditions. An Adafruit Feather 32u4 RFM95 transceiver was used to capture the RSSI measurements. Only one LoRa configuration was used during the experiments (BW = 125 kHz, SF = 8 and CR = 4/5). The results show that LoRa could achieve a localization accuracy better than 1.6 m in LOS and 3.1 m in NLOS conditions.

RSSI-based localization system using LoRa technology combined with regression and machine learning (ML) algorithms was investigated in [48]. The experiment analysed the feasibility of LoRa in both indoor and outdoor environments. The authors showed that the ML approach toward RSSI fingerprinting achieves promising results than other localization technologies.

On the other hand, LoRa technology can provide a localization solution based on the Time Difference of Arrival (TDoA) of the received signal [53, 54]. A performance evaluation and

comparison between RSSI-based and TDoA-based localization technique for the public LoRa network has been investigated in [54]. The experimental results showed that the location estimates using TDoA approach outperform all investigated RSSI approaches. The authors suggest that the TDoA can be used with the Angle of Arrival (AoA) to achieve better results.

Recently, a few number of research works are trying to mix RSS and TDoA technique with the AoA estimation method to improve the localization accuracy for the LoRa network [55, 56, 57]. In [55], a combination of TDoA localization and AoA localization using only two synchronized gateways was investigated in a large outdoor area using a LoRaWAN network. The simulations showed that when adding the AoA approach to the TDoA, the localization error decreases from 500 m to 399 m. Thus, an improvement of 80% was achieved with AoA. Similar study, as in the case of [55], was introduced in [56]. This study involves a particular filtering approach that combines TDoA and AoA to estimate the location in a dense urban environment. The results showed that when applying the AoA with the TDoA, the median error decrease from 199 m to 94 m. Thus, these results proved that combining AoA with TDoA provides better results in terms of accuracy and reliability.

LoRa for indoor localization: Challenges

As previously discussed, LoRa technology can provide localization solutions based on RSSI, TDoA, and AoA. There are a number of challenges involved with each approach:

- **RSSI-based approach:** The main characteristics of LPWAN technologies including LoRa is the use of a minimal amount of power and a narrow bandwidth to transmit signals. RSSI-based LoRa localization solution cannot guarantee good localization accuracy, since lowering the device's power consumption can result in lower RSSI quality and increased multipath effects. Moreover, due to its CSS modulation, LoRa devices can receive signals below the noise level. As a result, RSSI measurements can be affected by low SNR values, leading to high localization errors.
- **TDoA-based approach:** Time-based LoRa localization approaches such as TDoA and ToF require a large bandwidth to accurately measure the time of arrival of the received signals at the gateways. Therefore, the narrow bandwidth of the LoRa signal makes it unsuitable for localization. Furthermore, a high timestamp accuracy of the received signal is needed at the gateways side, which can affect the cost of the system.
- **AoA-based approach:** Addressing the limitations of RSSI-based localization solu-

tions and TDoA-based localization solutions can be achieved by using the AoA approach. First, unlike TDoA technique, AoA does not require large signal bandwidth or high timestamp accuracy at the receiver. In addition, AoA-based localization solutions measure the angle between the transmitter and the receiver by measuring the phase of the received signal at the array-antennas. Thus, the narrow bandwidth of the LoRa signal won't affect the phase of the received signal, and therefore, not affect the accuracy of the AoA. Lastly, since AoA depends only on the phase of the received signal, not on its received signal strength, the phase will not be affected by multipath and channel fading.

2.4/ LOCALIZATION SIGNAL PROPERTIES

In this section, the most commonly used signal metrics that are used to locate the end device, will be discussed.

2.4.1/ RECEIVED SIGNAL STRENGTH INDICATOR (RSSI)

The received signal strength indicator (RSSI) is the one of the mostly used metric for indoor localization. The idea behind localization using RSSI is to exploit the attenuation of the signal strength and to find an estimation of the distance between the end node and the AP without using complicated calculations [58]. A higher RSSI value indicates a lower distance between the transmitter and the receiver (the transmitter and the receiver are close to each other). The distance d can be calculated using various different path loss models (signal propagation models) given that the transmission power (TP) of the end device is known. The RSSI value is related to the distance d using a simple path loss propagation model [59, 60]:

$$RSSI = -10n\log_{10}(d) + C \tag{2.6}$$

where n is the path loss exponent that depends on the nature of indoor environment (value is ranging from 2 in free space to 4 in other loss indoor environments), d is the distance between the transmitter and the receiver, and C is a fixed constant that refers to the RSSI value at a known distance from the receiver. During the experiments, the RSSI values are averaged, and the distance can be calculated with the followng equation:

$$d = 10^{\frac{C-RSSI}{10n}} \tag{2.7}$$

RSSI-based localization system requires at least three references points (AP) to estimate

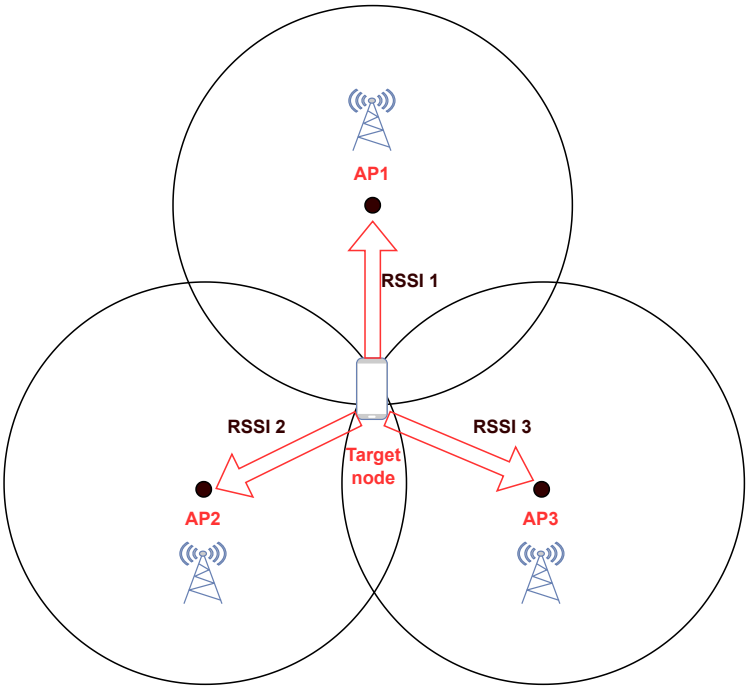

Figure 2.4: Localization based on RSSI

the distance relative to the target node as shown in Figure 2.4. Then, a trilateration is used to measure the location coordinates.

RSSI approach is widely used due to its simplicity and cost effectiveness, since no additional hardware is required on the receiver side. However, it suffers from poor localization accuracy, since signal strength measurements can be affected by NLOS conditions, interference, multipath fading, and noisy environment [28, 27].

2.4.2/ Time of Arrival (ToA)

Time of Arrival (ToA) or Time of Flight (ToF) is the time that takes a signal to propagate from the transmitter to the receiver [61]. Multiplying the ToA or ToF value by the speed of light ($c = 3 \times 10^8 m/sec$) gives the distance *d*:

$$d = c \times ToA \tag{2.8}$$

and

$$ToA = t_{received} - t_{transmmited} \tag{2.9}$$

where $t_{received}$ is the time of receiving the packet at the receiver, and $t_{transmitted}$ is the time of transmitting the packet from the transmitter.

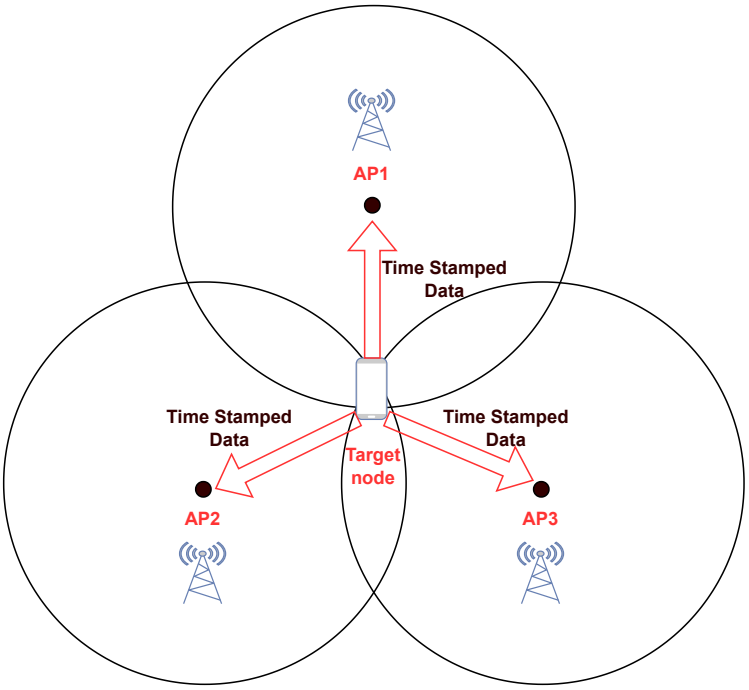

Figure 2.5: Localization based on ToA

Typically, ToA schemes requires a minimum of two or three references nodes to estimate the distances between the references nodes (AP) and the target node. A trilateration (three references nodes) is used to estimate the location in 2D environment and a multilateration (four references nodes) is used to estimate the location in 3D environment. ToA approach requires the transmitter and the receiver to be synchronized to achieve high localization accuracy [62], or in some cases, timestamps are transmitted during the communication protocol [63]. Figure 2.5 illustrates the ToA-based localization approach.

While localization solution using ToA can achieve centimeter-level accuracy in LOS conditions, it suffers in multipath and NLOS conditions. In fact, when there is no LOS between the transmitter and the receiver, the transmitted signal can be reflected by walls, obstacles, and other materials, which results in the signal traversing the longest path and taking the longest time to reach the receiver. Consequently, location coordinates will be inaccurate since distance estimation will be affected. Another drawback is the miss-synchronization between the transmitters and the receivers since the transmitter's clock is not synchronized with the receiver's clock [62]. As a result, there will have inaccurate measurement with the ToA or ToF and, thus, location errors.

2.4.3/ Time Difference of Arrival (TDoA)

Time Difference of Arrival (TDoA) is another time measurement approach, where the difference of arrival times (timestamps) for signals arriving between all receivers is used to

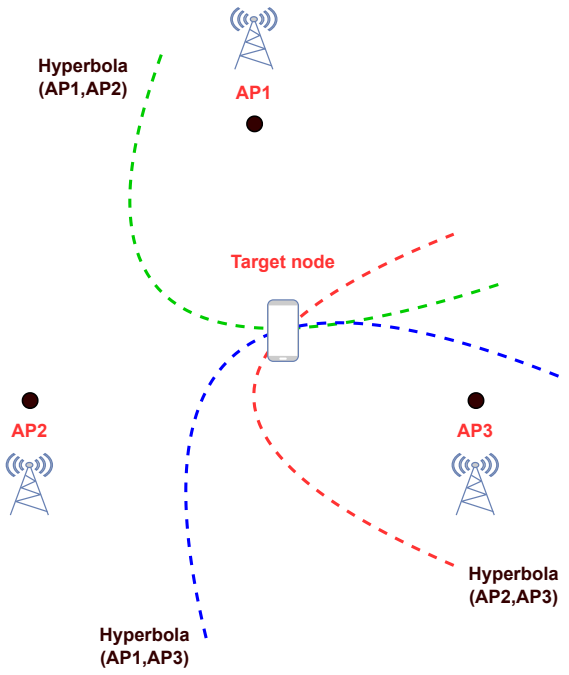

Figure 2.6: Localization based on TDoA

estimate the location coordinates [64]. The main difference between ToA and TDoA is that ToA requires the knowledge of the emitting time of the signal from the transmitter, but in TDoA, the emitting time is not necessary; thus; the difference in Time of arrival between a pair of receivers is used to draw an hyperbolic curve which presents the possible location of the target node. At least three receivers are required to perform the TDoA and the location can be computed by the intersection of the three hyperbolic curves as shown in Figure 2.6.

The main advantage of TDoA is the that a strict synchronization between the transmitter and the receivers is not needed. However, a synchronization between the receivers is required [65]. Another challenge for TDoA is the necessity of a high receiver bandwidth and sample rate in order to deal with multipath effect [66].

2.4.4/ Angle of Arrival (AoA)

The Angle of Arrival (AoA) localization approach is a method that indicates the direction of the signal received by a receiver composed of an antenna-arrays system [67, 68]. This angle-based technique requires a minimum of two receivers to determine the location of the target node by using a triangulation method as shown in Figure 2.7. In general, AoA can be computed by exploiting the time or the phase difference between the signals at different elements of the antenna-array system.

Using AoA-based localization system presents many advantages. First, it requires less

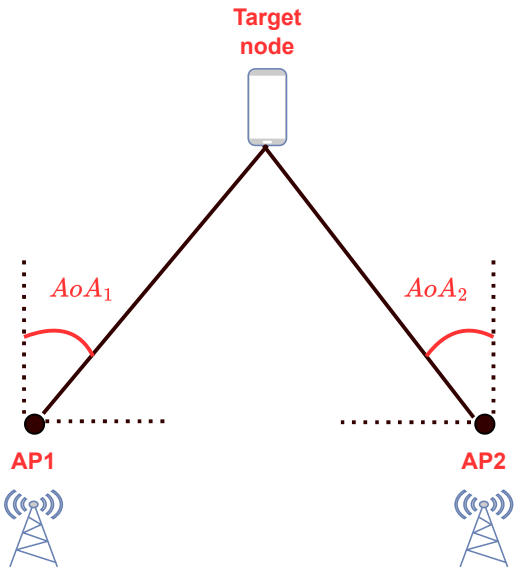

Figure 2.7: Localization based on AoA

receivers as only two AP are required to estimate the target's location in 2D environment, or three AP in 3D environment, which is advantageous over ToA and TDoA that require more AP [69]. Although, AoA can provide a high localization accuracy without the need of time or clock synchronization between the receivers. The angle between the transmitter and the receiver is computed by measuring the phase of the received signal at each elements of the antenna-array. However, complex hardware and coherent phase detector system is needed to provide a high level localization accuracy [70].

2.4.5/ Channel State Information (CSI)

Channel State Information (CSI) is another possible localization solution used to locate the target node. In opposite to RSSI-based localization system which can provide an estimate of the distance based on averaging the signal's amplitude over the entire bandwidth, CSI is more advantageous and has more fine-grained features than RSSI since it can provide signal's phase and amplitude of each sub-carrier frequency band [71]. The CSI-based localization system use the physical layer channel state information in order to obtain the amplitude and the magnitude in the frequency domain. CSI can provide target's location by using fingerprinting, triangulation and trilateration.

CSI-based solution can achieve a high-level localization accuracy compared to RSSI [72, 73]. Moreover, CSI is more efficient than RSSI, since it involves the frequency diversity with different sub-carrier scheme which is more robust to noise and multipath effects [74]. Nowadays, IEEE 802.11 networks known as WiFi have Networks Interface Controllers (NICs) which can provide CSI measurements and high localization accuracy. However,

not all the gateways or receivers has integrated NICs or can provide CSI measurements.

2.5/ Summary and Conclusion

This chapter summarizes in detail the different current localization technologies and signal's metrics used for indoor localization. An important number of indoor localization technologies have been proposed, and can be classified into two categories:

- **RF-based technologies:** for indoor localization, RF-based technologies such as WiFi, BLE, RFID, UWB, etc., are short-range radio (with a range of a hundred meters at best) communication technologies. When applying in real world indoor environments, these technologies require a high density of Access Points (APs) and target nodes to be deployed, resulting in a high cost of the entire localization system. In addition, many indoor localization applications require low power connected devices to be distributed over a wide geographical area. Therefore, RF-based technologies are not the best candidate for low-power and long-range tracking-based applications.
- **LPWAN-based technologies:** In contrast to RF-based technologies, LPWAN-based technologies such as LoRa is able to connect devices over long-range communication (up to ten kilometers). A small number of LoRa gateways can cover a large indoor area (building, universities, shopping malls, etc.), and thus, can support target's localization at low-cost. Moreover, LoRa can achieve low-power communication since the LoRa devices can communicate with a battery lifetime up to 10 years. LoRa is a physical layer scheme that operates in the license-free ISM band (868 MHz in Europe). Its CSS modulation technique makes it a good candidate for most of indoor environments, where a various of phenomena can be observed such as signal's attenuation, multipath and channel fading.

In this chapter, we also investigate the most used localization measurements including RSSI, CSI, ToA, TDoA, and AoA. Once the localization technology is chosen and applied in real world indoor environment, the choice of the localization technique is always a challenge. Despite the many advantages of the LoRa technology for indoor localization, the following challenges should be considered:

RSSI-based localization solutions for LoRa technology has their limitations, due to their sensitivity to strong signal attenuation caused by the multipath effects and channel fading. On the other hand, time-based approaches such as ToA and TDoA cannot achieve high localization accuracy, due to the narrow bandwidth of the transmitted signals and the demand of strict time-synchronization. The AoA-based approach is the most promising

solution for LoRa localization since the AoA estimation only depends on the phase of the received signals at different elements of the antenna-array.

This thesis seeks to implement an AoA-based localization system using mainly the phase approach, which we believe is most suitable and promising for LoRa technology. Thus, in order to achieve high localization accuracy, phase-based approach faces many challenges, such as coherent phase detectors and complex hardware and software development.

The next chapter examines the Software Defined Radio system in both hardware and software platforms, along with the GNU Radio software used to investigate the profile of the LoRa physical layer and implement AoA-based localization system.

3

SOFTWARE DEFINED RADIO

3.1/ INTRODUCTION

In this chapter, we explore the concept of the Software Defined Radio (SDR) platform in both hardware part and software part. We introduce a background of the Universal Software Peripheral (USRP) and the GNU Radio project that form the essential technical elements of the contributions.

3.2/ SOFWARE DEFINED RADIO (SDR)

Most of Traditional radio systems use integrated circuits (electronic circuits) and specialized equipment for implementing a radio communication system. Radio traditional systems are made up of traditional radio hardware components including mixers, amplifiers, filters, analog/digital converters, modulators/demodulators, and detectors.

On the other hand, a revolutionary concept named Software Defined Radio (SDR) was introduced and replaced the analog traditional radios. SDR is a radio communication system in which many of the traditional hardware components are replaced by a single device that performs signal processing functions. Most of the functionality of the SDR are implemented in Software rather than in hardware. The main idea of a SDR is digitization which is the conversion of the analog radio signal into digital format using an analog-to-digital (ADC) converter, so it can then be processed by a software. According to GNU Radio founder Eric Blossom, SDR is the technique of getting code as close as possible to the antenna. It turns radio hardware problems into software problems [75]. The figure 3.1 illustrates the block diagram of a typical SDR system.

As described before, SDR is a radio transmitter/receiver system composed by hardware part and software parts. In transmitting mode, the RF front-end converts the baseband signal to the carrier radio frequency (RF) signal to be transmitted by the antenna. The RF front-end is composed of a RF amplifier, RF filter and a Mixer with a local oscillator which

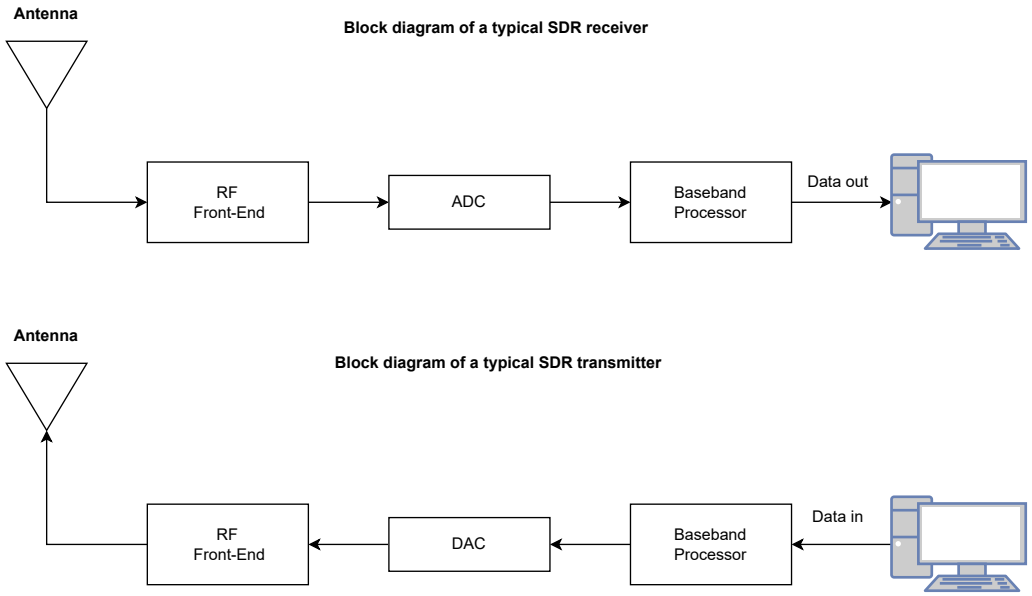

Figure 3.1: Block diagram of a typical SDR system

converts the baseband signal (centered around 0 Hz frequency) to a RF signal (ranging between MHz and GHz frequency).

The receiving mode is just a reversed procedure of the transmitting mode. The carrier RF signal received by the antenna is converted by the RF front-end to baseband signal and then being digitized by the ADC and sent to the baseband processor and the computer for signal processing. The signal processing functions including filtering, decimation, detection, demodulation and decoding can be realized by components and configured by software. These components include a digital signal processor (DSP), a field-programmable gate array (FPGA) and a general-purpose processor (GPP).

The SDR approach provides a variety of benefits over the traditional radio approach. These advantages include:

- **Time and cost reduction:** Using an SDR platform can reduce the time of deploying new products. In fact, a common SDR platform composed of a hardware and software part can be used to design and deploy new products for the industry market. Additionally, SDR in its software can be reused or reprogrammed to support with new RF technologies and functionalities. As a result, new products can be deployed more quickly and at reduced cost.
- **Multi-frequency/modulation:** One of the key advantage of the SDR is the capability to be reconfigured to handle different frequency ranges and modulations. The end user can choose different frequencies (ranging from kHz to GHz) and different modulation methods such as Amplitude Modulation (AM), Frequency Modulation (FM), Frequency Shift Keying (FSK), Phase Shift Keying (PSK) and many others

with only a standard platform.

- **Multi-channel:** A SDR has the advantage of being able to operate at multiple frequencies at the same time. When using an SDR platform, it is possible to demodulate more than one RF channel simultaneously. With coherent multi-channel SDR receivers, an antenna-array direction finding system and digital beamforming applications can be easily deployed and implemented.

- **Interference avoidance:** An important challenge in RF communication is dealing with interfering signals. SDR offers the opportunity to detect and avoid interference with other communication channels. The detection of the interfering signal and the determination of its frequency can be done with specific filters by software. Thus, the interfering signal can be filtered to obtain the signal of interest.

3.3/ HARDWARE ARCHITECTURE

The market includes a list of SDR hardware ranging from low-cost to high-cost transceivers. Ettus research headed by Eric Blossom and Matt Ettus [76] is one of the companies that have developed an open source hardware platform dedicated to the SDR. The development was focuses on the Universal Software Radio Peripheral (USRP). The USRP is the most popular cost-effective SDR platform used in research applications. The USRP is characterized by its flexibility, accuracy, phase and frequency stability, large bandwidth, and good prices compared to other hardware systems. This open source device defines the interface between the analog RF domain and the General purpose processor and can generate and receive any kind of RF signals. The USRP can receive radio waves captured by the antenna and converts these waves into digital signals that can be processed by the computer using an analog to digital converter (ADC). On the other hand, to generate a radio wave, the USRP converts a radio wave processed by the computer into a RF signal using a digital to analog converter (DAC). A block diagram of the USRP hardware is shown in Figure 3.2. We present the block diagram of the USRP SDR receiver in both hardware and software part. In this thesis, we use specifically the USRP B210 device.

3.3.1/ THE B210 MOTHER BOARD

The type of the USRP used in this thesis as shown in Figure 3.3 is the B210. This device covers a wide frequency range (70 MHz to 6 GHz) with a maximum bandwidth of 56 MHz, which make it a suitable candidate for a various number of RF applications [77]. This SDR board combines the AD9361 RF module called daughterboard (section

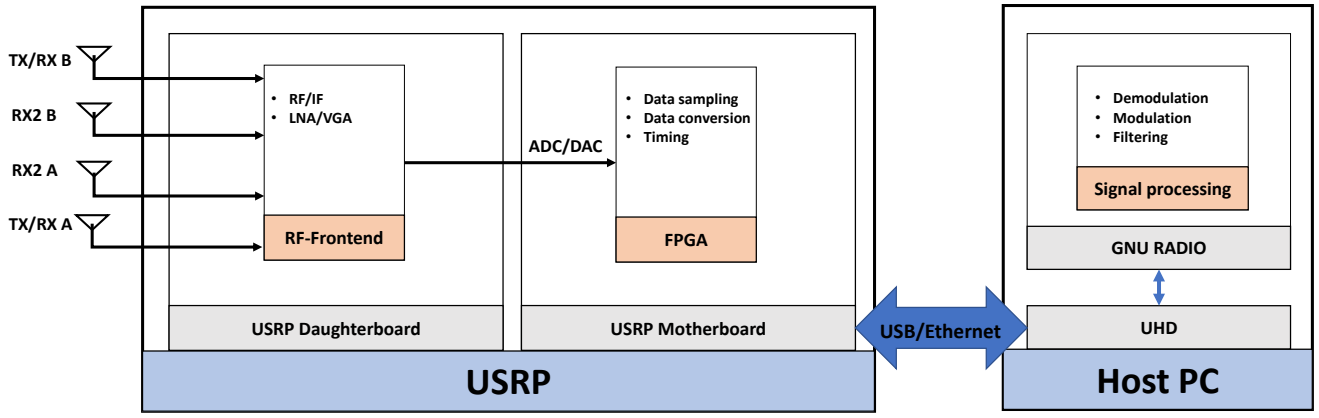

Figure 3.2: Block diagram of a USRP based SDR receiver

3.3.2) and the Xlinx Spartan-6 FPGA board. In reception mode, the signals received by the the daughterboard will be amplified and converted from its High-Frequency (HF) to the Intermediate Frequency (IF) band. After that, the filtered signal is converted and digitized by the ADC, which has 12 resolutions bits for each In-phase and Quadratic (I/Q) samples, and a sampling rate equals to 61.44 Msps (Mega sample per second). The B210 Spartran 6 FPGA has the role decimating and reducing the sample rate *(fs)* by a factor of *N* resulting in samples that will be sent to the host PC with a reduced throughput. The B210 can be connected the Host PC via a Gigabit Ethernet high speed interface or a USB 2.0/3.0 cable and is compatible with the GNU Radio development platform.

3.3.2/ THE B210 DAUGHTER BOARD

The B210 motherboard is connected to the AD9361 daughterboard [78] which has the role of receiving and transmitting analog signals. The AD9361 provides four independent RF chains, two transmitter (TXA and TXB) and two receiver (RX2A and RX2B) chains, which share the same clock source. This fully coherent property between the two RX chains make this board an ideal candidate for computing the phase difference without a phase offset between the two RX chains. Each RF chain is connected to a set of amplifiers, filters and local oscillators that convert the signal from the RF frequency band to the baseband frequency. The daughter board is the interface to the real world, while the mother board takes care of ADC/DAC conversion, sampling, decimation and connection to the host machine. The block diagram of the AD9361 daughterboard is shown in Figure 3.4.

In this thesis, the AD9361 daughterboard is used to cover the 868 MHz LoRa frequency band. In addition, the coherence between its two RX ports is an important feature for computing the phase difference and AoA, as indicated by the thesis objective.

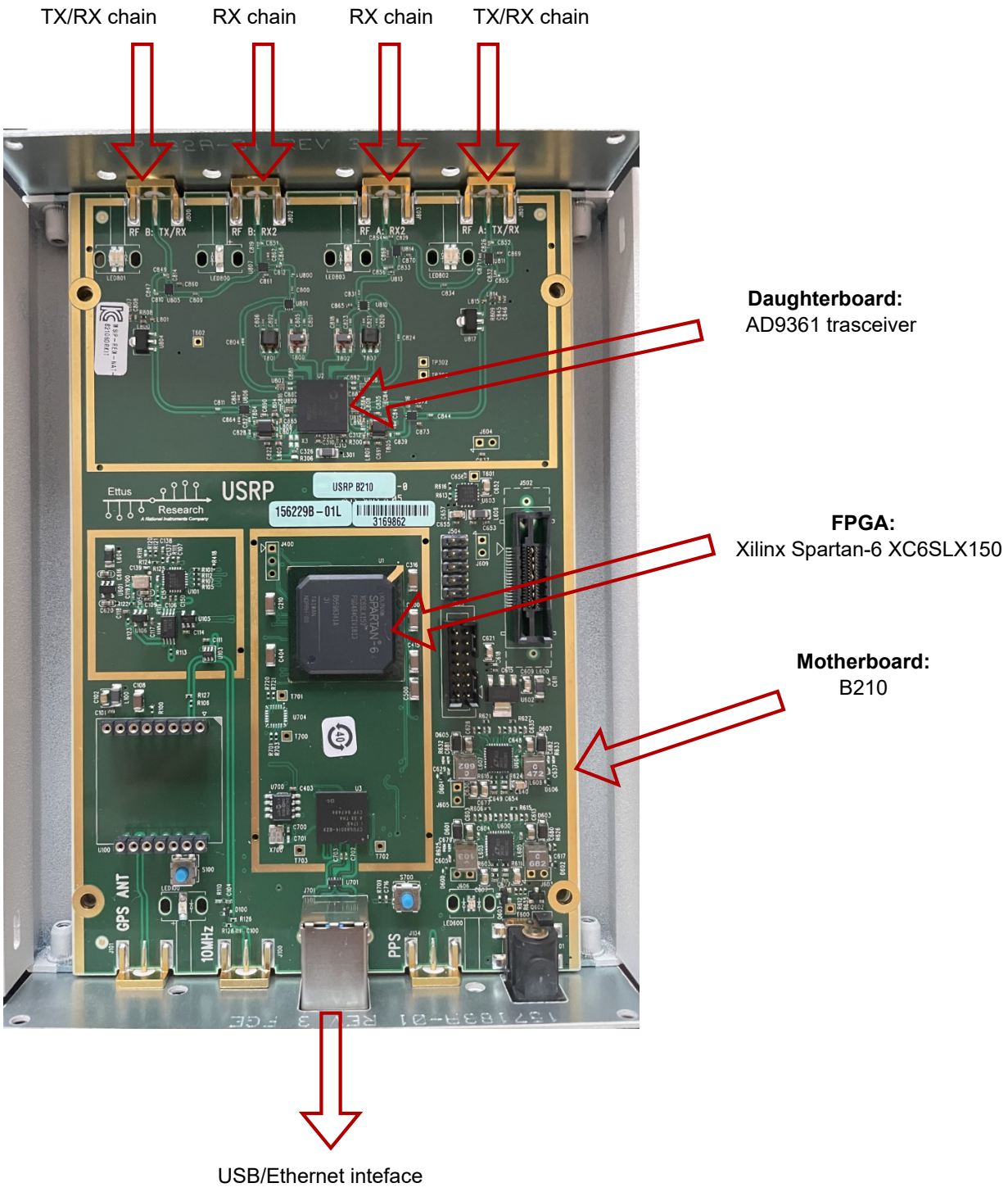

Figure 3.3: USRP B210 hardware architecture

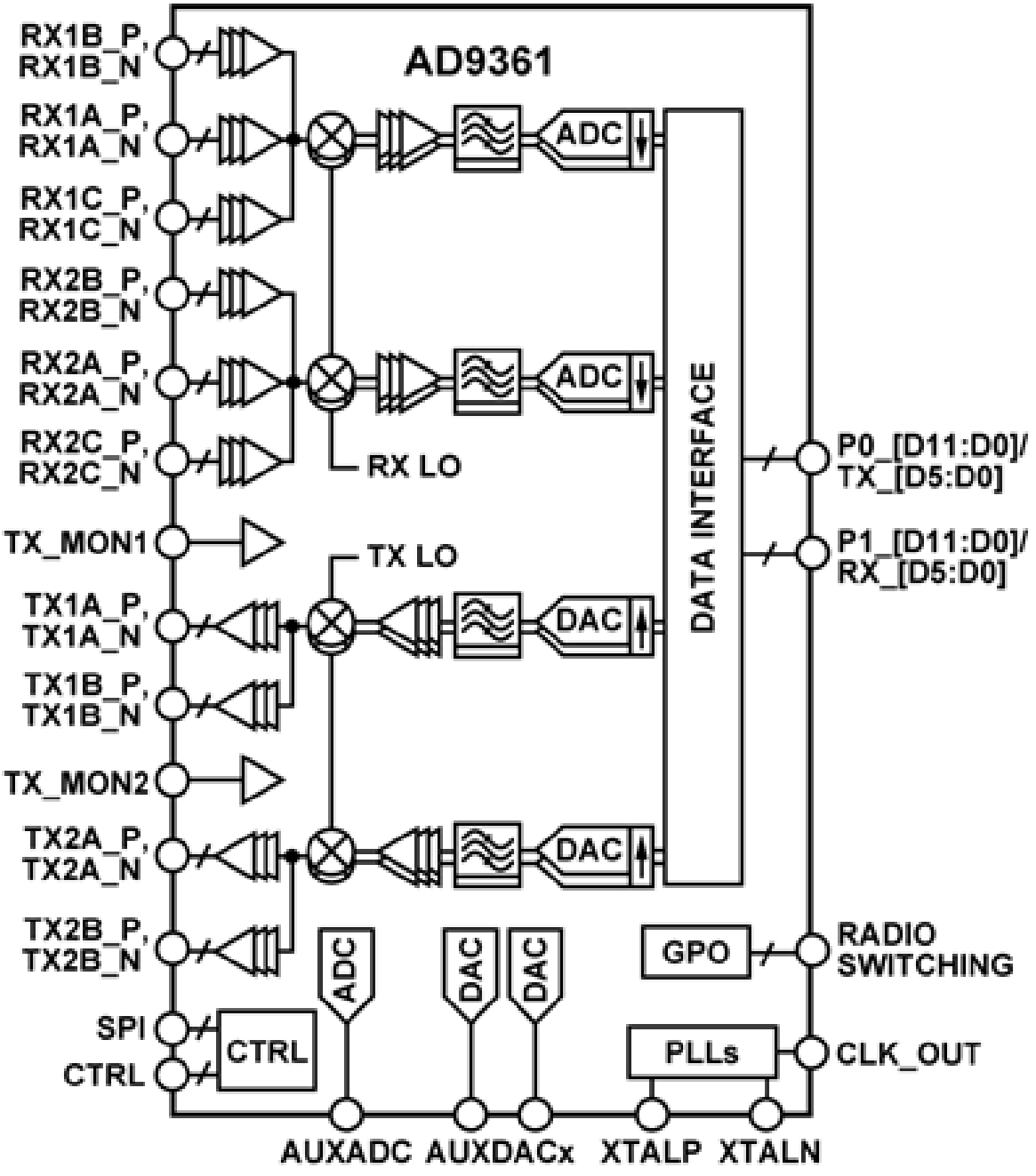

Figure 3.4: Block diagram of the AD9361 [78]

3.4/ SOFTWARE ARCHITECTURE

As explained before, a SDR is a system composed of hardware and software, with most signal processing functions being performed in software instead using dedicated integrated circuits in hardware. In this section, we describe the GNU Radio framework which provides the most SDR functionality for signal processing.

3.4.1/ GNU RADIO FRAMEWORK

GNU Radio's philosophy revolves around the concept that hardware problems can be transferred to software problems. The GNU Radio project [79] is the most popular software framework used to interface with the USRP based SDR platforms. It was officially introduced to the community by Eric Blossom and John Gillmore in 2001 as part of the GNU package [80].

The project is a free and open source software development toolkit that is widely used in academic research, governmental sector, industry and commercial sectors for investigating and implementing radio communication systems. The GNU Radio applications provide a flow graph diagram composed of signal processing blocks written in C++ programming language and implemented on the CPU for performance and computational purposed. The Python programming language is used to create a flow graph diagram that depicts the flow of data between the blocks. Thanks to the SWIG (Simplified Wrapper and Interface Generator) interface that enables the signal processing blocks implemented in C++ to be connected over python. The architecture of GNU Radio is illustrated in Figure 3.5.

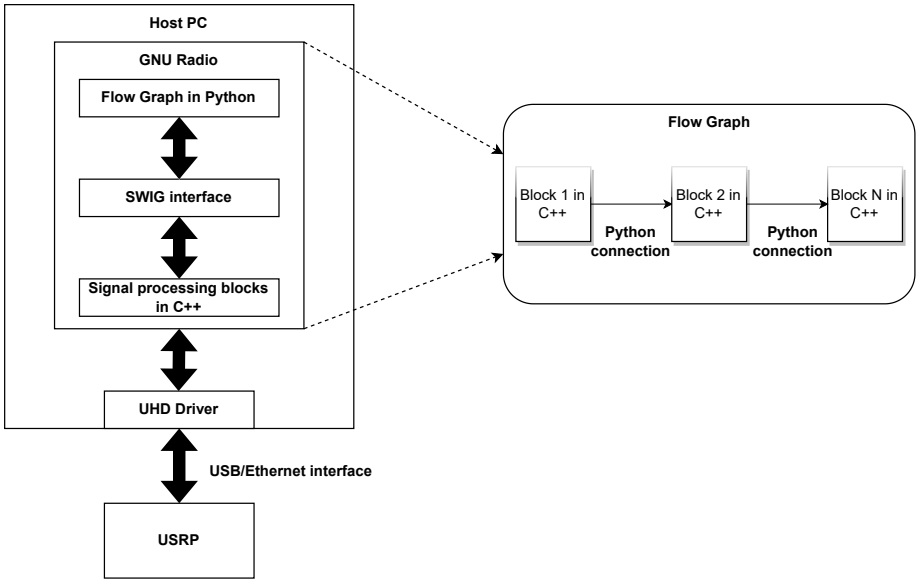

Figure 3.5: Architecture of the GNU Radio

The GNU Radio's signal processing blocks offer many signal processing functions including:

- **Analog Modulation:** Amplitude Modulation (AM), Phase Modulation (PM), and Frequency Modulation (FM).
- **Digital Modulation:** Quadrature Amplitude Modulation (QAM), Phase-Shift Keying (PSK), Orthogonal Frequency Division Multiplexing (OFDM), Gaussian Frequency-Shift Keying, and other modulation types.
- **Filtering:** Infinity Impulse Response Filter (IIR), Finite Implulse Response (FIR), Fast Fourier Transform (FFT), and many others.
- **Signal Processing:** Decimation, Interpolation, Down-sampling, Compression, and others.

GNU Radio's applications are usually represented as flows graph accessible through the GNU Radio Companion (GRC).

3.4.2/ GNU Radio Companion (GRC)

The GNU Radio companion (GRC) is a graphical user interface (GUI) tool developed by Josh Blum and released as free software in 2009, which allows the end user to design a GNU Radio flow graph and develop a GNU Radio application in a graphical environment. This GUI represents the front-end between the end user and the GNU Radio libraries. When compiling a GNU Radio flow graph in GRC, it generates and execute a Python source code that contains the designed and connected blocks.

Additionally to its role in designing GNU Radio flow graphs that interact with the external world via the USRP hardware, the GRC can be used to work on simulations. When the end user does not need to send or receive a real signal with the USRP, GRC can be used to create simulations and generate graphs for research and dissertation purposes as in our case in this section.

An example of GNU Radio flow graph is presented in Figure 3.6, which illustrates the replacement of a traditional oscilloscope. The flow graph is composed of a *signal source* block which generates a variety of waveforms such as *Sine*, *Cos*, *square*, and other types. In the example, the *signal source* sets the waveform equals to *sine* and the baseband frequency equal to 1 kHz. This signal is sent to the *Throttle* block which sets the average rate (output samples of the *Signal Source*) does not exceed the maximum sample rate (maximum samples per second). In this flow graph, we can define global variables for the sample rate and the baseband frequency.

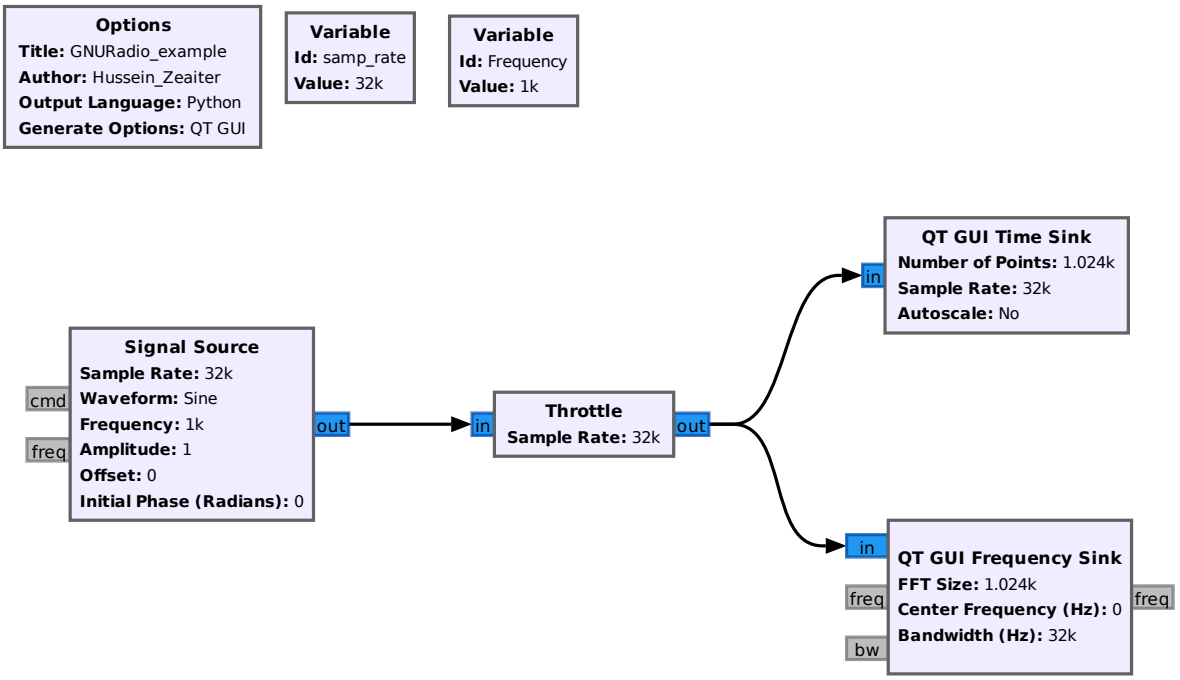

Figure 3.6: A simple GNU Radio flow graph. A signal source, QT GUI Time and Frequency Sink are used.

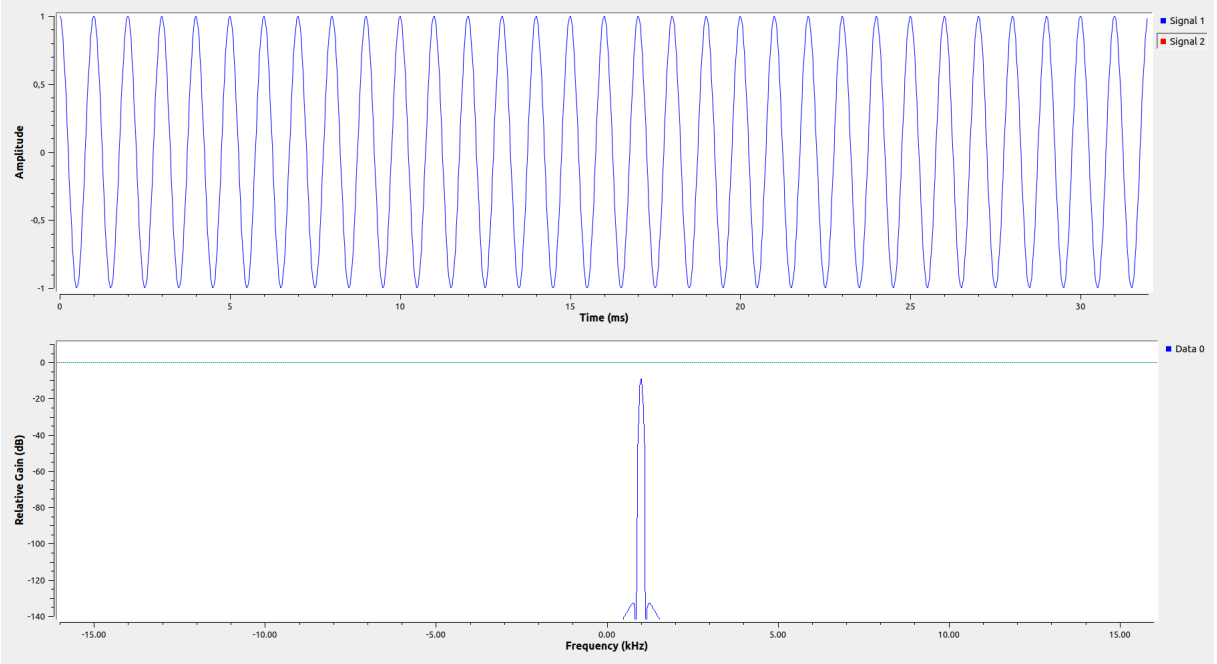

Figure 3.7: A GNU Radio flow graph output. A sine wave signal with a frequency centered at 1 kHz.

The sample rate should be at least twice the signal frequency (Shannon theorem). For example, for a sample rate equals to 32 kHz, the *Signal Source* block can generate a maximum frequency equal to 16 kHz. In addition, a *QT GUI Time Sink* and *QT GUI Frequency sink* are used to act as an oscilloscope and spectrum analyzer and represent the *Signal Source* in the time and frequency domain respectively. The output of the flow graph is illustrated in Figure 3.7.

GRC enables to capture a RF signal with the USRP. In reception mode, the *UHD: USRP Source* block is used to act as a receiver which receives and converts the signal to the baseband or intermediate frequency (IF). The Figure 3.8 below illustrates the receiving chain of a signal from the *USRP* via *UHD* driver.

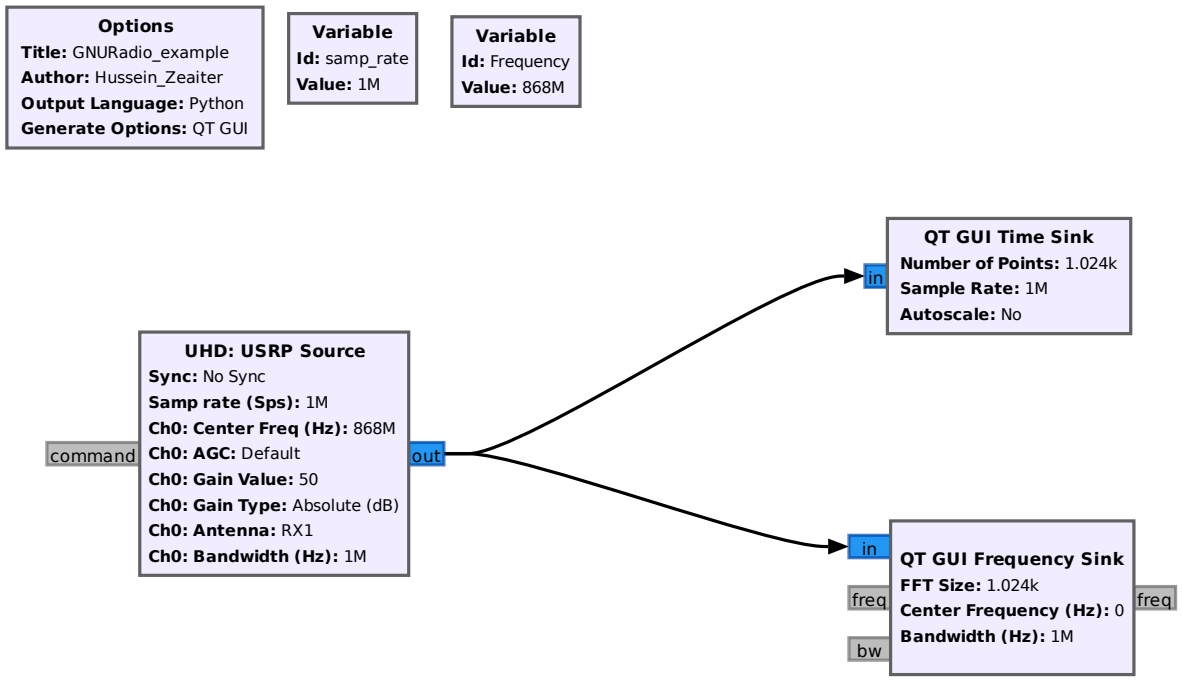

Figure 3.8: A GNU Radio flow graph of signal reception from the USRP via UHD driver.

3.4.3/ UHD DRIVER

UHD stands for *USRP Hardware Driver*, which is an open source user interface library developed by Ettus Research and supports all the USRP SDR devices family including all motherboards and daughterboards.

UHD presents the unique access method for the end user to take control, configure, and send or receive signals to and from the USRP hardware as shown in Figure 3.9. The end user can set the sampling rate, the center frequency, the antenna gain and select the receive and transmit antennas.

The UHD driver has a unique C/C++ API that supports many software such as GNU

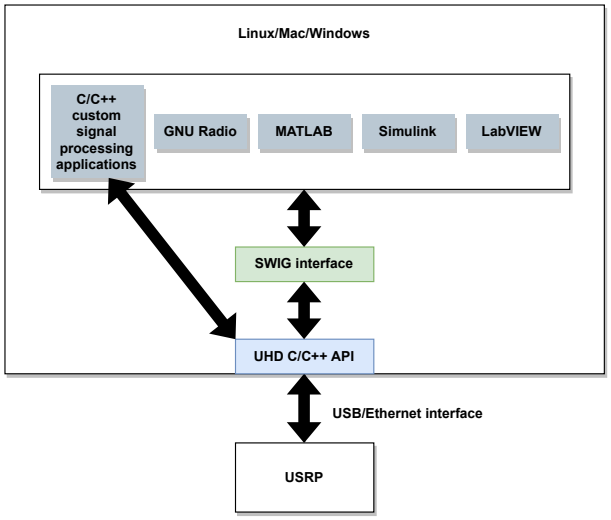

Figure 3.9: UHD interface between hardware and software.

Radio, MATLAB, Simulink, and LabVIEW. In addition, it offers the possibility for the end user to design and build a custom signal processing application on top of the C/C++ API without the necessity of the swig interface. UHD was mainly launched on Linux operating system, but it also supports operating systems such as Mac and Windows.

3.5/ SUMMARY AND CONCLUSION

In this chapter, we have presented the history and background of the Software Defined Radio technology. We examined in detail the essential components of an SDR platform including the hardware and software part. The software part includes of the GNU Radio development toolkit, which is used to study the profile of RF signals, design and develop signal processing applications. Additionally, the hardware part involves the USRP, which allows the transmission and reception of various types of RF signals.

In this thesis, the Software Defined Radio platform is used as the gateway for the purpose of measuring the angle of arrival of a transmitting LoRa device. In the next chapter, we will discuss our first contribution to implement a localization system based on the AoA approach.

III

CONTRIBUTIONS

4

SYLOIN: AN INDOOR LOCALIZATION SYSTEM FOR LORA SIGNALS

4.1/ INTRODUCTION

The Syloin project is an indoor localization system whose architecture is composed of a set of SDR/LoRa gateways deployed in a logistics warehouse in order to measure AoA from various locations. Following this, a triangulation function is performed, which results in a set of intersecting lines resulting in the location of LoRa objects deployed in the area. These objects linked to a single battery have been designed to send low-power signals to gateways in order to extend their lifespan as much as possible. Furthermore, adding more connected objects in the warehouse must not saturate the radio channels. This should be possible with a good management of collisions and interference.

As the first contribution, this thesis proposes a solution to track LoRa objects in an indoor environment using an SDR platform. This solution is based on measuring the phase difference between the signals received at the different antennas of the SDR gateway. When there is a phase shift between the received signals at each antenna, we calculate its value and provide its corresponding AoA.

To achieve this, we design and develop an embedded software to organize wireless radio communications between elements communication with the LoRa wireless network technology. As part of this first contribution, LoRa signal was processed and simulated using the SDR. The SDR facilitates easy visualization and study of the LoRa signal profile. The demodulation and decoding of the LoRa signal were also included in this first contribution.

Once we have finished the demodulation and decoding the LoRa signal, we move to the next step in calculating the AoA. The process is composed of three steps: Detecting the presence of the signal in the channel, measuring the phase of the received signal at each antenna of the receiver, and, finally, computing the phase difference and the AoA.

In this chapter, the solution to track a LoRa object using an SDR platform, along with

testbed and experimental results are presented.

4.2/ INVESTIGATING LORA SIGNAL USING SDR

Before proceeding to the detection, demodulation and decoding process of a LoRa signal, it is important to understand LoRa signal properties and its behaviour. LoRa technology used the CSS modulation technique to modulate and encode the signal. Therefore, to encode and send a signal, a LoRa transmitter must be configured and programmed at least with three essential parameters: the carrier or operating frequency (CF), the spreading factor (SF), and the channel bandwidth (BW). The LoRa technology operates at the 868 MHz ISM frequency band in Europe. LoRa can manage up to 16 channels in Europe with 3 channels set up by default (868.1, 868.3 and 868.5 MHz). Another important parameter is the channel bandwidth. LoRa allows mainly 3 channel bandwidth: 125, 250, and 500 kHz. Finally, LoRa introduces several spreading factors, typically 7 SF (from 6 to 12), that allows orthogonal transmission to avoid signal's collision.

LoRa configuration		
Frequency band	Channel Bandwidth	Spreading Factor
868 MHz	125, 250, and 500 kHz	6 to 12

Table 4.1: LoRa configuration parameters in Europe.

The first step in investigating the profile of the LoRa signal involves the use of a SDR platform. For signal acquisition and processing, we use the USRP B210 based SDR receiver and GNU Radio software. The LoRa signal acquisition process was started by transmitting at first a LoRa signal with the following parameters: Frequency equal to 868 MHz, Channel bandwidth equals to 125 kHz and spreading factor equals to 7.

At this point, the whole signal acquisition process will be done in GNU Radio. The entire signal acquisition process is illustrated in Figure 4.1. The flow graph starts by the *UHD:USRP Source* block which is responsible to receive the stream of data captured by the USRP B210 SDR receiver. *UHD:USRP Source* block allows of setting parameters for receiving a various number of RF signals. These parameters include:

- **Sample Rate:** The sample rate which is equal to the number of samples per second captured by the USRP B210. By respecting Nyquist-Shannon sampling theorem, we end up with a sampling rate equals to 1 MHz. In fact, the Nyquist's theorem establishes a sufficient condition for a sampling rate that permits to observe the total signal's bandwidth in Hz. Therefore, for a continuous signal *x(t)* in the time domain,

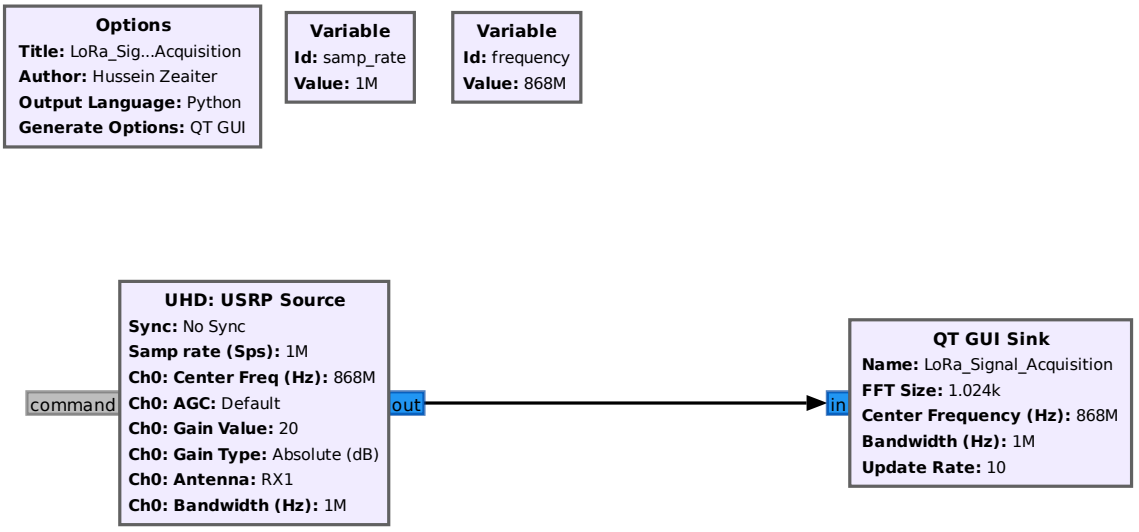

Figure 4.1: A GNU Radio flow graph of LoRa signal acquisition with USRP B210.

a sufficient sampling rate is anything greater than 2x*BW* samples per second [81]. The sufficient sampling rate (f_s) can be presented as follow:

$$f_s \geq 2 \times BW \tag{4.1}$$

As described earlier, LoRa technology enables three channel bandwidths: 125, 250, and 500 kHz. For all these bandwidths to be covered, the desired sampling rate must be at least twice the maximum LoRa bandwidth. For this reason, we set the sampling rate to 1 MHz ($f_s \geq 2 \times 500$ kHz).

- **Channel Center Frequency:** The center frequency refers to the carrier frequency of the frequency of interest. It must be the same frequency as the LoRa transmitted signal. Therefore, we set the channel center frequency to 868 MHz.
- **Channel Bandwidth:** The channel bandwidth refers to the bandwidth that is used by the USRP B210 anti-aliasing filter. in accordance with the Nyquist-Shannon sampling theorem, the anti-aliasing filter is used before the sampling process to limit the received signal's bandwidth. As a result, the USRP's receiving bandwidth is twice the LoRa's 500 kHz maximum bandwidth.
- **Channel Antenna:** There are several possible antennas that the user can choose from. The possible antenna selection is described in the description of the daughterboard (Section 3.3.2).

At this stage, the LoRa signal is captured by the *UHD:USRP Source* block and sent to the *QT GUI Sink* block. The *QT GUI Sink* block has the role to represent the signal graphically in time and frequency domain respectively. It uses the Fast Fourier Transform (FFT) to

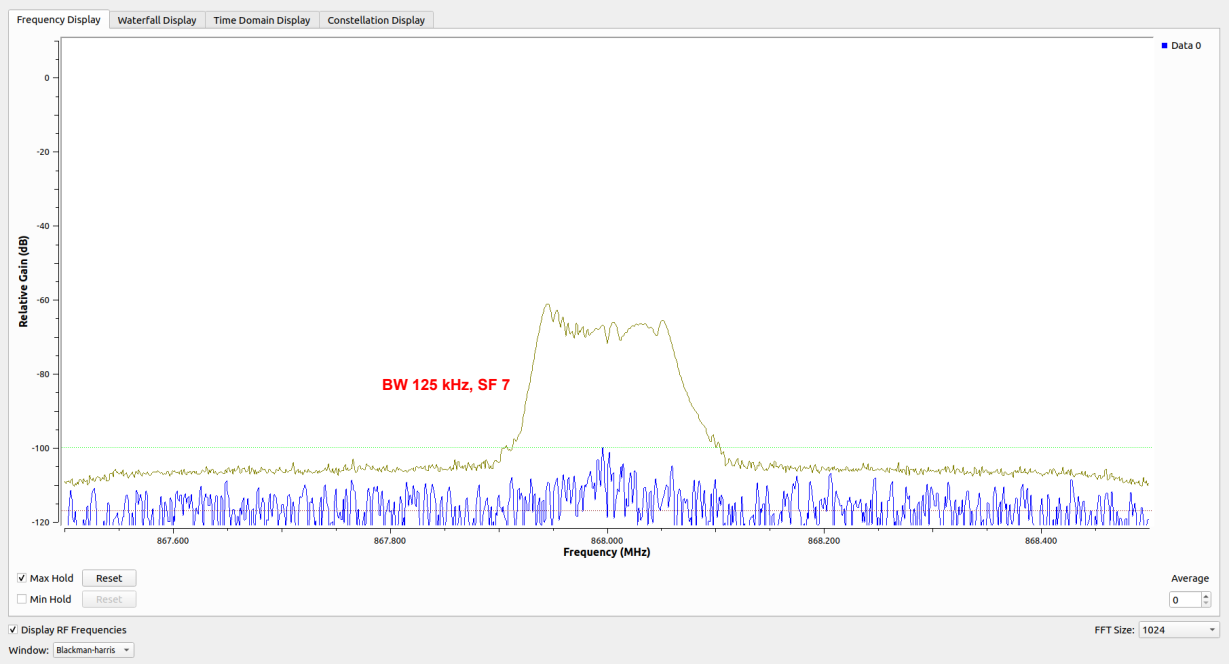

Figure 4.2: FFT frequency representation of LoRa signal (BW = 125 kHz and SF = 7).

represent the frequency components of the signal. The result of this implementation is illustrated in Figure 4.2. As we can see, the center frequency of the LoRa signal is 868 MHz, which is our frequency of interest (carrier sent frequency). We can determine the bandwidth of the transmitted signal by examining the different frequency components of the FFT. In fact, the bandwidth of a LoRa signal is equal to the difference between the highest and lowest frequency components of an FFT . We can therefore conclude that the bandwidth has a value of 125 kHz and matches our interest bandwidth.

We have now identified the LoRa signal frequency and bandwidth of interest. We still need to identify the spreading factor used by our LoRa transmission. It can be seen from Figure 4.2 that the chirps are transmitted at a very fast rate. In fact, the spreading factor determines the chirp rate, and hence, the data transmission rate. Consequently, lower spreading factor results in faster chirps, making it difficult to visualize chirps in real time. For this reason, the spreading factor of the transmitting signal has been changed from 7 (lowest value) to 12 (highest value). The frequency and time domain results of the new configuration are illustrated in Figure 4.3 and 4.4 respectively .

Figure 4.4 shows the time domain of a LoRa signal with the spreading factor equal to 12. The LoRa signal begins with a serie of increasing frequencies (up-chirps) followed by a serie of decreasing frequencies (down-chirps) that indicates the end of the LoRa's preamble. After the preamble, we can clearly see the LoRa encoded data.

At this level, we have identified a LoRa transmission with two different configurations in the frequency and time domain respectively. We have successfully identified the type of

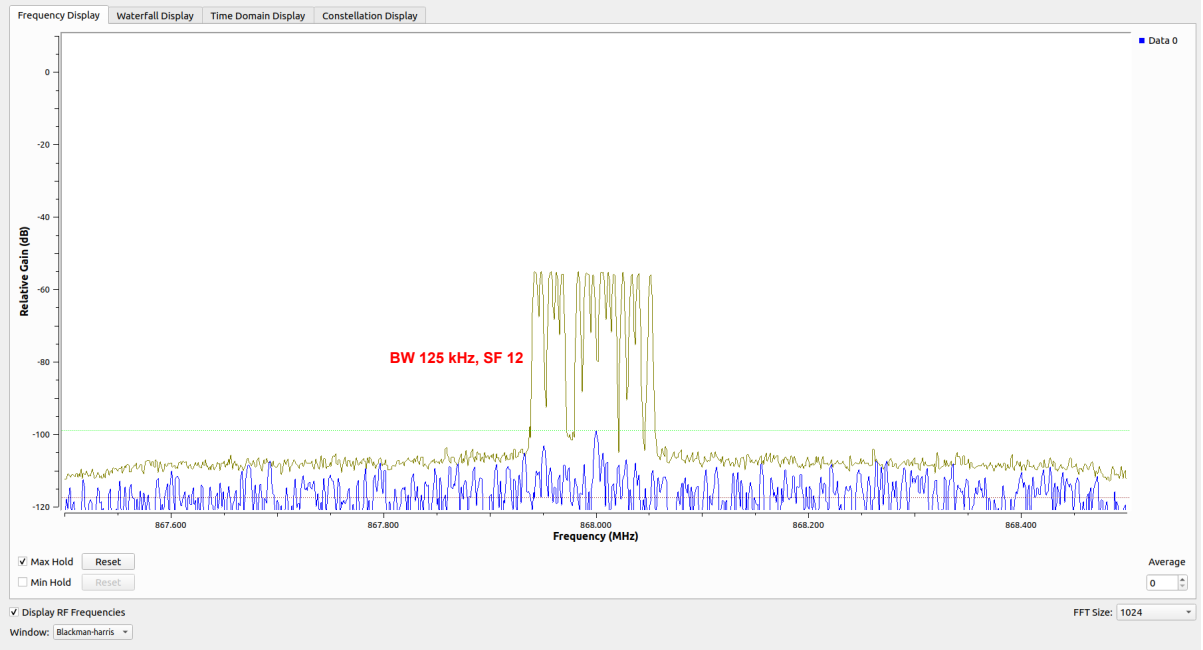

Figure 4.3: FFT frequency representation of LoRa signal (BW = 125 kHz and SF = 12).

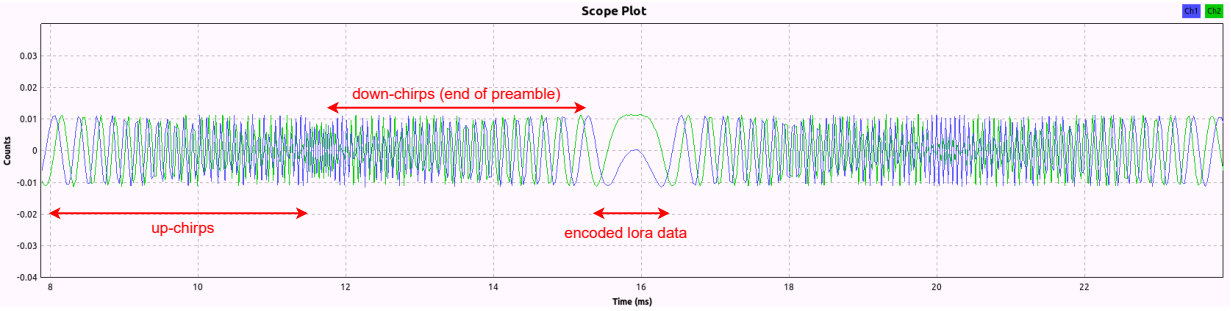

Figure 4.4: Time domain representation of LoRa signal (BW = 125 kHz and SF = 12).

modulation used by LoRa. The next step is to go further to demodulate and decode the signal.

4.3/ DEMODULATING AND DECODING LORA SIGNALS

4.3.1/ RELATED WORK

The LoRa wireless technology is a proprietary physical layer developed by Semtech. There are not enough open-source references and documentation available for designing and implementing the LoRa physical layer in an open environment. For the research community, studying and implementing the LoRa PHY remains challenging.

A lot of research has been focused on LoRa PHY layer using SDR over the past few years

[82, 83, 84, 85]. The aim of these studies is to reverse engineer the LoRa PHY layer to end up with an implementation. A reverse engineering project involves identifying the radio communication protocol used in the LoRa network. In [82] and [83] provide in-depth details about the LoRa PHY layer.

The first implementation, [82], introduces a modulation and encoding technique of the LoRa PHY. An open-source software implementation ,*gr-lora*, is also presented. *Gr-lora* is an open-source LoRa PHY layer implementation using the SDR platform and the GNU Radio software development toolkit. Based on reverse engineering methods, if defines signal processing blocks for receiving and transmitting LoRa RF signals. However, this implementation only supports receiving and transmitting LoRa signals with a spreading factor equals to 8, a coding rate equals to 4/8, and all bandwidths. It is due to the fact that the whitening sequences are not processed correctly that the rest of the spreading factors and coding rate fail.

In the second implementation, [83], a Multi-channel software decoder for the LoRa PHY layer was introduced usind the SDR platform and the GNU Radio. The authors presented a reverse engineering algorithm based on real LoRa transceivers. Three steps are involved in the algorithm: signal detection, synchronization, and real-time decoding of LoRa frames. The decoder in this implementation, *gr-lora*, can decode LoRa frames from multiple channels simultaneously. According to the authors, the decoder can work with all possible combinations of spreading factors and coding rates, and can communicate with existing LoRa transceivers, including the SX1272 (Semtech), RN2483 (Microchip), and RFM96 (Hope RF).

In this thesis, the LoRa PHY layer implementation presented in [83], is used to detect and decode LoRa signals. This decoder will be used in conjunction with our proposed localization solution. In the next section, we will discuss in details the GNU Radio decoder of the LoRa PHY.

4.3.2/ GR-LORA: GNU RADIO DECODER OF THE LORA PHYSICAL LAYER

Gr-lora is an open-source GNU Radio signal processing project that provides signal processing blocks used for receiving and transmitting LoRa RF signals using a software defined radio platform. The project relies on a fully reverse engineering process in order to implement the LoRa PHY with GNU Radio. In this project, demodulating, decoding, and therefore, modulating and coding LoRa signals are handled correctly with 100% spreading factors accuracy. The GNU Radio implementation of the LoRa PHY is illustrated in Figure 4.5.

As illustrated in Figure 4.5, we have added a *LoRa Receiver* block to our flow graph. This block is responsible for demodulating and decoding LoRa signals. Before executing the

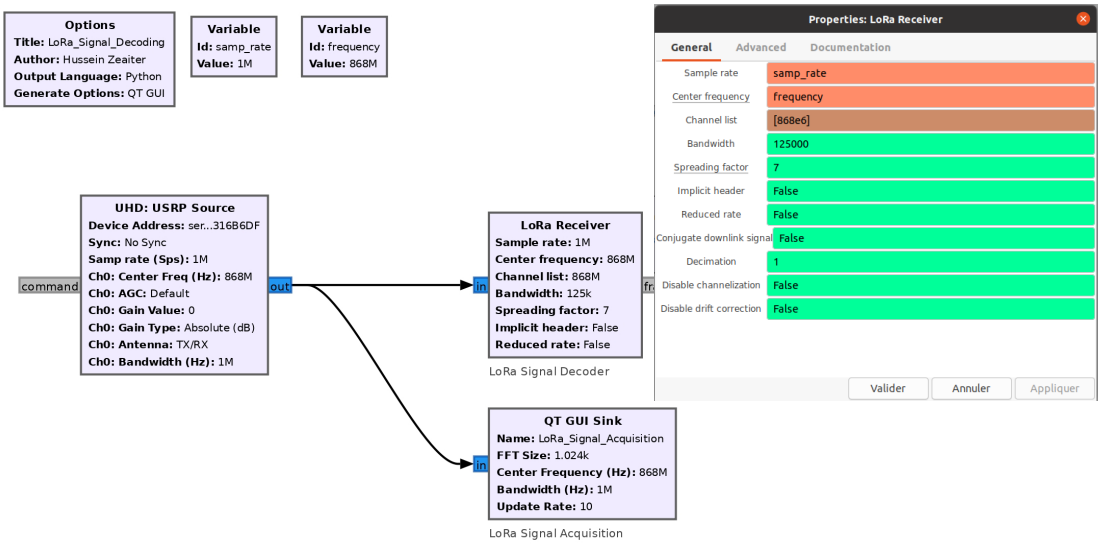

Figure 4.5: A GNU Radio flow graph of LoRa signal decoder with USRP B210.

flow graph, different parameters must be filled in: the center frequency of the LoRa signal, 868 MHz, the channel bandwidth, 125 kHz, and the spreading factor with a value equal to 7. The result of this flow graph is shown in Figure 4.6.

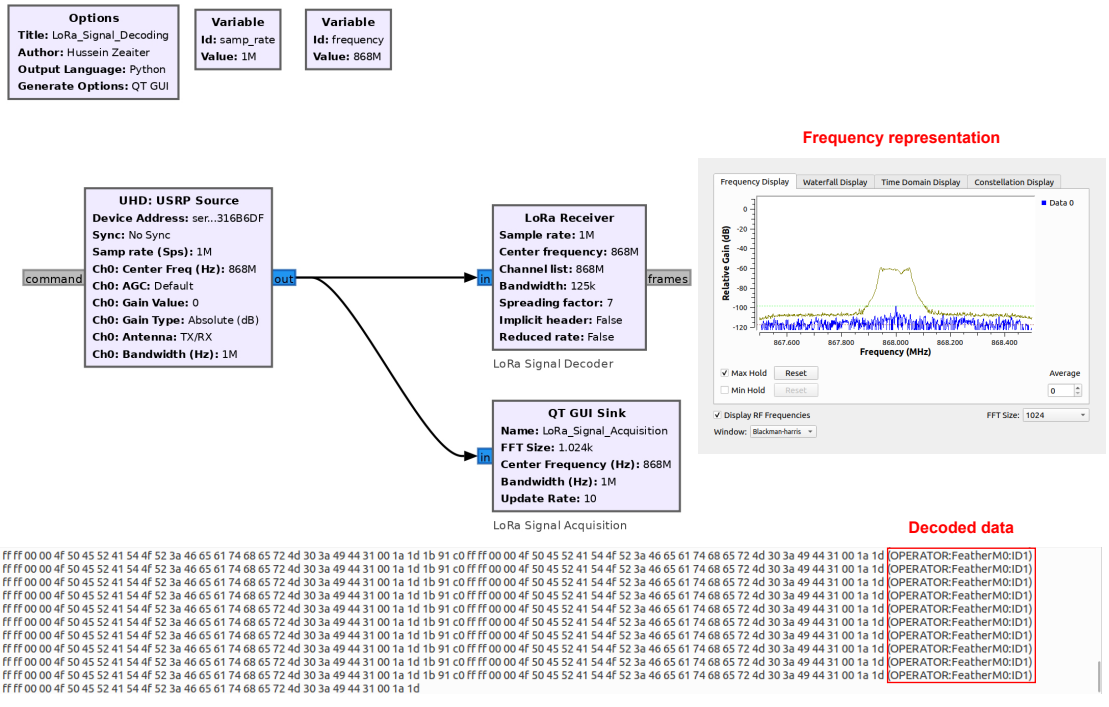

Figure 4.6: A GNU Radio flow graph of decoded LoRa signals.

In the above figure, the result of the executed flow graph is the frequency representation of the LoRa signal (top right) and the decoded data (bottom) in hexadecimal and the corresponding ascii format.

Having investigated, demodulated and decoded LoRa PHY signals in GNU Radio with SDR platform, we will proceed to implement an angle of arrival based localization system for LoRa signals. Our localization algorithm will use the *gr-lora* decoder as a signal decoder.

4.4/ An innovative AoA-based localization system for LoRa signals using SDR

4.4.1/ Related work

Localization based on Direction of Arrival (DoA) or Angle of Arrival (AoA) techniques have been used in a wide range of wireless sensors and communication applications. DoA refers to measuring the AoA where a signal was received. There have been several advances in AoA techniques in the literature. The most common AoA techniques include spectral techniques including the Capon Beam-forming technique [86], typical technique including Maximum Likelihood (ML) [87], and subspace decomposition techniques. Subspace decomposition approaches include the Multiple Signal Classification (MUSIC) technique [88], and the Estimation of Signal Parameters via Rotational Invariance Technique (ESPIRIT) [89]. In spite of this, these techniques have many drawbacks. While Beam-forming based technique offers a low computing complexity, it is susceptible to noise or interference in the received signal. In terms of noise robustness (better performance under low SNR), Maximum Likelihood based technique has better performance than other DoA techniques, but its computational complexity is higher. Finally, Subspace decomposition based techniques provide a compromise between computation time and complexity, and robustness to low SNR.

As SDR evolves in the field of radio direction finding engineering, new opportunities are provided to study existing algorithms and create new ones. Various SDR based direction finding systems are described and presented in the literature. In [90], the authors proposed a DoA estimator based on 4-element linear array consisting of 4 independent RF receivers that need to be phase-synchronized. In the DoA estimator, the AoA of the received signal was estimated using the MUSIC algorithm. Another direction finding approach was implemented in [91] using 4 USRP2 based SDR platforms. The 4 RF boards are synchronized using an external 10 MHz reference clock signal. The authors in [92] proposed a low budget SDR direction finding system based on the USRP N200 using a single two-channel SDR platform. According to the authors, the average absolute er-

ror between the real and the estimated AoA is 3 degrees for angles between [-30, +30] degrees.

Recently, a few AoA based localization solutions for LoRa technology have been introduced in the literature. An AoA localization technique for LoRa signals based on a SDR receiver has been proposed in [93]. Based on the proposed method, an estimation error of 2 degrees was found for LOS and 10 degrees for NLOS conditions. This method, however, used an 8-element uniform linear array (ULA). In order to achieve synchronization between the 8 ULA, a handcrafted crystal oscillator is required for 8 independent SDR receivers.

In order to solve the problem of synchronization requirements between RF channels of different SDR boards, some AoA solutions have been presented. An implementation of a time-modulated array (TMA) with only one hardware and two antennas was implemented in [57]. This system has the advantage over systems that depend on multiple receivers to localize. However, an hybrid RSSI and AoA signal's information must be implemented, which require more time and computational complexity.

In this thesis, we propose a novel direction finding approach based on phase interferometry [94]. The interferometry method involves computing the phase difference of the signal received by two antennas spaced at a known distance. The main purpose is to determine the target's direction based on the phase difference between the two antennas of the SDR receiver. By measuring the phase difference of the captured signal, the AoA can be calculated. The next section describes the theory behind AoA estimation base on phase difference measurements at two antennas.

4.4.2/ PHASE INTERFEROMETRY DIRECTION FINDING

4.4.2.1/ PHASE INTERFEROMETRY

The AoA based localization system can be implemented using a phase measurement system based on the interferometry principle as shown in Figure 4.7.

In Figure 4.7, two RF signals propagate from the transmitter to the two antennas. These RF signals can be assumed to be parallel if the distance between the transmitter and antennas is greater than the distance between the antennas. A phase difference between the received signal at two antennas can be described by the following equation:

$$\phi = 2\pi\left(\frac{d\cos\theta}{\lambda}\right) \tag{4.2}$$

where θ is the angle of arrival of the incident signal relative to the interferometry baseline, d is the distance separating the two antennas, and λ is the wavelength of the RF signal.

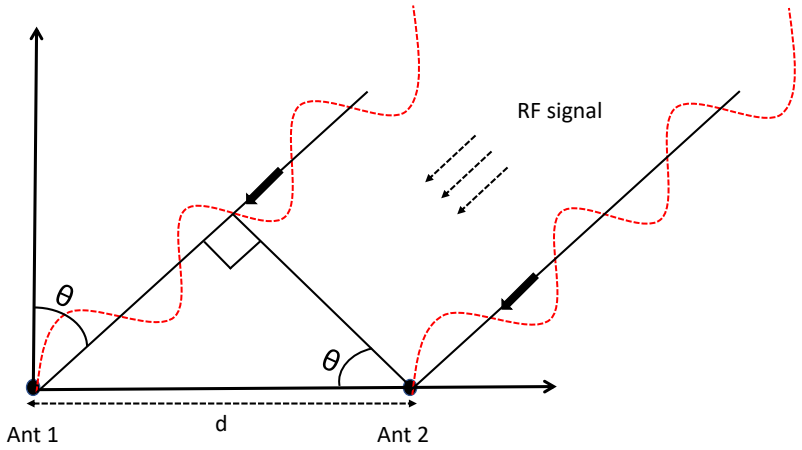

Figure 4.7: AoA measurement using two antennas element interferometry

Equation 4.2 only provides unambiguous values of ϕ when $d \leq \lambda / 2$. If $d > \lambda / 2$, ϕ can exceed the range of [-π,+π] which causes an ambiguity, in other words, we are not able to determine a unique and accurate value of θ which leads to multiple solutions of AoA.

A third antenna is typically added to the system to resolve the ambiguity. Our research work assumes that $d \leq \lambda / 2$, so that the ambiguity problem is not considered.

According to Equation 4.2, an angle of arrival can be calculated given a phase difference between the two antennas, and can be represented by the following equation:

$$\theta = \cos^{-1}\left(\frac{\lambda}{2\pi d}\phi\right) \tag{4.3}$$

At this point, the angle of arrival of an incident LoRa signal can be calculated using the phase interferometry measurement shown in Figure 4.7 and its corresponding formula calculation in Equation 4.3. It is possible to calculate the phase and corresponding AoA of the LoRa signal using only a single SDR receiver equipped with two antenna elements.

The next section will discuss how the Fourier transform algorithm can be used to extract the phase of a LoRa signal.

4.4.2.2/ FFT PHASE INTERFEROMETRY MEASUREMENT SYSTEM

The Fast Fourier Transform (FFT) is one of the most popular tools in Digital processing applications. As its name implies, the FFT is a fast version of the Discrete Fourier Transform (DFT). The FFT algorithm computes DFT much faster than any other available algorithm by performing a series of DFT computations. Due to this, the number of calculations will

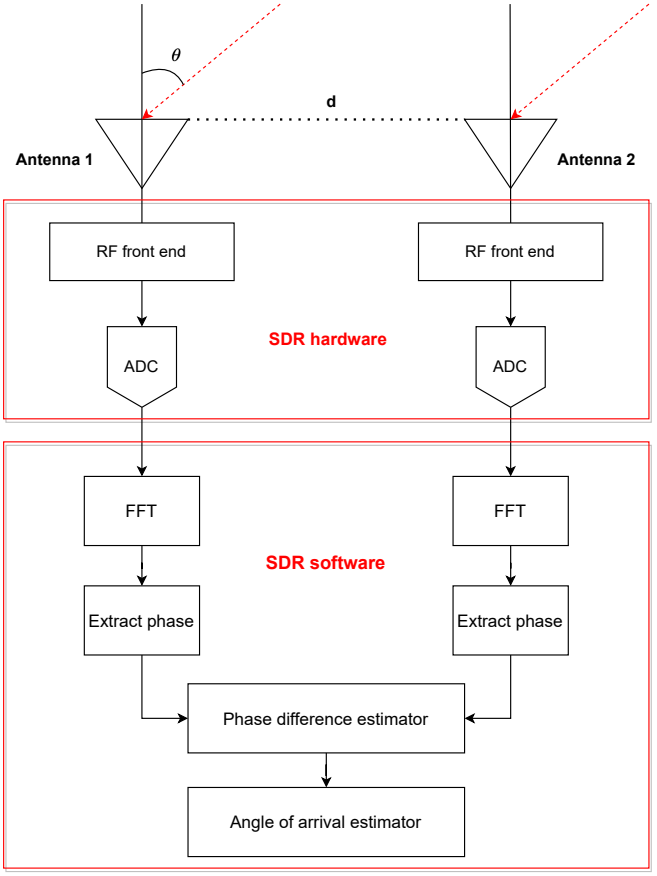

Figure 4.8: FFT Phase Interferometry measurement system.

be reduced by using FFT.

Given a discrete signal *x(n)* in the time domain, the DFT transform of *x(n)* is the following:

$$X_k = \sum_{n=0}^{N-1} x_n e^{\frac{-i2\pi kn}{N}} k = 0, 1, 2, .., N-1 \tag{4.4}$$

Equation 4.4 provides the DFT computation of *N*-point data sequence with $O(N^2)$ multiplies and adds. Thus, when applying FFT, the computation would take $O(NlogN)$ multiplies and adds.

A key function of the FFT is to transform a digital signal from the time domain to frequency domain. Since FFT can provide the phase and the frequency on a RF signal, an FFT phase interferometry direction finding system can be implemented. The system architecture of an FFT phase interferometry direction finding system is illustrated in Figure 4.8.

As shown in Figure 4.8, in the hardware part, the RF signal received by each antenna of the RF front-end is sampled, digitized by the ADC and sent to the software part where the FFT is computed. Each resolution element of the FFT consists of a real and an imaginary

part which we must scale and convert to polar form to obtain the phase information. The phase ϕ_n of each FFT output can be calculated by the following equation:

$$\phi_n = \tan^{-1}\left(\frac{Imag\_Output(FFT)}{Real\_Output(FFT)}\right) = \frac{I_n}{R_n} \tag{4.5}$$

where the $\tan^{-1}$ function return phase values between [-π, +π]. Equation 4.5 refers to the phase FFT output of each channel. After subtracting each FFT output's phase, the phase difference is calculated.

Given the phase difference between the two antennas, the AoA can be calculated for each frequency element of the FFT. The proposed measurement system can also measures the AoA of multiple signals if their frequencies do not intersect.

The FFT phase interferometry system can also identify interfering signals. If the received signal is accompanied by interfering signals around the frequency of interest, the FFT of each RF front-end output computes simultaneously the phase difference of each frequency cell.

4.4.2.3/ FFT Frequency and Phase of Interest

In the previous section, we presented how phase interferometry direction finding system could be implemented using FFT. The most critical step in this measurement is determining the FFT frequency of interest of our LoRa signal. In order to determine the phase and the AoA, the algorithm must be able to identify the exact frequency of interest in the FFT measurement.

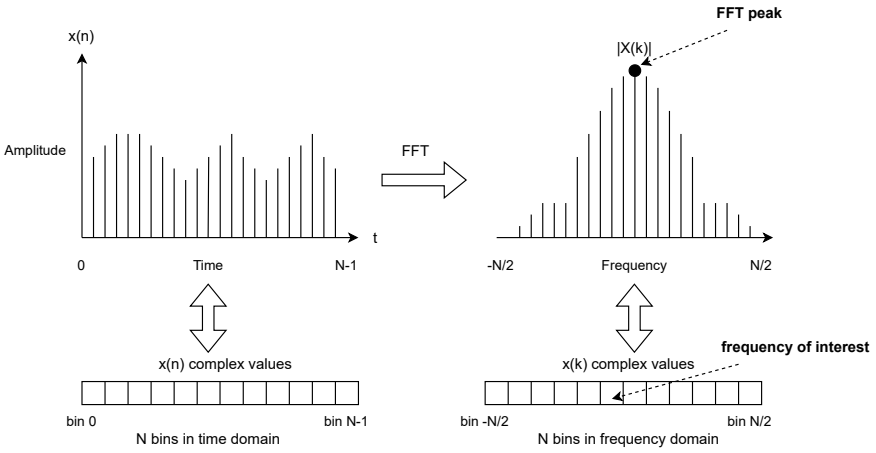

Figure 4.9: FFT representation showing bins frequency

Let *x(n)* be the discrete time domain signal computed in software as shown in Figure 4.9 with a variable amplitude and its FFT transform respectively. It should be noted that

Figure 4.9 has been provided for demonstration purpose.

In the frequency domain, each FFT bin represents the total energy that the signal has at that specific frequency. Thus, our frequency of interest lies in a part to be determined between these bins. The frequency of interest can be defined as the frequency at which the signal has the highest power which is the FFT peak.

Until this point, our goal is to extract the bin with our frequency of interest. When taking N-points FFT of the signal, the FFT transformation creates N frequency bins. Each bin represents of energy that the signal has at that specific frequency. The bin width defines the frequency resolution of the FFT and is the difference in frequency between each bin. The bin width can be calculated as the follow:

$$bin\_width = \frac{f_s}{FFT\_width} \tag{4.6}$$

where f_s is the sampling frequency (samples per second) and FFT_width is the size of the FFT transformation.

Given the *bin_width*, the bin of interest can be calculated as follow:

$$bin\_of\_interest = \frac{carrier\_frequency}{bin\_width} \tag{4.7}$$

Let a captured LoRa signal with a carrier frequency of 868 MHz, sampled at 2 MHz and with an FFT size equals to 2048 bins. The FFT transformation will have a bin width or frequency resolution if 0.847 MHZ or 847000 Hz. The bin of interest can be obtained by dividing the signal's carrier frequency by the bin width. Thus, the bin of interest of 868 MHz LoRa signal is equal to 1024. An ideal FFT would show a peak at 868 MHz as shown in Figure 4.10, and the energy will be split between bins 1023 and 1025 (867.1 MHz and 868.9 MHz).

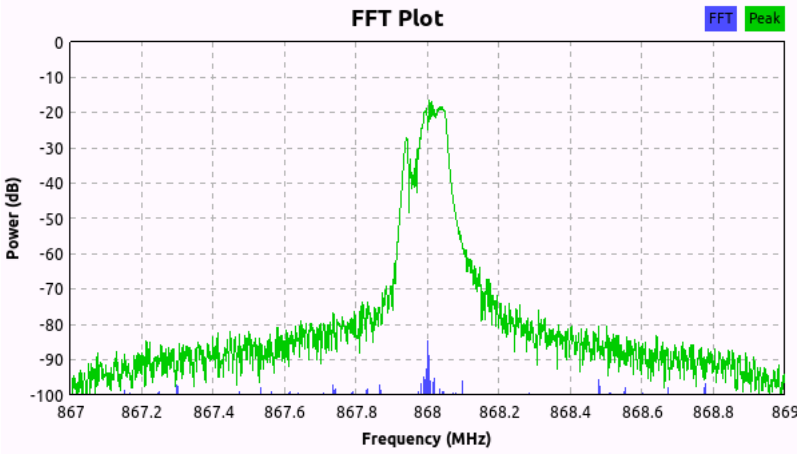

Figure 4.10: FFT plot of 868 MHz LoRa signal

Now, with the given bin of interest, the algorithm must be able to detect this bin, extract the desired phased, and measure the AoA of the incoming signal.

In the following section, we will discuss the signal detector and its role in our direction finding system.

4.4.2.4/ SIGNAL DETECTOR

The most important step in the direction finding system is the signal detection. Signal detector indicates if there is a signal present or not in the channel. The incoming data converted to the digital domain by the ADC are passed through a signal detector block. The signal detector block decides whether or not to forward the data for further phase and AoA processing as shown in Figure 4.11.

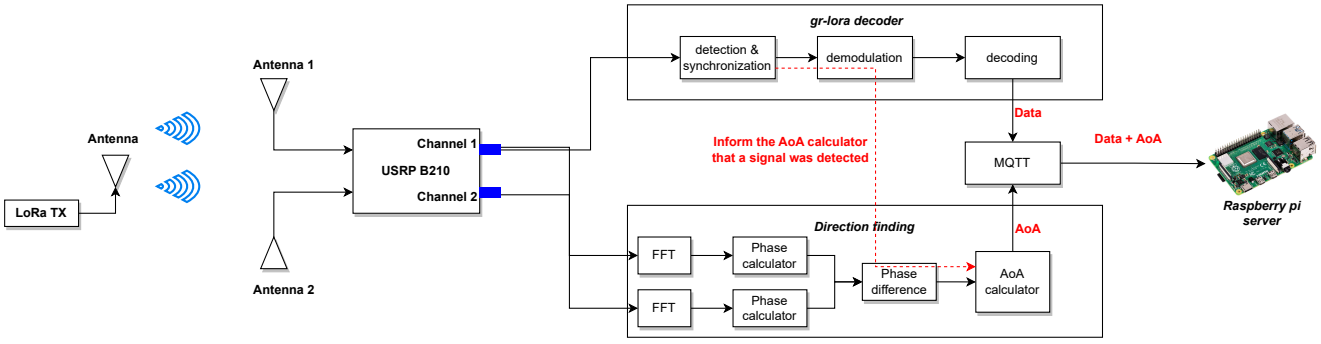

Figure 4.11: Blocks diagram of direction finding system.

Figure 4.11 illustrates our proposed system consisting of a USRP B210 receiver and a LoRa TX transmitter. The signal received at each antenna of the receiver in converted by the RF front-end from its carrier frequency to its baseband frequency. Then, ADC converts the signal to the modulation bandwidth. On the other hand, the processing of the converted signal can be done in the GNU radio.

The GNU Radio part is divided into two paths. the first path consists of the *gr-lora* decoder which is responsible for the detection, synchronization, demodulation and decoding. To decode a LoRa frame, the decoder must know the beginning of the frame. Each LoRa frame is composed of a preamble of a few symbols (mainly 8 up-chirps). Once the preamble is detected, the first path of the direction finding system informs the second path that a LoRa signal has been detected. Therefore, the second path will calculate the phase difference and the AoA of the detected signal. To solve the problem related to the exchange of information between the two paths, a publish/subscribe method was implemented. The communication between the two paths is based on the *Message Passing* protocol which we will be described in the next section.

4.4.2.5/ MESSAGE PASSING PROTOCOL

To enable the communication between the Signal detector and the AoA calculator, a communication protocol has been used.

Typically, the data transfer between signal processing blocks in GNU Radio is based on a data streaming mechanism. The samples captured by the SDR hardware are converted by the ADC to digital data which is a number of bits. Data streaming mechanism can handle to receive and send bits between blocks. However, it can not handle metadata, messages, and packet structures.

Message Passing interface is the solution that can handle these cases. *Message Passing* interface is based on Polymorphic Types (PMTs) in GNU Radio which allows the carrier data transfer between blocks or threads in GNU Radio [95]. The fundamental concept on which *Message Passing* interface is implemented is that of an event or action. Each GNU Radio block has its own messages queues to receive incoming messages and send messages to the message queues of other blocks.

As shown in Figure4.12, the signal detector block has to declare its output message port. The output port is identified by a specific name. Once the LoRa signal is detected, the signal detector block publishes a message on this particular port. The AoA calculator block must subscribe to this port in order to receive the event and calculate the AoA of the detected signal.

The first path and the second path publish the decoded data and the AoA to the MQTT block, respectively. In the following section the MQTT protocol will be discussed in details.

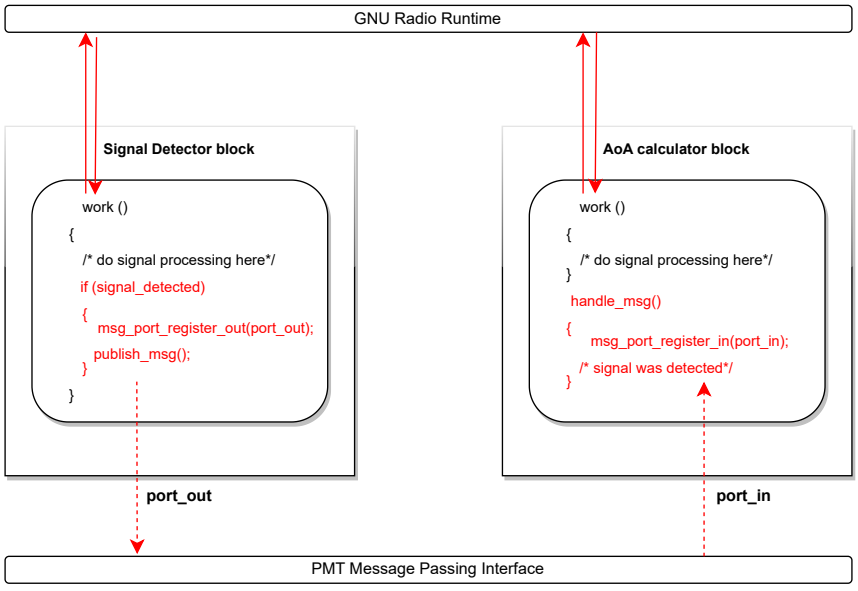

Figure 4.12: Blocks diagram of Message Passing Interface.

4.4.2.6/ MQTT PROTOCOL

Message Queuing Telemetry Transport (MQTT) is a publish/subscribe messaging protocol used by IoT devices to transport messages in a very simple way. It was originally designed for devices with low-bandwidth, low power consumption, and low-latency requirements. This protocol is based on the TCP/IP communication protocol and can work with Web Socket. The following are some of the reasons why MQTT is widely used in IoT applications:

- Reduces power consumption and network bandwidth due to its lightweight structure (low header size and low packet size).
- High update rates per second are achieved due to its low latency.
- It is less complex and saves more development time because it requires less development code.
- Provides an authentication protocol that uses usernames and passwords to secure communication.

The MQTT protocol is based on a Client-Broker or server model. The MQTT client can be a portable computer, server, smartphone, microprocessor, or microcontroller that runs the MQTT library and can send and receive data from the MQTT broker. We call the client a publisher when it sends data to the broker, and a subscriber when it receives data from the broker.

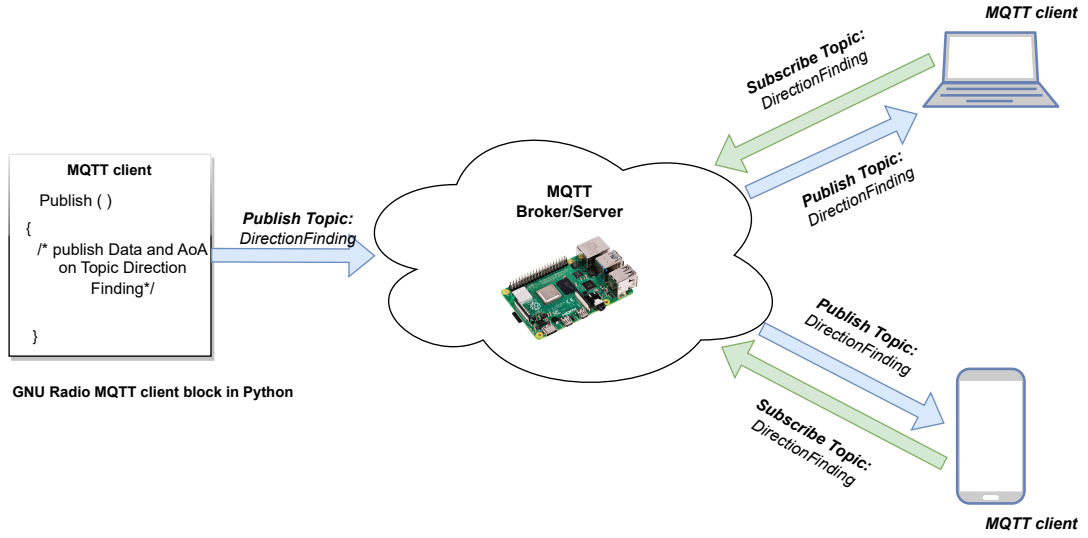

Figure 4.13: MQTT client in GNU Radio.

As shown in Figure 4.13, MQTT client was developed in GNU Radio with the help of python language. The client block publishes the data and AoA on a particular topic which

is the "*DirectionFinding*" to the broker which is installed and configured on a Raspberry Pi microprocessor. Once the broker has received the messages, it forwards them to subscribing clients. Subscribing clients must subscribe to the "*DirectionFinding*" topic. It should be noted that the MQTT is based on TCP/IP communication protocol. Thus, TCP/IP stack must be configured on subscribing clients.

The following section provides the complete implementation of the direction finding system in GNU Radio.

4.4.3/ Direction Finding System implementation in GNU Radio

The GNU Radio flow graph as shown in Figure 4.14 illustrates the Direction Finding system of our LoRa signal.

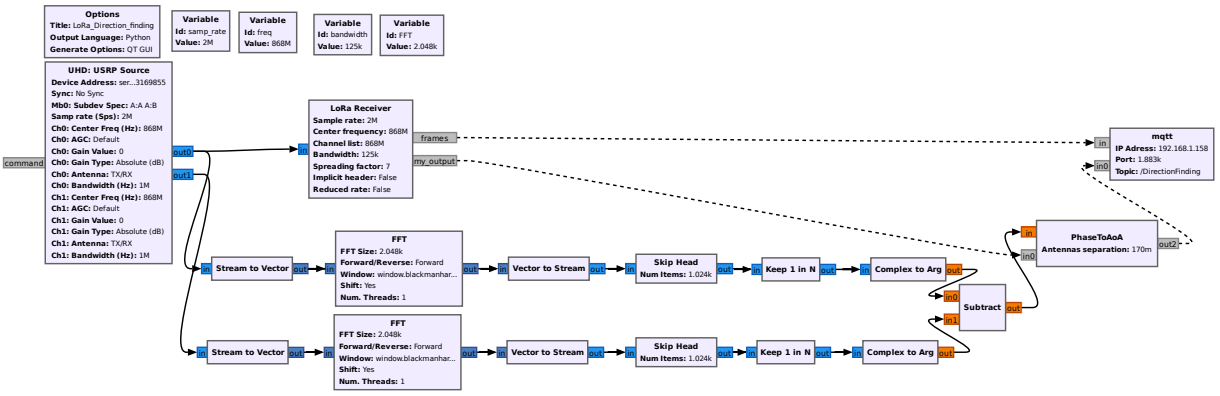

Figure 4.14: Direction Finding - GNU Radio Flowgraph.

The flow graph starts with the *UHD:USRP Source* block which is responsible for receiving the stream of data captured by the USRP SDR receiver. The stream of data are sent to the *Stream to Vector* block which converts the stream of data to vector (real and imaginary) format. The size of *Stream to Vector* is set to 2048 which is also the size of the FFT. Once the data are in vector format, the *FFT* block performs the Fast Fourier Transform and converts the data from the time domain to the frequency domain for further processing. The *Vector to Stream* block brings back the output of the *FFT* block to the stream format. The stream of data are now in the frequency domain. In order to determine the phase and the AoA, the algorithm must first determine the frequency of interest (bin of interest) of the LoRa signal.

As previously discussed in section (4.4.2.3), the bin of interest of a 868 MHz LoRa signal is equal to 1024. Now, with the given bin of interest, the algorithm can skip to that bin.

This is done by the *Skip Head* and *Keep 1 in N* block. Up until this point, the output of all the blocks are in complex format, which is good since we can use this to compute the phase. The *Complex to Arg* block takes the complex number as its input and gives the arg value in float format as its output. The *arg* value represents the angle between the real and the imaginary component of the FFT which is equal to the phase of the signal.

The flow graph in Figure 4.14 shows that there are two paths, one for each antenna. The extracted phase difference is obtained by subtracting the phase values from each other. The *PhaseToAoA* block takes the phase difference as its input and calculate the corresponding AoA. Finally, the *mqtt* block publishes the decoded data and the AoA to the server. The end user can visualize the data and the AoA in real time.

4.5/ EXPERIMENTAL AND RESULTS IN INDOOR ENVIRONMENT

In order to evaluate our direction finding system approach, a field of experiments was conducted in a $8m \times 8m$ ground floor laboratory environment. In this experiment, we first introduce the materials used, and we will then discuss the experimentation and the results.

4.5.1/ EXPERIMENTAL SETUP

The experimentation was performed utilizing the USRP B210 as the SDR receiver, and the RFM95 LoRa transceiver as the transmitter. The RFM95 LoRa transceiver is equipped with a USB port and USB-to-Serial communication, so it can be programmed using the microcontroller development software Arduino IDE. The RFM95 LoRa module was configured using the RadioHead library.

The transmitter was configured to send a LoRa signal with the following parameters:

- Carrier frequency: 868 MHz.
- Spreading factor: 7.
- Channel bandwidth: 125 kHz.
- Coding rate: 4/5.

The devices were mounted on the tripod, and at a height of approximately 1 meter in order to have an Fresnel Ellipsoid without any obstacle. The complete installation is shown in Figure 4.15.

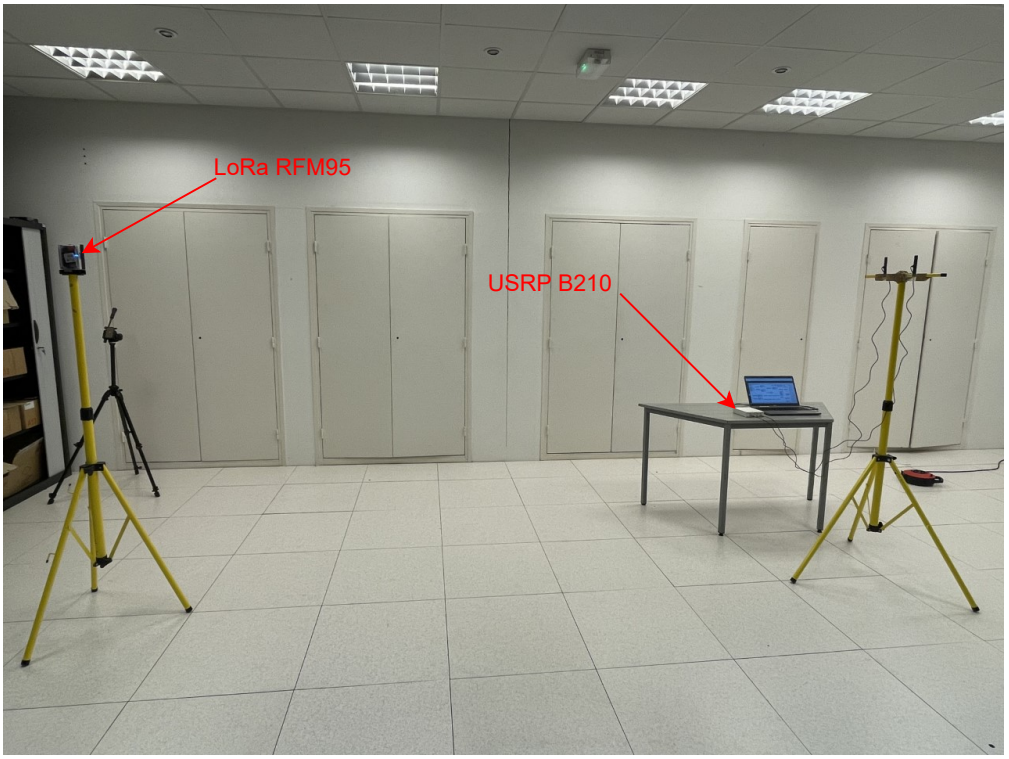

Figure 4.15: Experimental setup - two antennas direction finding system using USRP B210 and LoRa RFM95 transceiver.

4.5.2/ Measurement Data

Our experiments were conducted into two parts: the first one to identify the spacing *d* between the antenna elements of the SDR receiver. The second to measure the AoA estimation errors for AoAs in the [0,180] degrees interval.

4.5.2.1/ Antenna spacing

In the first experiment, we measured 300 AoA points with antenna spacing equals to $\lambda/4$ and $\lambda/2$ respectively as illustrated in Figure 4.16. The AoA values for each antenna spacing were measured from three different positions (45 degrees, 90 degrees and 135 degrees).

Figure 4.17 and Figure 4.18 show the measured phase difference in radians for antenna spacing equals to $\lambda/4$ and $\lambda/2$ respectively. In Figure 4.17, we can clearly observe the measured phase difference for each LoRa transmitter position. Also we can notice the presence of ambiguous phase difference values. The ambiguous values correspond to measured phase difference that exceed the interval $[-\pi,+\pi]$.

Figure 4.18 shows more ambiguous phase difference values when the antenna spacing is equal to $\lambda/2$. This is the reason why that increasing the baseline length (antenna spacing

of the receiver) can increase the ambiguity in phase difference measurements.

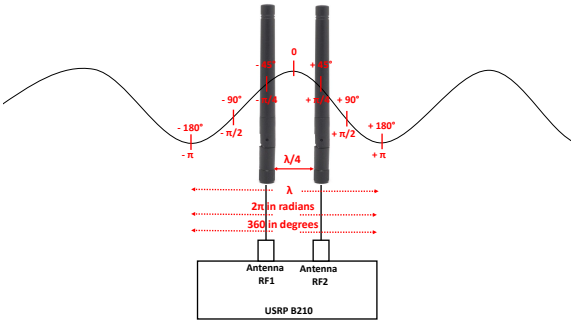

(a) Antenna spacing $\lambda/4$

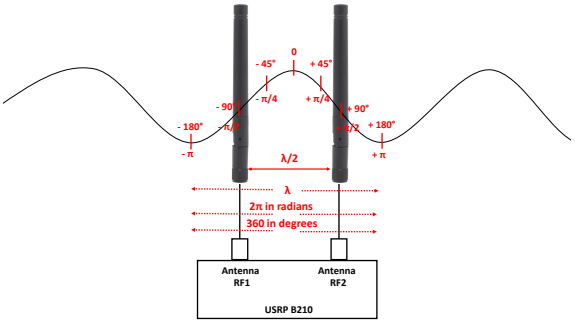

(b) Antenna spacing $\lambda/2$

Figure 4.16: Antenna spacing of the USRP B210

AoA measurements for each antenna spacing can be obtained by applying Equation (4.3) in Section (4.4.2.1). The measurement results are illustrated in Figure 4.19 and 4.20 respectively.

The results show that the AoA accuracy is better when the antenna spacing is equal to $\lambda/2$ than $\lambda/4$. However, we obtained more ambiguous values with $\lambda/2$ than $\lambda/4$. From these results, we can learn that the AoA accuracy is mostly proportional to the antenna spacing, hence a long antenna spacing improves the AoA accuracy. Even though that increasing the antenna spacing can lead to phase difference and AoA ambiguity.

In the section (4.4.2.1), we demonstrated that when the antenna spacing is less or equal to $\lambda/2$ ($d <= \lambda/2$), the phase difference and the AoA ambiguity will be ignored in the range of [$-\pi$,$+\pi$]. However, our results show that the ambiguity problem still exists for both antenna spacing. To resolve this problem, we suppose that the reason of the ambiguity is the following:

- **Hypothesis 1:** The ambiguous AoA values result from the incorrect estimation of the phase difference between direct and reflected LoRa signals (echos) by walls and materials. It follows that the phase difference between the two signals will exceed

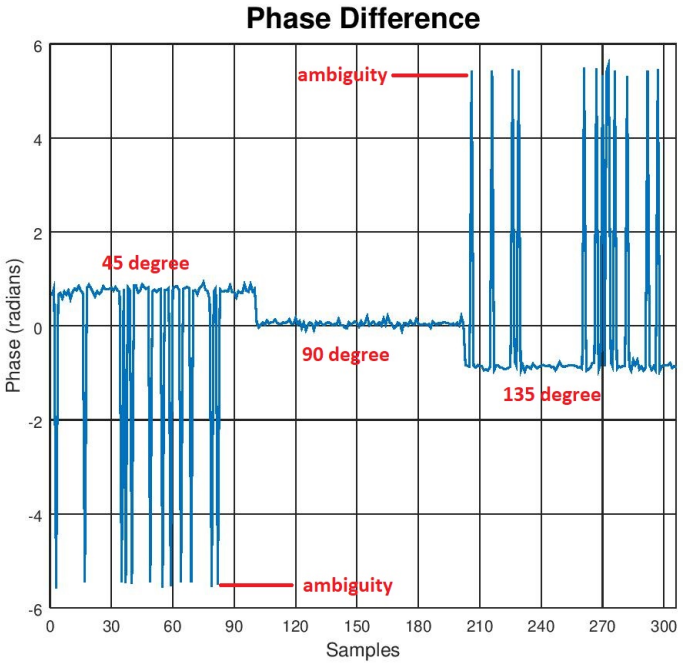

Figure 4.17: Phase difference measured for three positions (45, 90, and 135 degrees) for antennas spacing equals to $\lambda/4$.

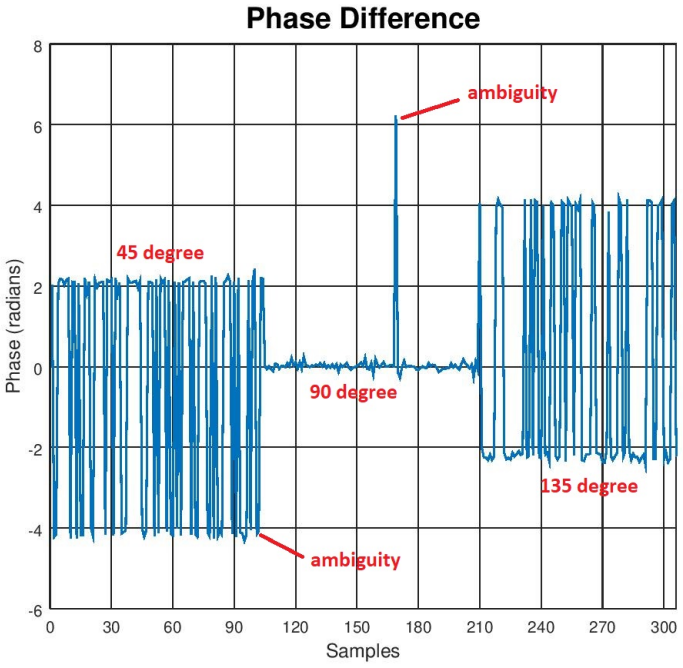

Figure 4.18: Phase difference measured for three positions (45, 90, and 135 degrees) for antennas spacing equals to $\lambda/2$.

the range [-π,+π].

- **Hypothesis 2:** The ambiguous AoA values result from the incorrect estimation of

the frequency and the phase of interest of the Lora signal.

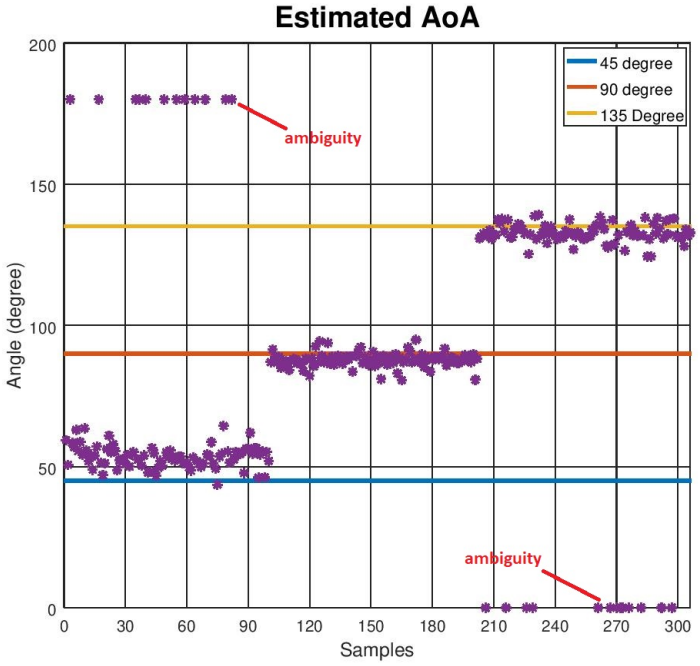

Figure 4.19: AoA measured for three positions (45, 90, and 135 degrees) for antennas spacing equals to $\lambda/4$.

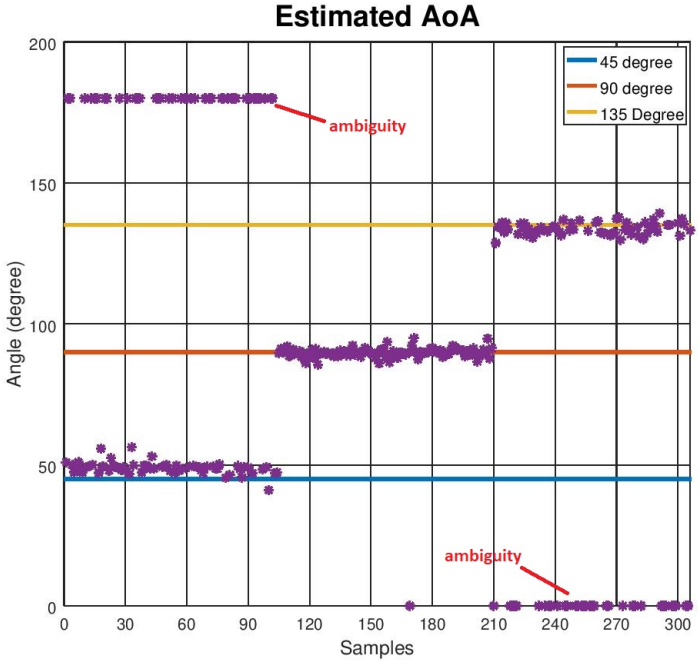

Figure 4.20: AoA measured for three positions (45, 90, and 135 degrees) for antennas spacing equals to $\lambda/2$.

In order to resolve this problem, we started with hypothesis 1, and then conducted a field

experiment in an anechoic chamber. The next section describes our anechoic chamber experiments.

4.6/ EXPERIMENTAL AND RESULTS IN ANECHOIC CHAMBER

In order to confirm our first hypothesis, we conducted experiments in the anechoic chamber at the University of Toulouse, IUT of Blagnac. An anechoic chamber is a non-reflective or non-echoing closed room designed to absorb and suppress reflections of signals. It will ensure that our experiments are isolated from the outside environment.

4.6.1/ EXPERIMENTAL SETUP

The line of sight experiment was conducted in the IRIT Laboratory at the University of Toulouse, IUT of Blagnac. The test was conducted in the anechoic chamber with a RFM95 LoRa transceiver and the USRP B210 SDR receiver. The LoRa transceiver was configured to send a LoRa signal with the following parameters: carrier Frequency (868 MHz), spreading Factor (7), Channel bandwidth (125 kHz), and coding rate (4/5).

The LoRa device was mounted on a tripod and the two antenna array system was fixed on a rotating table piloted with the MQTT explorer application. A complete installation is shown in Figure 4.21.

4.6.2/ MEASUREMENT DATA

From our previous experiments in the laboratory indoor environment, antenna spacing d was chosen as $\lambda/2$.

Our first hypothesis was validated by measuring 100 AoA points in the range of [15,90] degrees with 15 increments between each measurement in both indoor laboratory and anechoic chamber, and then calculating the ambiguity rate. The ambiguity rate is calculated by computing the ratio between the number of ambiguous measurement values and the total number of measured AoA (100 AoA points). The result of this measurement is illustrated in Figure 4.22.

Based on the results obtained, the ambiguity rate tends to be minimal for AoA equals to 90 degrees and starts to increase for angles less than 90 degrees in both environments. However, the anechoic chamber has a lower ambiguity rate than the laboratory room. It is possible to explain the decrease in ambiguity rate by the nature of the anechoic chamber, which blocks reflections that could cause errors in calculating the phase difference and the angle of arrival.

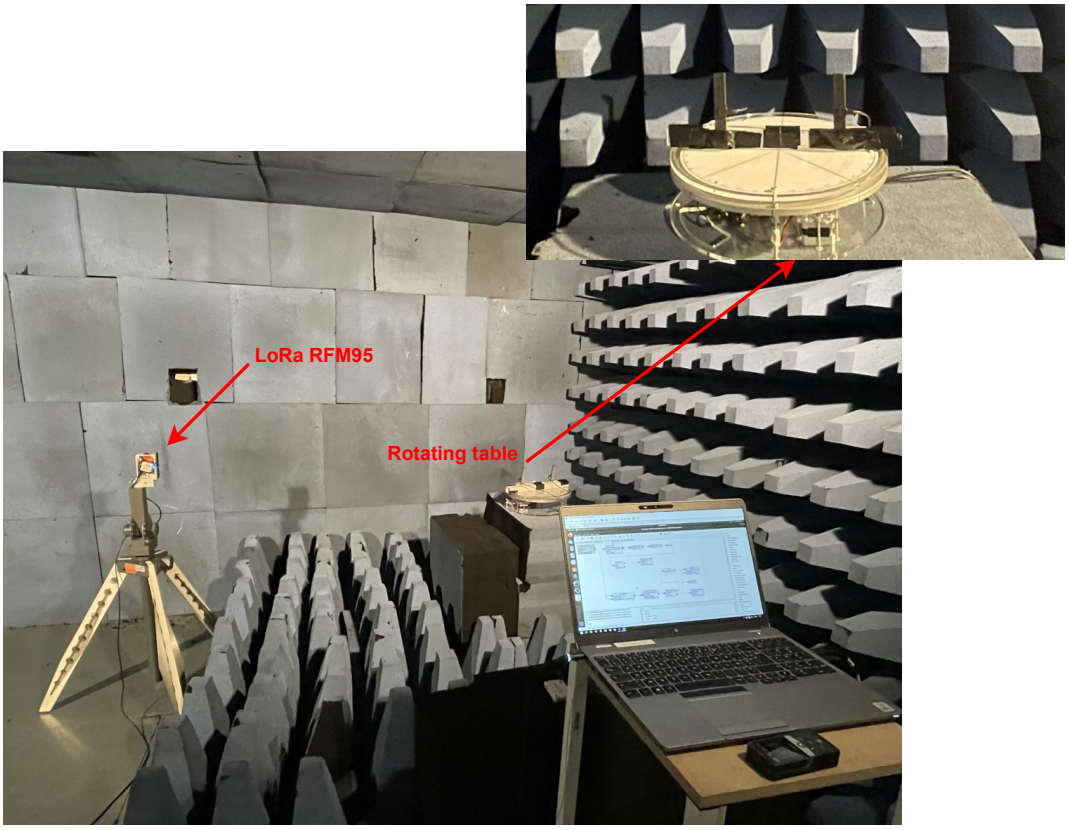

Figure 4.21: Experimental setup - two antennas direction finding system using USRP B210 and LoRa RFM95 in anechoic chamber.

From these results, we can concluded that one advantage of using anechoic chamber for measuring phase differences and AoA is that it minimizes the effects of reflections and reverberations, which can distort the signal wave and cause errors in phase measurements.

From these measurements, it is worth noting that although an anechoic chamber can minimize the effects of reflections, there are still some ambiguous phase difference and AoA values that affect the accuracy of our algorithm. Consequently, we will proceed with the second hypothesis.

In the next section, an ambiguity removal and accurate AoA estimation for LoRa signals will be discussed.

4.7/ AMBIGUITY REMOVAL AND ACCURATE AOA ESTIMATION FOR LORA SIGNALS

In this section a method for resolving ambiguity in the phase difference and AoA measurements for LoRa signal is introduced.

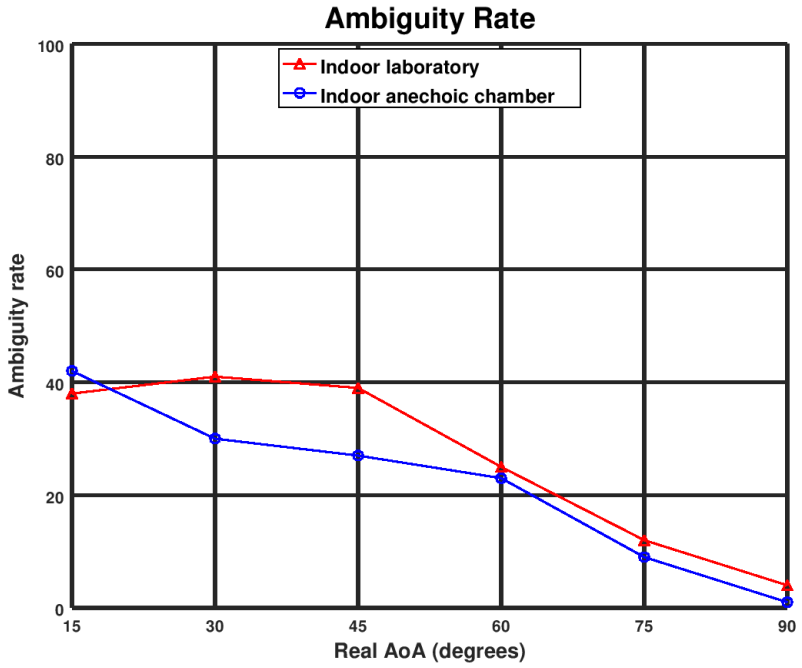

Figure 4.22: Ambiguity rate for 100 measured AoA points in indoor laboratory and anechoic chamber.

4.7.1/ INTERFEROMETRIC AMBIGUITY RESOLVING

Interferometric ambiguity is a common issue in interferometry direction finding system. It arises when the phase difference between two signals received by two antennas is greater than one cyle (phase difference exceeds the range of [-π,+π], leading to ambiguity in determining the exact phase difference and the direction of arrival (AoA).

One approach to solve the interferometric ambiguity is to use a third antenna. With three antennas, it is possible to solve the ambiguity by measuring the phase differences between all three antennas. This is knwon as *trilateration* and can be used to determine the position of a target.

Another approach to solve the interferometric ambiguity in two-antenna interferometry is to use an approach called phase unwrapping. Phase unwrapping is the process of removing the integer multiples of 2π from the measured phase values to obtain the exact continuous phase.

To perform phase unwrapping, it is necessary to have some prior knowledge of the instantaneous phase values. Hence, prior knowledge of LoRa instantaneous phase is required.

4.7.1.1/ LoRa INSTANTANEOUS FREQUENCY AND PHASE

The phase of a signal is commonly represented as a value between $-\pi$ and $+\pi$ radians or between -180 and +180 degrees. This is known as the *unwrapped* phase. However, in certain situations, the phase of a signal can *wrap* around at these limits and jump from $-\pi$ to $+\pi$ radians or from -180 to +180 degrees.

One common situation where phase wrapping can occur is in systems that use frequency modulation (FM) to encode information onto a carrier signal. In these systems, the phase of the signal is directly related to the frequency of the modulating signal. If the modulating signal changes rapidly, the phase of the carrier signal can wrap around.

In LoRa communication, the instantaneous frequency refers to the frequency of the signal at any given point in time. In opposite to radio signals which have a constant frequency, LoRa signals use the chirp spread spectrum modulation which changes the frequency of the signal over the time.

The LoRa signal's frequency changes in a predictable pattern, following a chirp waveform. The frequency of the signal starts at a low frequency and gradually increases to a high frequency or vice versa, depending on the direction of the chirp.

The instantaneous frequency of a chirp signal is given by:

$$f(t) = Kt + f_0 \tag{4.8}$$

Where, *f(t)* is the instantaneous frequency in Hertz of the chirp at time *t*, f_0 is the starting frequency of the chirp signal, and *K* is the chirp rate, which determines the speed of the signal respecting to time. Thus, the rate of a chirp signal can be represented as follow:

$$K = \frac{f_1 - f_0}{T} \tag{4.9}$$

Where, f_0 is the starting frequency, f_1 is the ending frequency, and *T* is duration time.

Given the instantaneous frequency, the instantaneous phase of the chirp is given by:

$$\phi(t) = 2\pi f_0 t + \pi k t^2 \tag{4.10}$$

Where, $\phi(t)$ is the instantaneous phase signal at the time *t*, $2\pi f_0 t$ represents the initial phase of the chirp, and $\pi k t^2$ represents the additional phase as the frequency of the chirp changes linearly in time.

Figure 4.23, shows the time-varying frequency and phase for a LoRa-like symbol with a bandwidth of 125 kHz . From the observation, the chirp is starting at a frequency of 0

kHz and is ending at a frequency of 62.5 kHz, with a discontinuity in frequency from 62.5 kHz to -62.5 kHz following.

Translating the instantaneous frequency into instantaneous phase, we clearly notice that the phase is wrapped at ϕ_1 (phase discontinuity between $\phi_1 = +\pi$ and $\phi_2 = -\pi$, $\delta(\phi) = \phi_2 - \phi_1 = 2\pi > \pi$).

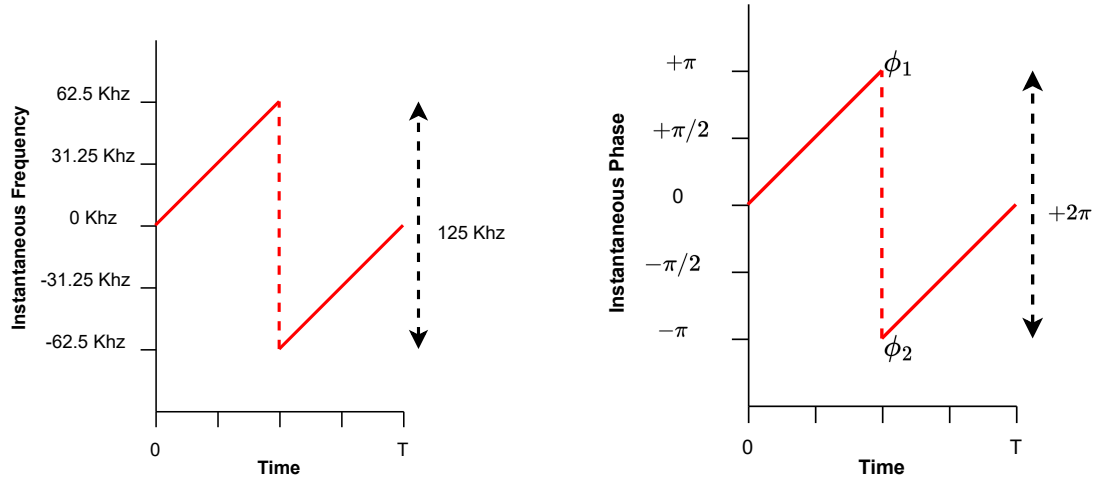

(a) Instantaneous frequency of a LoRa-like symbol

(b) Instantaneous phase of a LoRa-like symbol

Figure 4.23: An example of LoRa instantaneous frequency and phase

To ensure that the chirp phase is continuous in time, we implement a phase unwrapping process. Phase unwrapping is the process of removing the phase discontinuity between successive phase measurements. This is done by subtracting or adding 2π recursively from non-continuous samples until the result obtained $\delta(\phi) < \pi$.

4.7.2/ Experiments and Results

In order to validate our phase unwrapping process, we conducted three experiments.

During the first experiment, we measured the phase difference of the received signal of the LoRa transmitter with an angle of 15 degrees to 90 degrees, with 15 degrees increments between each measurement. This measurement was conducted in both wrapped phase and unwrapped phase process. The result of this measurement is illustrated in Figure 4.24.

Figure 4.24 (a) shows the expected phase difference when unwrapped phase processing is not applied. It can be clearly observed that phase difference ambiguities exist due to the phase difference exceeding the interval [$+\pi$, $-\pi$) (phase wrapped over $-\pi$). Furthermore, We can notice an increase in wrapping when the angle is decreased from 90 degrees to 15 degrees.

Figure 4.24 (b) shows that we are able to reliably eliminate wrapped phase difference values using our unwrapped phase process. The algorithm we developed can extract a phase difference purely though ambiguity removal at a high rate and with a high phase difference accuracy.

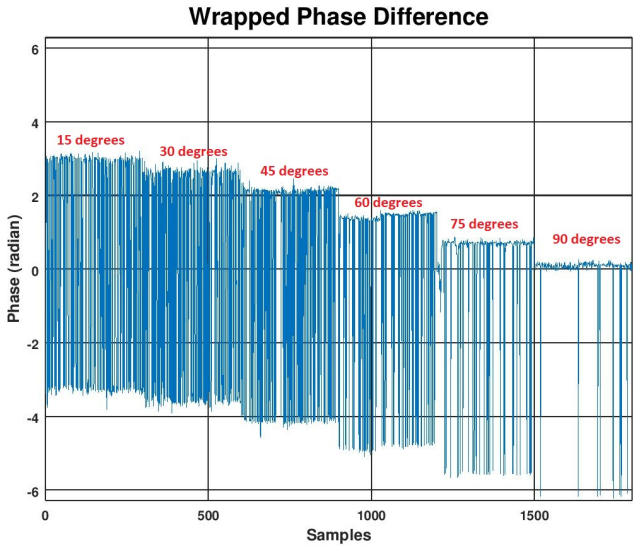

(a) Wrapped phase difference

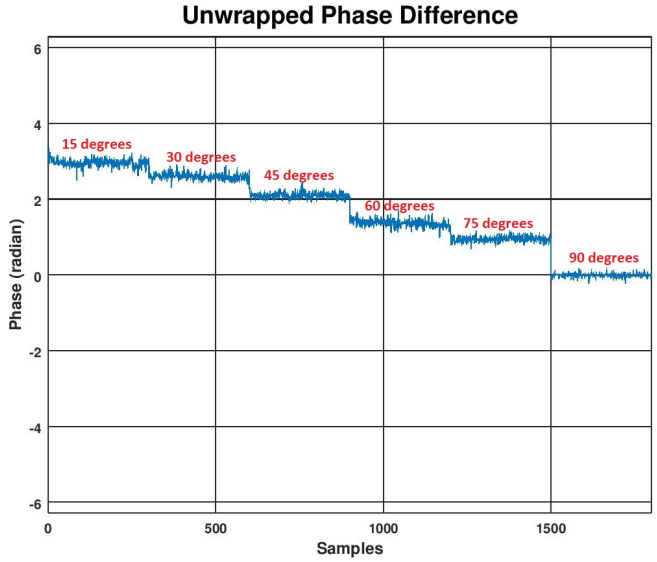

(b) Unwrapped phase difference

Figure 4.24: A phase difference of a LoRa signal

During the second experiment, we determined the accuracy of our phase unwrapped process and hence the AoA. We calculated the deviation error of the AoA from angles in the range of [5, 175] degrees. The deviation error of the estimated angle versus the real angle is shown in Figure 4.25. AoA can be successfully estimated in the range of [5, 175] degrees. There is a maximum error of 5 degrees at 5 degrees and 175 degrees, while a minimum error is close to zero at 90 degrees.

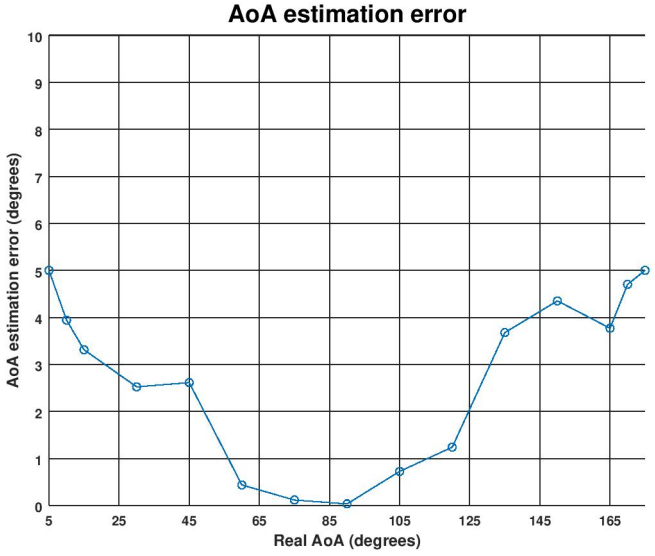

Figure 4.25: AoA estimation error versus real AoA.

In the third experiment, we evaluated the performance of our phase unwrapped direction finding system. Our transmitter was programmed to transmit a LoRa signal with different SFs (7 to 12) and BWs (125, 250, and 500 kHz). For each BW, AoAs were measured with SFs ranging from 7 to 12. In Figure 4.26, 4.27 and 4.28, angle deviation error is shown for three different BWs and for all SFs.

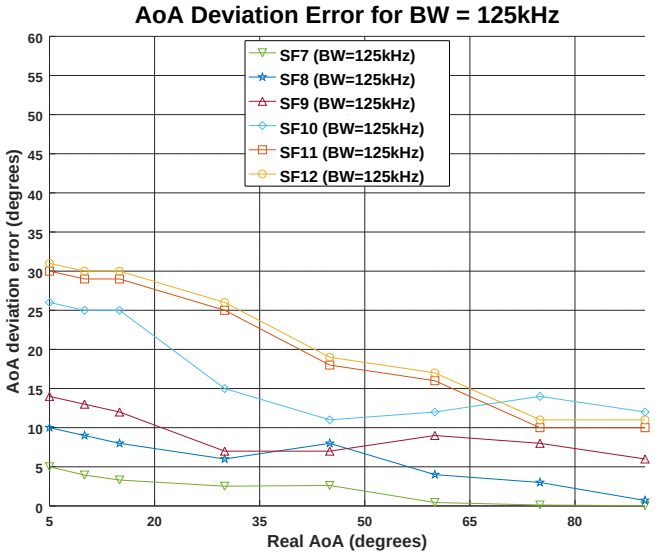

Figure 4.26: AoA estimation error for BW = 125 kHz .

From Figure 4.26, We can distinguish that using a BW equal to 125 kHz, the algorithm gives the best performance for SF equals to 7, 8, and 9, respectively, and can accurately measures the AoA with an estimation error less than 5 degrees for SF equals to 7. However, the angular deviation error increases exponentially as SF increases from 9 to

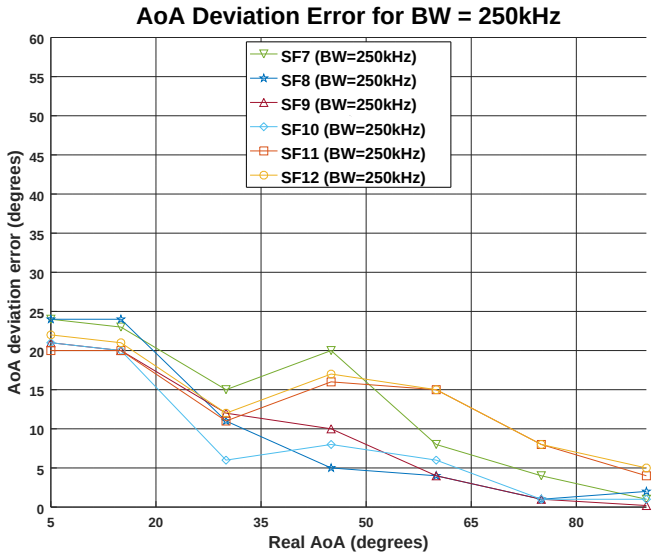

Figure 4.27: AoA estimation error for BW = 250 kHz .

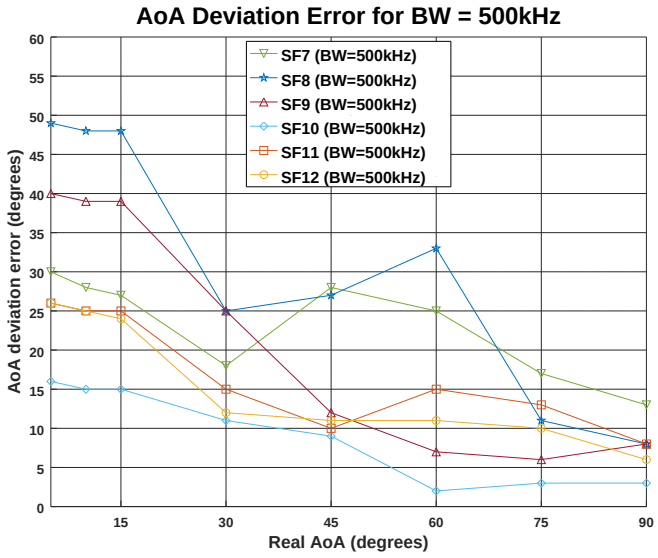

Figure 4.28: AoA estimation error for BW = 500 kHz .

12.

Figure 4.27 shows that, when the BW is equals 250 KHz, the deviation error increases for lower SFs and decreases for higher SFs. However, in this configuration, it is difficult to find a spreading factor that gives the best performance.

Finally, for a BW equals to 500 kHz, the algorithm provides better performance for the highest SFs (10, 11 and 12) and a poor performance for the smallest SF (7 and 8).

From these results, we can conclude that the AoA accuracy is higher when a small SF is combined with a small BW, or when a high SF is combined with a large BW. Moreover, we

recommend using a LoRa configuration with a SF of 7 and a BW of 125 kHz for optimal performance. With this configuration, we can achieve an accuracy of less than 5 degrees.

4.8/ EXPERIMENTAL AND RESULTS IN REVERBERATION CHAMBER

In order to evaluate the performance of our indoor tracking signal system, we conducted another experiment in a reverberation chamber. The use of a reverberation chamber was essential to test the robustness of our approach under hard indoor conditions where signal reflections and multipath propagation can greatly affect the accuracy of the AoA measurements. The reverberation chamber represents a confined environment with high levels of signal reflections, allowing us to evaluate the performance of our method in a challenging scenario.

4.8.1/ EXPERIMENTAL SETUP

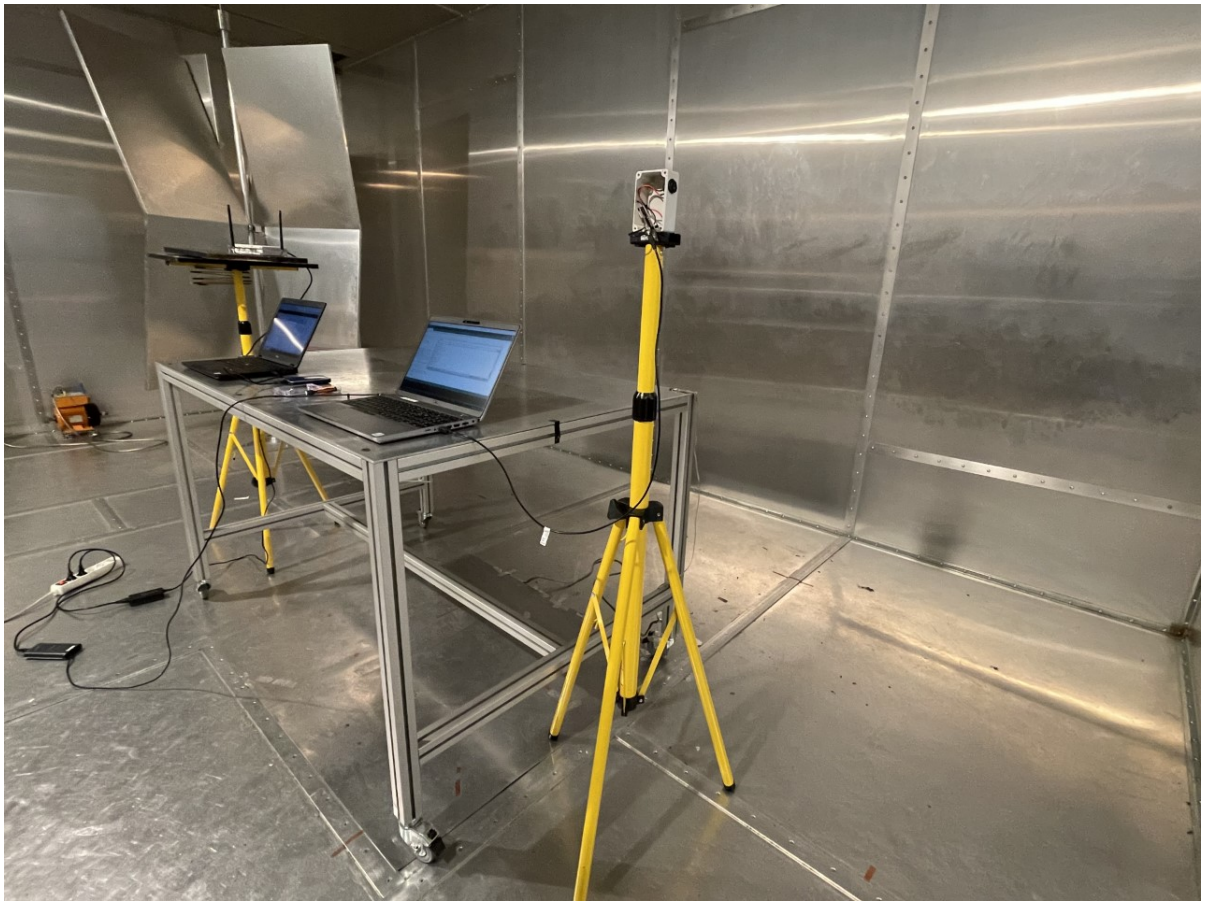

Figure 4.29: Experimental setup - two antennas direction finding system using USRP B210 and LoRa RFM95 in reverberation chamber.

The experiment was conducted in the Université de Technologie de Belfort Montbéliard (UTBM), in the city of Belfort. The test was conducted in the reverberation chamber with a RFM95 LoRa transceiver and the USRP B210 dual antenna receiver. According to the results obtained in the previous section, the transceiver was configured to send signal with the best configuration: Frequency = 868 MHz, SF = 7, BW = 125 kHz, and CR = 4/5.

The complete installation setup is illustrated in Figure 4.29.

4.8.2/ MEASUREMENT DATA

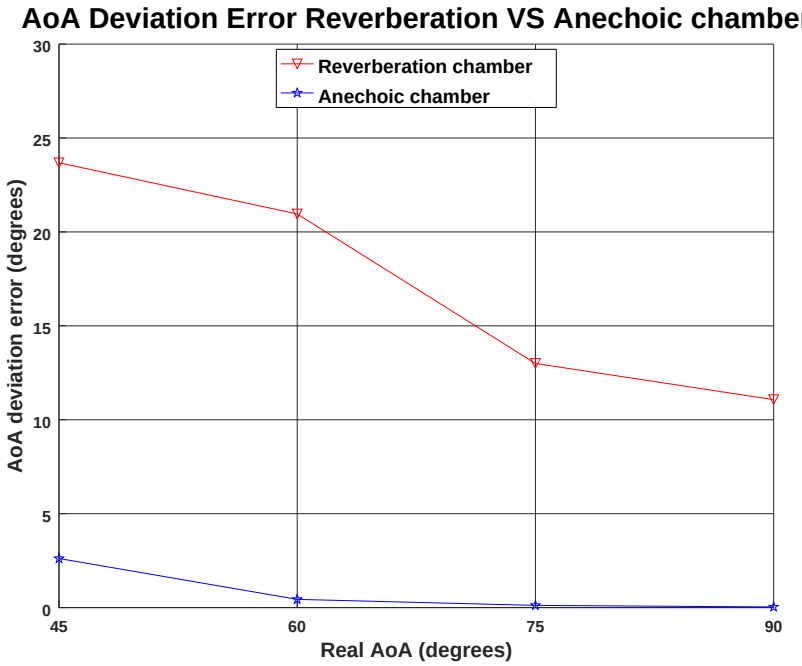

Figure 4.30: AoA deviation error in Reverberation VS Anechoic chamber.

The measurement data was obtained by measuring the AoA of a LoRa signal in the range of 45 to 90 degrees, and the corresponding deviation error was also recorded. The comparison was then made between the results obtained in an anechoic chamber and a reverberation chamber as shown in Figure 4.30.

In the anechoic chamber, there is no reflection of the signal, which means that the signal arrives at the dual antenna receiver without any reflection of multipath. As a result, the deviation error in an anechoic chamber will be very low (below 3 degrees for a true angle equals to 45 degrees). In opposite, in the reverberation chamber, there are multiple reflections of the signal, which make it difficult to accurately estimate the AoA, and also can lead to a higher deviation error (24 degrees for a true angle equals to 45 degrees) compared to the anechoic chamber.

Overall, it is important to highlight that the reverberation chamber represents a very chal-

lenging and hard indoor environment, where there are multiple reflections and multipath. In reality, most indoor environments are not as severe as a reverberation chamber.

4.9/ INDOOR LOCALIZATION OPERATING ON THE ANGLE OF ARRIVAL OF A LORA SIGNAL

4.9.1/ INSTALLATION OF GATEWAYS

For the location service to work, a minimum of 2 gateways measuring the angles of arrival of the radio signals must be installed. The angle of arrival is a relative measurement depending on the location of the gateways. So we need to know the coordinates of each gateway and the direction of the axis of the 2 measuring antennas for this service to be activated. There are 2 methods to initialize these values, either they are entered manually by the installer or they are calculated automatically during an initialization phase. By asking the installer to enter these values, there is a risk of input errors in the parameters. The purely automatic method will initialize approximate values without being exact, which will slightly increase the calculation error of the coordinates of the objects to be located. The proposed method consists of initializing these values automatically and then proposing to the installer to refine these values so that they are close to the exact values. Thus, most human errors are removed, such as the inversion of gateway identifiers or the entry of coordinates that are far away from reality. This automatic phase is both an assistance to the initial setup and a coordinates verification entered by the installer.

In order for the automatic initialization phase to take place, we reverse the location function. Instead of calculating the coordinates of an object in the environment from known gateway coordinates, we will calculate the gateway coordinates from objects in the environment whose coordinates are known. The simplest way is to be able to use a GNSS interface but not from inside the building where the GNSS signal is not received but from outside locations near the building where the GNSS signal is receivable. This unit consists of a LoRa object connected to an Android Smartphone in order to use the GNSS interface of the Smartphone to know its WGS84 position composed of latitude, longitude and altitude. Some recent smartphones have a dual-frequency L1/L5 (1575.42 MHz/1176.45 MHz) or E1/E5 GNSS receiver such as the Qualcomm Snapdragon 8 Gen 1. The announced accuracy is one meter under good reception conditions. *SYLOINinit*, the Android and Arduino initialization application for the SYLOIN project was developed by Maanrifa Bacar Ali, member of our research team. *SYLOINinit* guides and assists the installer in order to respect the initialization procedure by proposing to place at least 4 misaligned outdoor locations on a background map and to perform a series of LoRa exchanges with all the gateways by broadcasting the WGS84 coordinates of each

location inside LoRa signals. All the data collected by the gateways combined with the signal reception characteristics including RSSI and angle of arrival are transmitted to a MQTT broker. The *SYLOINcoordinatesGateway* module collects these measurements in subscriber mode and broadcasts the coordinates/direction of each gateway in publisher mode in order to initialize and activate the location system at the end of this procedure. *SYLOINcoordinatesGateway* needs the reception measurements of 3 misaligned outdoor locations to calculate the coordinates of a gateway. Two outdoor locations allow to define a circle of possible gateway locations from the two angle of arrival measurements. Figure 4.31 illustrates this result. The points A and B represent the 2 outdoor locations broadcasting LoRa signals. According to the 2 angles of arrival measured from the gateway, the only possible locations are located on the circle of center C and radius r (inscribed angle theorem), with the following formulas:

$$\begin{cases} r = \frac{d}{2} \cdot \left| k + \frac{1}{k} \right| \\ C = (H_x + (k + \frac{1}{k}) \cdot d \cdot \frac{cos(\alpha)}{4}, H_y - (k + \frac{1}{k}) \cdot d \cdot \frac{sin(\alpha)}{4}) \end{cases}$$

where,

H,the midpoint of the segment [AB],

d,the distance of the segment [AB],

α,the slope angle of the line (AB),

$k = tan\left(\frac{A_a - B_a}{2}\right)$,half the difference of the 2 angles of Arrival measured on the gateway from A and B. G1 and G2, two of the points of the circle where the difference of the 2 angles A_a and B_a is 65° in Fig. 4.31.

With 3 outdoor locations A,B and C, it is possible to construct 3 circles from the 3 pairs A,B; A,C and B,C. The intersection of the 3 circles making 1 point if the measurements are accurate. Figure 4.32 represents this result by associating one difference of angles to each pair of outdoor locations. This calculation is done for each gateway and allows to calculate the coordinates of all the deployed gateways. When the coordinates of a gateway are known, the orientation of the axis of the 2 antennas can be deduced with the following formula:

$$\begin{cases} Orientation(A, G) = 180 + \frac{180}{\pi} \cdot atan \frac{A_x - G_x}{A_y - G_y} \\ AntennaOrientation = orientation(A, G) + A_a \end{cases}$$

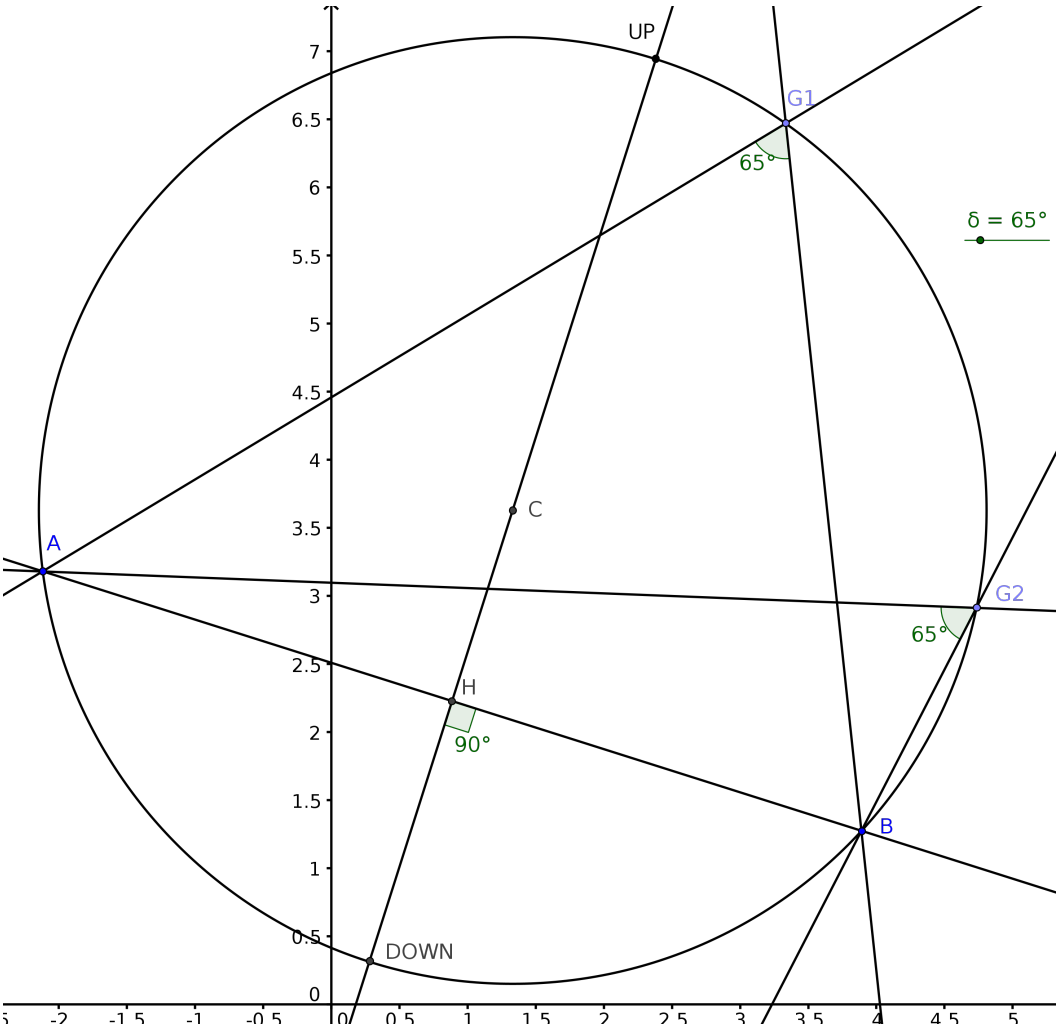

Figure 4.31: Circle of all possible positions of the gateway (e.g. G1, G2) of 2 signal measurements from points A and B

where,

A_a, is the angle of arrival of signal sent from A and received on the gateway

Now the location service is ready to calculate the coordinates of objects transmitting a LoRa signal from inside the building. If necessary, the installer can slightly refine the calculated values.

4.9.2/ CALCULATING THE COORDINATES OF AN OBJECT

When the location service is ready, it is enough to measure 2 angles of arrival from 2 different gateways to calculate the intersection point. When there are 3 or more gateways in reception, we will measure the distances between each intersection point in order to

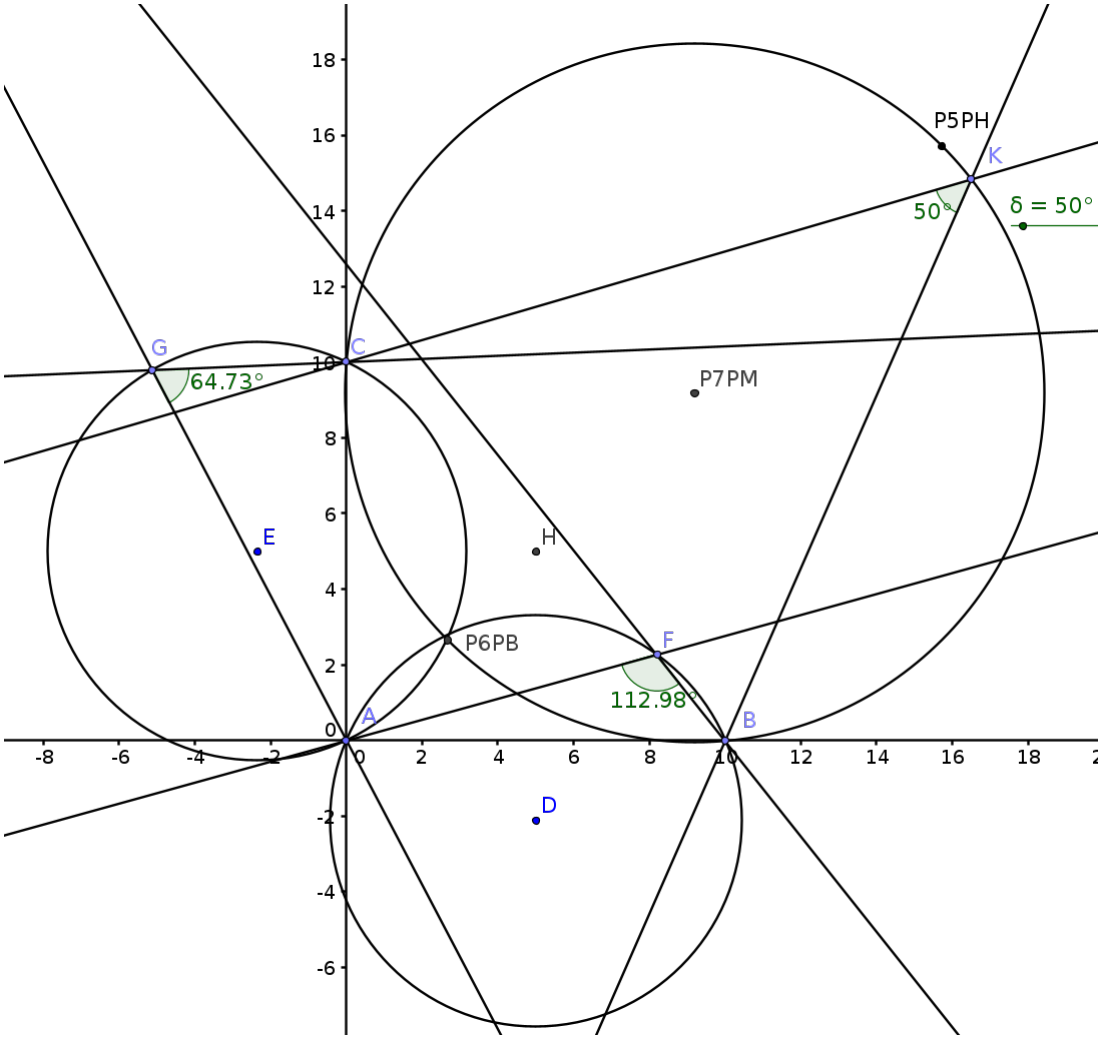

Figure 4.32: Graph representing the point of intersection P6PB of the 3 circles symbolizing the possible points of the gateway

verify the quality of the measurements obtained. When a point of intersection is too far from the others, this will focus us to interpret that the quality of the measurements of the pair of gateways concerned from this point of transmission causes measurement errors in reception. These errors generally represent the multipaths reception of secondary signals and a main signal not received. In figure 4.33, for each signal reception and an associated angle of arrival from a gateway $G(G_x, G_y)$, the equation of the associated line is as follows:

$$\begin{cases} y = a \cdot x + b \\ G_y = a \cdot G_x + b \end{cases}$$

$$\begin{cases} \text{for half plane oriented in the building} & a = orientationAntenna - O_a \\ \text{for half plane oriented outside the building} & a = orientationAntenna + O_a \end{cases}$$

where,

$O_a$is the angle of arrival of a signal received from the object O,

$a = tan(90 - G_a + O_a)$

$b = G_y - tan(90 - G_a + O_a) \cdot G_x$

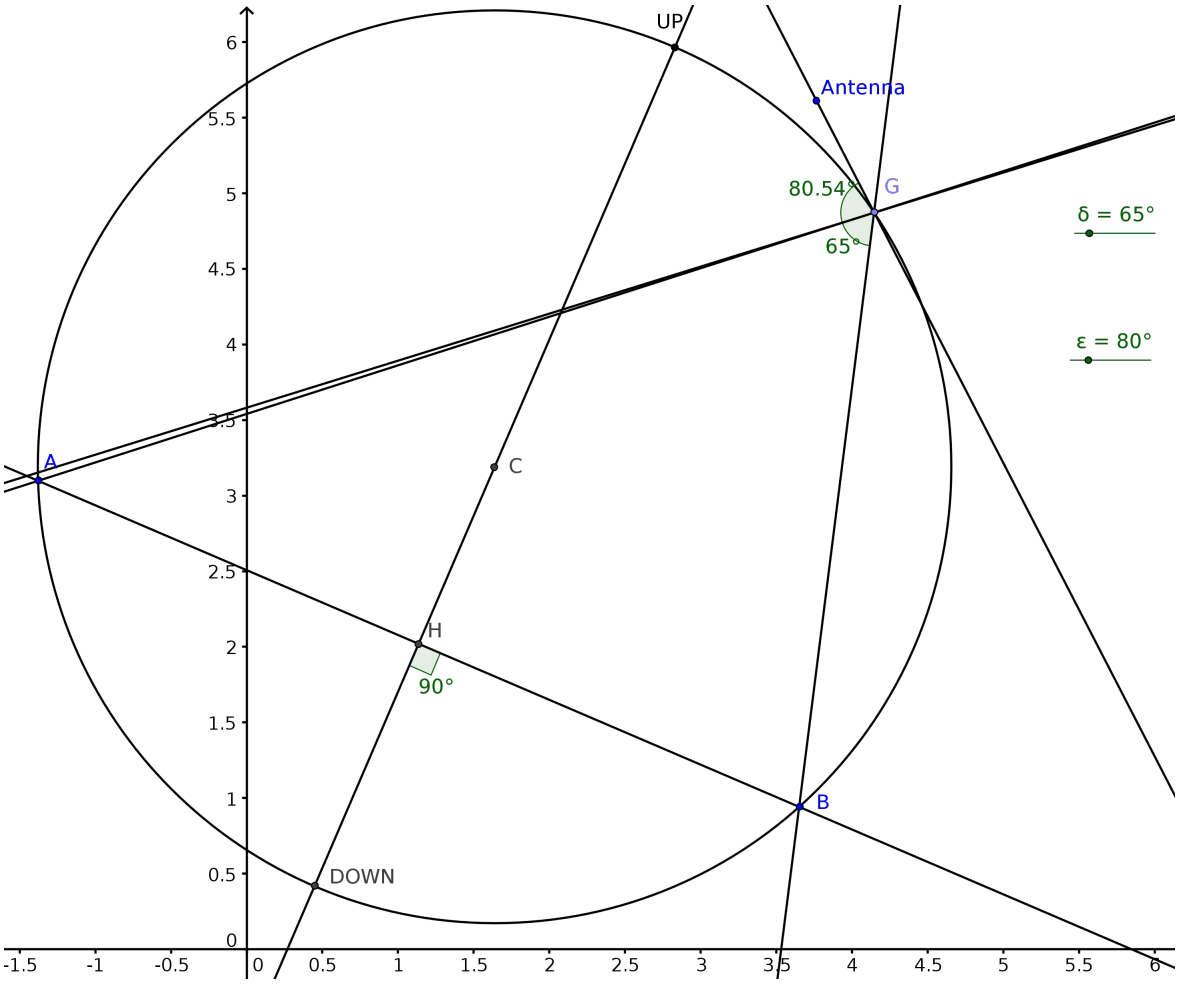

Figure 4.33: Illustration of the calculation of the line induced by the angle of arrival of a signal received from point A with the antenna orientation (G, Antenna)

4.10/ SUMMARY AND CONCLUSION

In this chapter, we proposed an indoor tracking system based on the angle of arrival technique and LoRa wireless technology. We presented the study and processing of the LoRa signal using the SDR platform. The SDR is intended to provide facility for examining and studying the LoRa physical layer characteristics. Thus, the processing, demodulation, and decoding of the LoRa signal was accomplished using the *gr-lora* library in GNU radio.

Additionally, a dual interferometry antenna was designed and developed as a direction finding approach for SDR platforms. The approach was accomplished based on the phase difference between LoRa signals received at each antenna of the SDR receiver, as well as the AoA. This method involved detecting the presence of the LoRa signal in the channel and measuring the phase difference and its associated AoA. Accordingly, the following approaches were proposed for finding the LoRa signal's direction of arrival:

- **Detecting the presence of the LoRa signal:** A new paradigm of LoRa digital carrier signal detection was investigated using GNU Radio and USRP B210 operating at a carrier frequency of 868 MHz. By leveraging LoRa modulation properties, we can determine whether a user's signal is present in the channel. Once the LoRa's signal was detected, it can be used by our algorithm to compute the phase difference of the received signal between each pair of antenna elements, and estimate the AoA.

- **Measuring the phase difference and the AoA:** The phase difference was determined using the FFT transform which is an advanced signal processing technique used to analyse and extract valuable information from LoRa signal in the frequency domain. We have demonstrated that by using FFT, we can provide the frequency and the phase of the LoRa signal. This approach is considered the most feasible for identifying and extracting the phase of interest of the LoRa signal. Once the phase of interest is extracted, the algorithm proceeds to calculate the phase difference and AoA.

This direction finding system was implemented and tested using a real an RFM95 LoRa transmitter and a commercial USRP B210 SDR receiver, in two types of indoor environments: an office laboratory and an anocheic chamber. Furthermore, we have presented the results of AoA as a function of the separation distance between the dual antenna of the USRP B210.

The results showed a significant association between the separation distance and the AoA measurement accuracy. We have learned that with a distance separation equals

to λ/2, we have more accurate AOA estimation than a distance separation equal to λ/4. Using a distance separation equals to λ/2, we obtained a maximum AoA measurement errors around 5 degrees. The 5 degrees error was obtained using a LoRa configuration with a SF of 7 and a BW of 125 kHz. We learned that best performance can be achieved using this configuration.

The next chapter, we will provide a new signal processing approach that can be used to detect a weak LoRa signal with SNR<0, and compute its associated AoA. The new approach can be used to determine whether a signal is present in a noisy environment based on the FFT and the autocorrelation function.

5

MEASURING ACCURATE AOA FOR WEAK LORA SIGNALS

5.1/ INTRODUCTION

In the previous chapter, we provided a solution to measure accurately the angle of arrival of a LoRa signal based on a SDR platform with an estimation error around 5 degrees. However, our system can only achieve an accurate AoA measurement with a high signal-to-noise ratio (SNR > 6dB) communication.

In this chapter, we aim to validate our direction finding system with a very low SNR down to -20 dB. A new approach is proposed to detect and measure the AoA of a very weak LoRa transmission signal. The presented approach is based on dual antenna reception to exploit the Fast autocorrelation signal detection and the phase difference measurement. We, therefore, believe that an accurate AoA of a weak LoRa signal reduces the battery consumption of the transmitter, extends the communication lifetime, and secures the communication of the LoRa devices. To the best of our knowledge, we are the first to implement a real time AoA for a very weak LoRa signal.

In the next section, we will provide a background of the signal processing methods used to detect a weak RF signals.

5.2/ BACKGROUND OF WEAK SIGNAL DETECTION

The detection of weak RF signals in digital signal processing is a rapidly developing area of science and technology these days. Developing new methods to deal with such problems is always a challenge for the research community.

Most of the time, a signal that is received is accompanied by noise, and therefore, detecting the signal of interest becomes more difficult. There are several signal processing

engineering methods for detecting the presence of a weak signal with a specific frequency band. Most of these methods include chaotic oscillators signal detection or noise detection [96, 97, 98]. The idea of chaotic oscillators detection is to detect the same frequency and non-frequency signals located in the different frequency ranges.

A Stochastic Resonance (SR) approach was used in [99] to detect weak signals in underwater communication. In [100], a SR algorithm was developed for Software Defined Radio (SDR), Amplitude Modulated (AM) receiver. SR is a mechanism observed in nonlinear systems where adding a strong noise can improve signal detection and the SNR. However, the computational complexity and cost in SR systems is very high due to match the nonlinear characteristics of the system with the characteristics of the noisy received signal.

Another approach based on Machine learning can also be used for detecting weak signals. A machine learning model like Artificial Neural Network (ANN) is one such algorithm. ANN is a set of mathematical tools and computations that simulate the human-brain processes. Using neural networks, [101] proposed a method for detecting RF signals. The process involves computing the neural network output and comparing the results with the ground truth data. The weight of the neural network is then updated using an optimizing algorithm such as stochastic gradient descent.

A Weak signal can also be detected using Time-Frequency Analysis and Processing. Time-Frequency Analysis and Processing is a collection of theories, techniques, and algorithms that study a signal in both time and frequency domain using time and frequency characteristics. Fast Fourier Transform (FFT) and Wavelet Transform (WT) are the most used in signal Time-Frequency analysis and processing.

A threshold signal denoising method based on time-frequency analysis is developed in [102]. A time-frequency joint denoising approach is presented using LabVIEW programming. FFT was used to convert the signal to the frequency domain to find useful information in the channel. The noise is removed by comparing the signal with a decision threshold. Wavelet threshold (WT) denoising method [96], and empirical mode decomposition [103], use also time-frequency denoising approach based on threshold decision. Wavelet and EMD threshold denoising methods are mainly used in the underground communication, acoustic communication, navigation, and tracking, where there is a large amount of noise present in the signal.

Weak signal detection method is implemented in [104] using FFT transform and filtering approach. The FFT Transform method involves decomposing the signal in the frequency domain by applying different window functions and selecting pass bands to extract the signal of interest. FFT only provides accurate detection when the Signal to Noise Ratio (SNR) of the received signal is high. In low SNR situations, the signal components are hidden by the noise components, which makes it impossible to recognize the signal.

Signal detection algorithm using Discrete Wavelet Transform (DWT) is used in [105] for the analysis of radar signal. A DWT-based detection method is more accurate than a conventional one, and the authors present a method to detect radar signals with very low SNR.

Another approach for detecting weak signals from a strong noise is correlation analysis. In a noisy signal, noise is defined by its randomness, while the signal of interest is defined by its periodicity. The detection of a periodic signal is possible with some mathematical tools such as autocorrelation or crosscorrelation. Several articles in the literature use autocorrelation to detect a signal in strong noise.

Detection of a weak low-frequency electromagnetic signal based on multi-layer autocorrelation is implemented in [106]. Multi-layer autocorrelation is based on a similar principle to autocorrelation detection. However, the output signal of multi-layer autocorrelation must undergo autocorrelation repeatedly after each computation phase. As a result, increasing the number of autocorrelation increases the Signal to Noise ratio (SNR) and detection accuracy.

A study of peak finding algorithm of speech signal using autocorrelation function is used in [107]. The authors proposed a peak autocorrelation detection to the pitch of the voiced signal. The proposed algorithm can estimate the fundamental frequency of the speech signal accurately with low computational complexity and in real-time.

An acquisition of weak GPS signals is presented in [108]. The proposed technique searches the coarse/acquisition (C/A) code phase of the GPS signal in the FFT-based correlation domain. A peak-finding algorithm is implemented using autocorrelation analysis. The results show that the proposed method can detect the GPS signals efficiently in indoor environments, even at a very low SNR level.

Based on the autocorrelation approach, we propose a dual antenna fast autocorrelation method for detecting weak LoRa signals in an indoor environment. The basic idea of our method consists of measuring the autocorrelation function of the LoRa signal in the frequency domain using a FFT transform. Performing the autocorrelation function combined with FFT will increase the detection accuracy and the SNR. The proposed method has many advantages. First, the processing time is reduced by using a FFT compared to other detection techniques. Second, applying the signal's autocorrelation in the frequency domain increases the detection accuracy compared to other detection techniques.

In the following section, we will provide an overview of the dual antenna fast autocorrelation technique for weak signal detection.

5.3/ DUAL ANTENNA FAST AUTOCORRELATION

5.3.1/ AUTOCORRELATION FUNCTION

An autocorrelation is a signal processing tool used to separate useful signal from noise. The autocorrelation analysis consists of finding the presence of useful segments in a signal. The autocorrelation of a signal is just the correlation coefficient. However, instead of applying the correlation between two different signals, the correlation is between the two segments of the same signal at times T_i and T_{i+k}.

Given a two continuous signals *x(n)*, *y(n)*, *n = 1,2,3,..,N*, where *N* is the number of samples. The discrete correlation function of the two signals can be computed by the following equation:

$$Corr(x,y)_k = \frac{1}{N}\sum_{n=0}^{N-1} x_{k+n}y_n \tag{5.1}$$

Equation 5.1, provides the correlation function of the two signals. When the two signals are similar, then their correlation coefficient will be 1, if a normalization factor is applied. However, if the two signals are different, then their correlation will not be equal to 1. If we suppose that *x(n) = y(n)*, then Equation 5.1 will be as follow:

$$Corr(x,x)_k = \frac{1}{N}\sum_{n=0}^{N-1} x_{k+n}x_n \tag{5.2}$$

Equation 5.2, computes the correlation between the same signal *x(n)* and *x(n+k)* separated by a time lag *k*, which is the autocorrelation function of the signal *x(n)*.

The autocorrelation function presented in Equation 5.2 reaches its maximum value at the lag=0, and is always symetric around zero, which means that the autocorrelation values are equals at lags *+k* and *-k*.

Using the autocorrelation properties, it is possible to detect weak signals. Using the FFT with the autocorrelation function will be described in the following section.

5.3.2/ FAST FOURIER TRANSFORM AUTOCORRELATION

Signal detection is a key function of the FFT. Using FFT and the autocorrelation function can accelerate the autocorrelaton computation. The Wiener-Khinchin theorem states that the autocorrelation function and the power spectral density (PSD) of the signal are Fourier pairs. The autocorrelation function is the Fourier transform of the PSD.

Let *x(n)*, *y(n)* be two discrete signals, the correlation function can be defined as:

$$Corr(x, y)_k \Leftrightarrow X(f)Y^*(f) \tag{5.3}$$

From equation 5.3, the correlation of the two signals can be computed by multiplying the FFT of one signal by the complex conjugate of the FFT of the other signal.

As the autocorrelation function of *x(n)* is the correlation with its delay version, the autocorrelation will therefore be the following:

$$Corr(x, x)_k \Leftrightarrow X(f)X^*(f) \equiv |X(f)|^2 \tag{5.4}$$

Where $|X(f)|^2$ is the PSD of the signal *x(n)*. Considering the properties of the autocorrelation and the FFT, it will be possible to detect weak signal buried in noise.

In the next section, we will describe how to detect weak signals, using autocorrelation, FFT, and dual antenna receiver.

5.3.3/ DUAL ANTENNA WEAK SIGNAL DETECTION

This section discusses the dual antenna fast autocorrelation detection approach, which consists of measuring the autocorrelation function between outputs of two sensors of the receiving antenna array.

The dual antenna approach is a very promising topic in radio communication systems, particularly for the receiver side. By using two antennas, it is possible to receive two replicas of the user signal, which can be used for various signal processing tasks.

One of the most common uses of the dual antenna approach is in signal detection and estimation. By using the correlation method, it is possible to determine whether the user signal exists or not. This is particularly useful in noisy environments, where it can be difficult to distinguish the user signal from the noise.

The correlation method works by comparing the two replicas of the user signal and calculating the correlation coefficient between them. If the correlation coefficient is high, it indicates that the two signals are highly correlated, and therefore, the user signal is likely present. On the other hand, if the correlation coefficient is low, it indicates that the two signals are not correlated, and therefore, the user signal is likely absent.

Figure 5.1 shows two signals *X1(t)* and *X2(t)* received by the antennas A1 and A2 respectively. When the transmitter and the receiver are in LOS conditions, there will be a time delay $\Delta(t)$ between the two signals received at the two antennas. Since the two signals *X1(t)* and *X2(t)* are the same time series data received at a different time by the

two antennas, $X1(t) = X2(t + \Delta(t))$.

Using the properties of the correlation function between two same signals separated by a time lag t given by Equation 5.2, and the fast autocorrelation function using FFT given by Equation 5.4, the detection of the signal using a dual antenna receiver is possible.

To perform signal detection using the dual antenna approach, it is necessary to collect enough samples of the received signals from the two antennas. Based on these samples, the fast autocorrelation of the signals can be built, which can then be used for signal detection.

The fast autocorrelation peaks need to be identified and analysed. These peaks correspond to the delay between the two received signals and can be used to determine the presence of the signal. The threshold value will be used to differentiate between the signal and the noise. If the peak amplitude is above the threshold, it indicates the presence of the signal, and if it is below the threshold, it indicates the absence of the signal.

In the next section, we will present our approach for detecting a LoRa signal using a dual antenna USRP B210 SDR receiver with the help of GNU Radio.

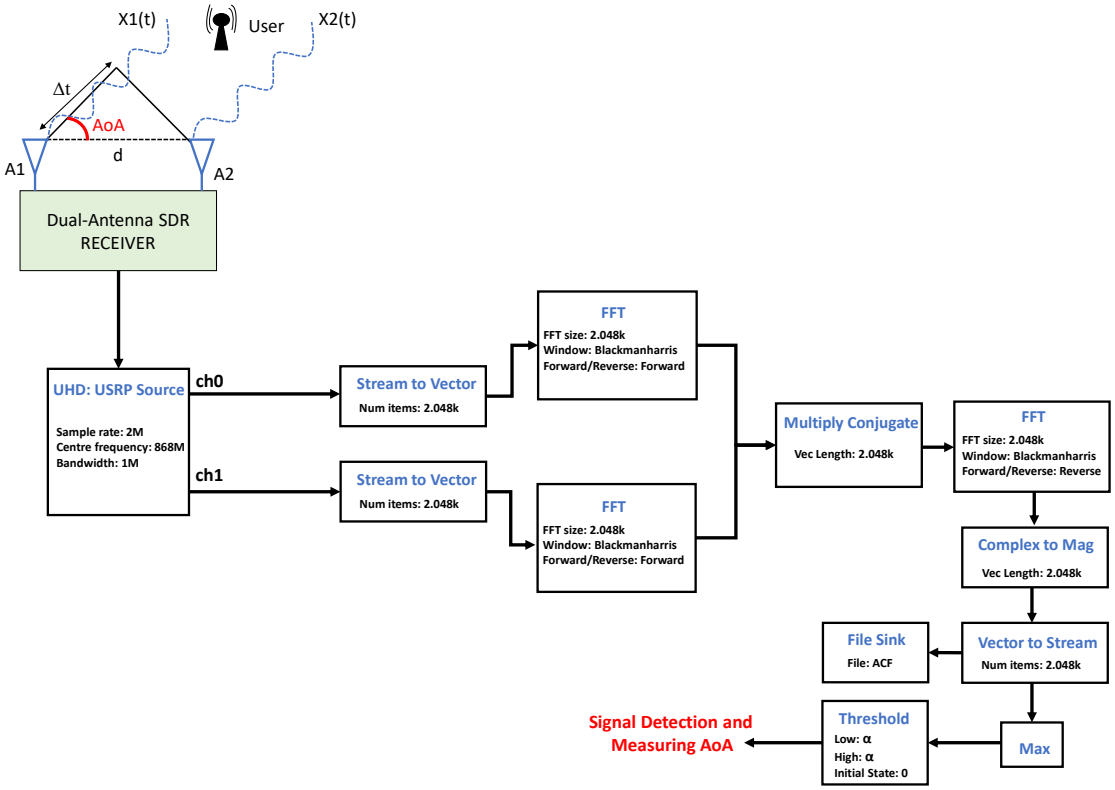

Figure 5.1: A block diagram of the Fast autocorrelation signal detection.

5.4/ PROPOSED METHOD

We developed a method for detecting weak LoRa signals on dual antenna receiver by measuring the fast autocorrelation function. In the first step, we use fast autocorrelation signal detection to determine whether LoRa signal exist in the channel. As a second step, we measure the AoA if the signal is detected. The USRP B210 SDR receiver and the GNU Radio form the basis of this method.

5.4.1/ USRP B210 FAST AUTOCORRELATION SIGNAL DETECTION

Figure 5.1 shows the basic principle of our proposed method. The process starts by extracting the LoRa signal received at the dual antennas using a *UHD: USRP Source* block which captures the data from the B210 receiver.

After that, the two signals diverge into two paths. For each path, the output of the *UHD: USRP Source* block is passed through a *Stream to Vector* block which converts the data in I and Q format. Now that the data are in I and Q format, the *FFT* block computes the FFT transform to transform the data from time domain to frequency domain.

Up until this point, the data are in the frequency domain for each path, the *Multiply Conjugate* block performs the multiplication of the output of the first path by the conjugate of the output of the second path. To get back the data in the time domain, the result of the *Multiply Conjugate* block is passed though the *FFT* block which performs a reverse FFT to convert the data from the frequency domain to the time domain.

Until now, the data are in complex vector format, the *Complex to Mag* block provides the magnitude in a float format. The *Vector to Stream* block performs the opposite function of the conversion done by the *Stream to Vector* block. It transforms the data back to the stream format and sends it to the *Max* block.

Up to the present, the data are in stream float format in the time domain. Since the autocorrelation function has a maximum peak at lag=0, the algorithm must find this peak.This is done by the *Max* block which takes a stream of data as its input and gives their maximum value as its output. Once the peak value is found, the output of the *Max* block is passed to the *Threshold* block. This block has two parameters: *High* and *Low* value. If the output of the *Max* block is higher than the value set for the *High* parameter, the output of the *Threshold* block is 1. On the other hand, if the output goes below the value set for the *Low* parameter, the output of the *Threshold* block is 0. The decision output of the Fast autocorrelation detection algorithm is given by the following equation:

$$Decision = \begin{cases} 1 & \text{if } Max > \alpha \\ 0 & \text{if } Max \leq \alpha \end{cases} \tag{5.5}$$

Where *Max* represents the peak of the Fast autocorrelation detection, and α is the predefined threshold. The predefined threshold is determined using a post processing analysis. The *FileSink* block is used to write the data in an empty file. The written data are processed in Matlab to determine the optimal threshold value.

The case when the value of the *Decision* is equal to 1, meaning that the signal is detected, and the case when the value is equal to 0, meaning that the signal is absent. Once the signal is detected, the algorithm computes the AoA using the phase difference method implemented in the Chapter 4.

5.4.2/ GNU Radio implementation

The Fast autocorrelation signal detection and AoA was implemented with GNU Radio and USRP B210 SDR receiver. The full GRC implementation is shown in Figure 5.2.

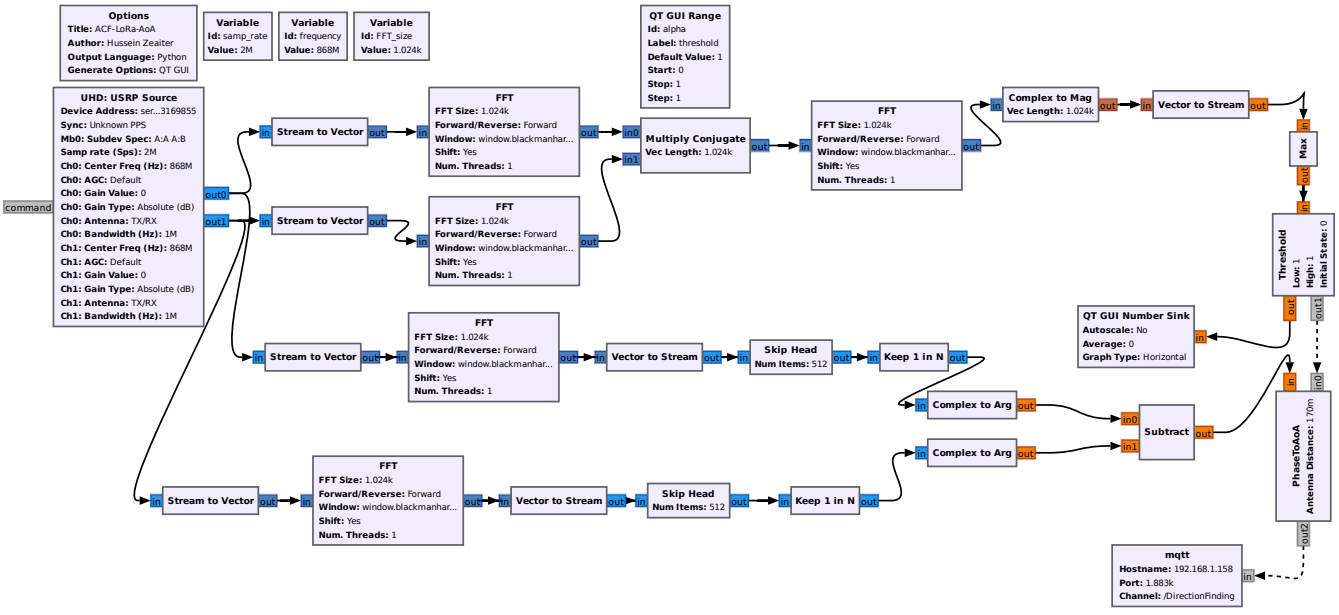

Figure 5.2: A GRC flow graph for the USRP B210 to compute the fast autocorrelation and AoA.

As shown in the figure above, our algorithm is able to capture in real time a LoRa signal received by the USRP B210, detect the presence of the signal in the channel using fast

autocorrelaiton, measure the phase difference between the two signals received by the two antennas and calculate the corresponding AoA. Finally, the AoA measurement is published in real time on a server using the MQTT protocol.

The experimental measurement and results will be discussed in detail in the following section.

5.4.3/ Experimental and results in indoor environment

5.4.3.1/ Experimental setup

In this experiment, a Feather M0 RFM95 transceiver was used to transmit a LoRa signal with the following configurations: carrier frequency = 868 MHz, BW = 125 kHz, SF = 7, and CR = 4/5. For the USRP B210, we assume a sampling frequency of 2 MHz, and the length of the signal (FFT size) of 1024 points (bins).

5.4.3.2/ Measurement Data

For the measurement data, we divided our experiment into two parts. Identifying the appropriate FFT size was the first step in improving detection accuracy at very low transmission power (TX) or signal-to-noise ratios (SNR). In the second step, we measured the AoA accuracy of the LoRa signal based on different SNR levels.

In experiment 1, the transmitter was programmed to send a signal with a transmission power ranging from -1 dBm (lowest TX) to +20 dBm (highest TX). The detection accuracy of the proposed system was measured for different FFT sizes. The performance of our algorithm is shown in Figure 5.3.

Figure 5.3 shows that, with an FFT size of 1024, the LoRa signal can be detected effectively if SNR is greater than -12 dB. In contrast, when the FFT size is equal to 65536, the detection of the LoRa signal decreases down to -20 dB. As the FFT size is increased, the autocorrelation of noise becomes smaller, which results in improved detection performance of the LoRa signal. In fact, increasing the FFT size can improve the frequency resolution of the autocorrelation function, which can lead to better estimation of the autcorrelation peaks. This can result in improved SNR for frequencies of interest.

Figure 5.4 and 5.5 illustrate respectively the autocorrelation peaks of LoRa signal with two different FFT sizes of 1024 and 65536, respectively. It clearly appears that when using an FFT equals to 65536 (frequency resolution = 30 Hz), the autocorrelation peaks are easier to detect than using an FFT size equals to 1024 (frequency resolution = 2 kHz). Therefore, the detection performance of the algorithm is better at high FFT size.

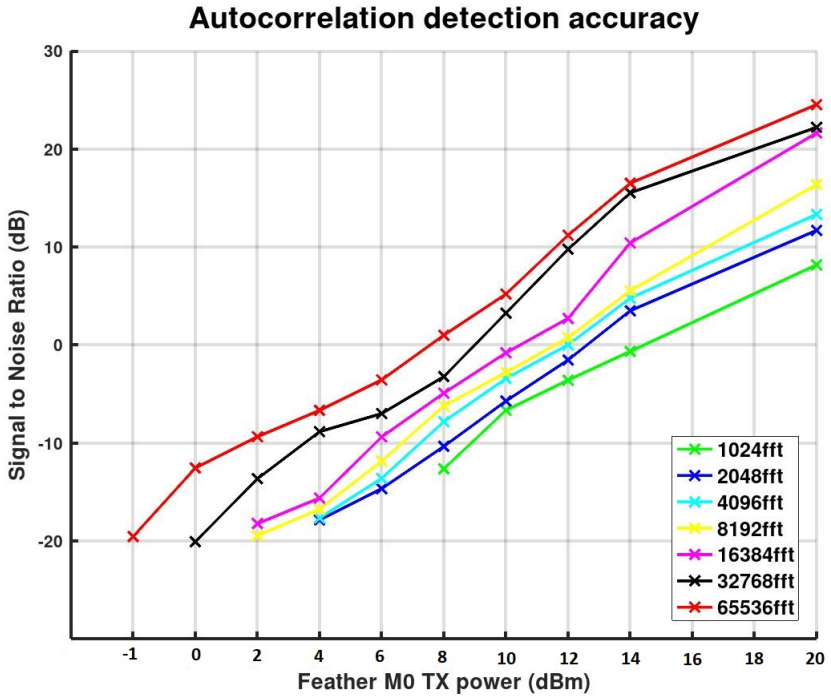

Figure 5.3: Autocorrelation detection accuray for different FFT size.

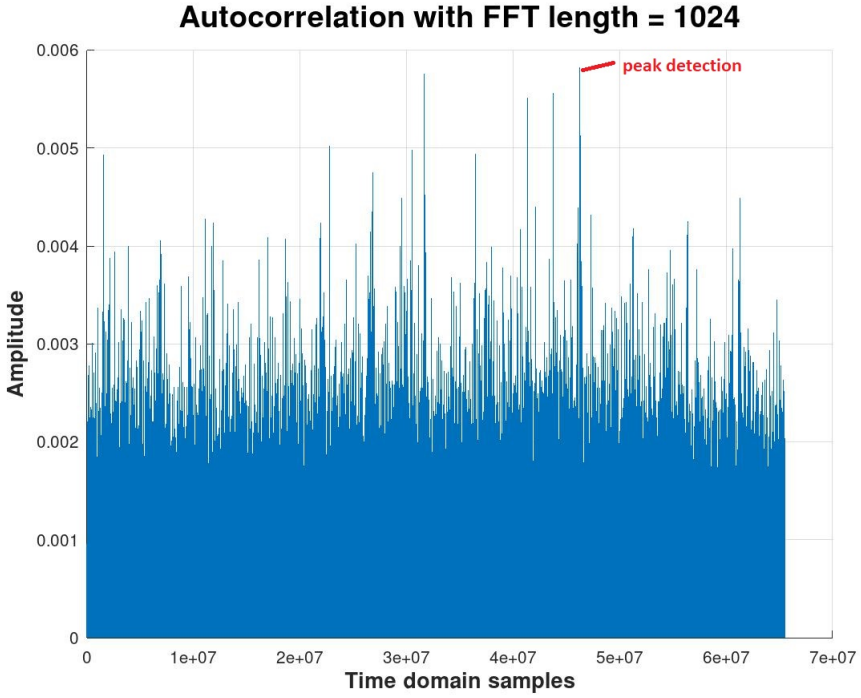

Figure 5.4: Autocorrelation peak detection for noisy LoRa signal with FFT size equals to 1024.

In the next experiment, the FFT size is chosen to be equals to 65536.

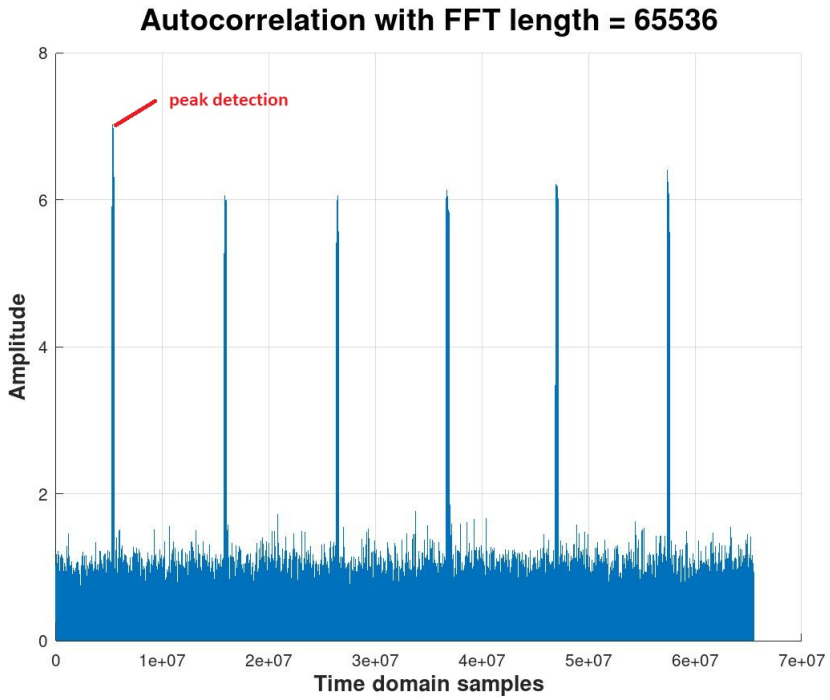

Figure 5.5: Autocorrelation peak detection for noisy LoRa signal with FFT size equals to 65536.

As part of experiment 2, we measured the AoA of a LoRa signal at three different SNR levels: 20 dB, 0 dB, and -20 dB. At each SNR level, the AoA was measured in 15 degrees increments between [5, 175] degrees. The results of this measurement are shown in Figure 5.6. Clearly, the measured values of AoA are very close to the real values when SNR is equal to 20 dB. The angular deviation increases significantly when the measurements were taken with SNR equals to 0 dB. Despite an SNR of -20 dB, the algorithm still provides good measurements accuracy for AoAs between 45 degrees and 135 degrees. Angular deviation increases exponentially for AoAs less than 45 degrees and greater than 135 degrees. Consequently, AoA accuracy is better for large angles when SNR is -20 dB.

The AoA deviation error for this experiment is shown in Figure 5.7. The algorithm can successfully measure the AoA with a deviation error of less than 5 degrees in the range of [45, 135] degrees, and less than 6 dergees for small angles when the SNR is 20 dB. Otherwise, when the SNR decreases to 0 dB and -20 dB, the deviation error increases to 10 and 12 degrees respectively for small angles.

Based on these experimental results, we can propose an efficient method for deploying an indoor location infrastructure that uses low AoA. Indeed, the alignment of the dual antennas of the LoRa gateways (USRP B210) must favor the angles located between 45 degrees and 135 degrees in the area so that the other angle values are as much as possible outside the building as can be seen in Figure 5.8.

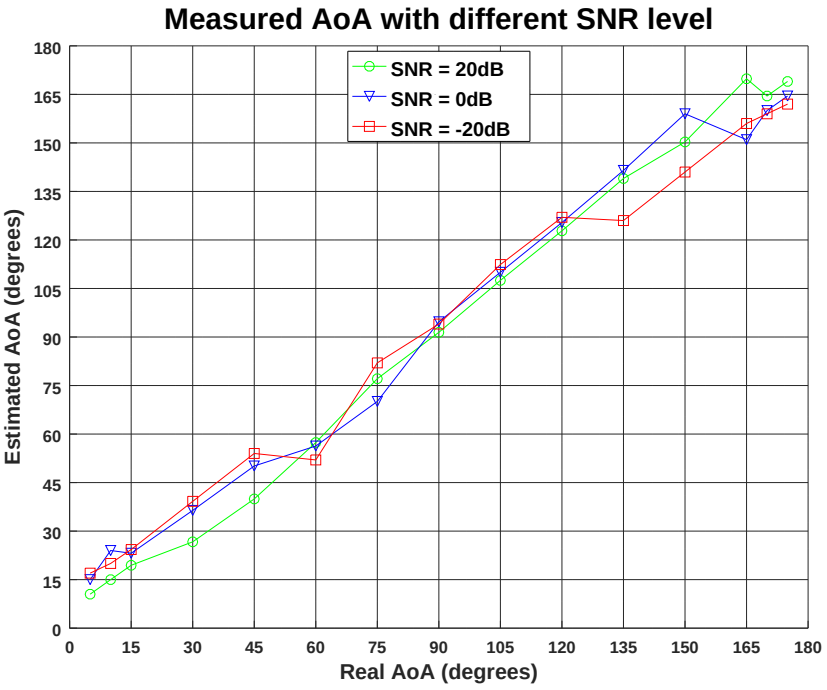

Figure 5.6: AoA measurements with different SNR level.

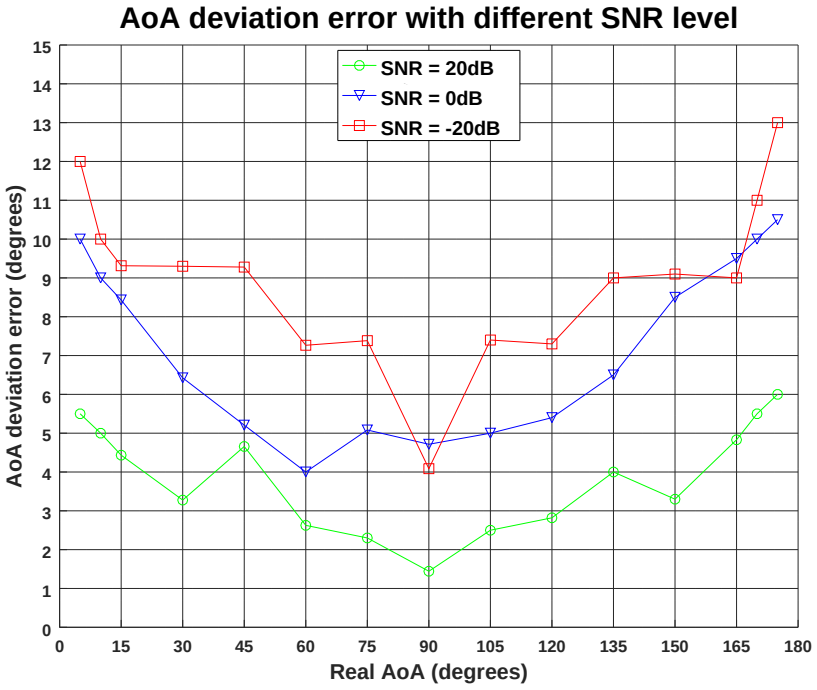

Figure 5.7: AoA deviation error with different SNR level.

By aligning the antenna in this manner, the accuracy of the AoA will be 9 degrees. This topology gives the best accuracy at the center of the building where the AoA are in the green area, and the worst accuracy at the building edges, where the AoA are in the red

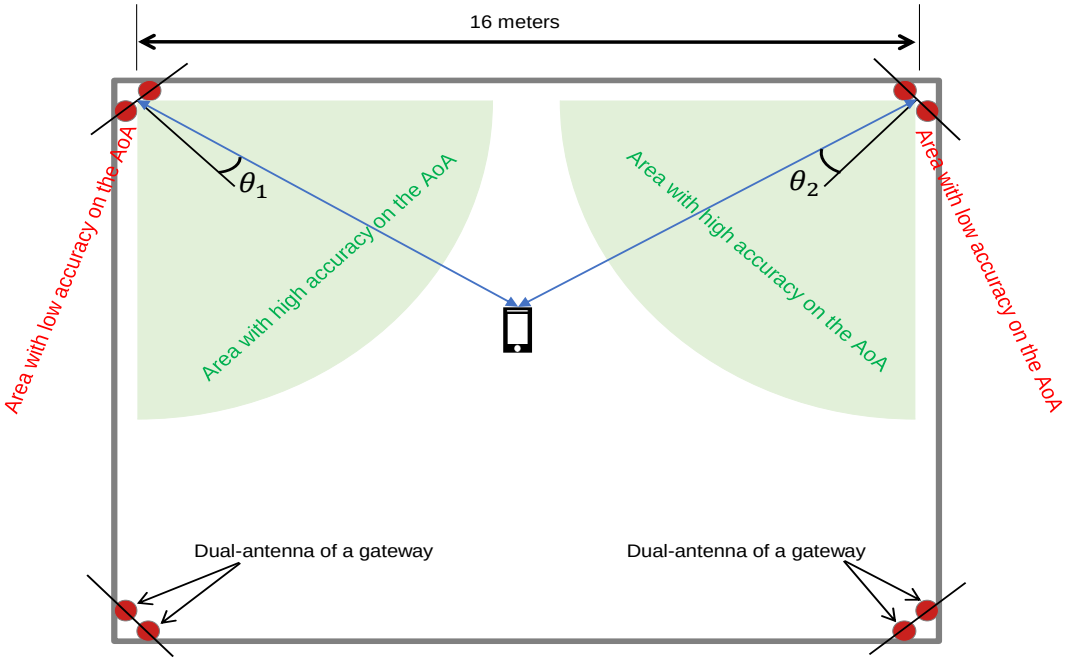

Figure 5.8: Indoor location infrastructure exploiting low AoA

area. If an object is in critical situation, a gateway can send a specific message in order to request a full transmit power reply so that AoA accuracy can be improved.

5.4.4/ Experimental and results in outdoor environment (Distance 3.8 km)

Determining the direction of arrival of LoRa signals over long distances can be a challenge due to a various factors that can affect the quality and reliability of the signal.

One of the main challenges is the attenuation and dispersion of the signal over long distances, which can cause the signal strength to decrease and the phase to be distorted. This can make it more difficult to accurately estimate the phase and the AoA of the signal, particularly if the signal is weak or noisy.

Despite these challenges, we have been able to measure the AoA of LoRa signals over long distances using our dual antenna USRP B210 receiver and the fast autocorrelation signal detection and AoA measurement method.

5.4.4.1/ Experimental setup

We conducted an experiment to test our LoRa direction finding system in an outdoor environment. The LoRa direction finding system was connected to a dual USRP B210

antenna spaced half a wavelength of the 868 MHz carrier frequency. On the other hand, the transmitter was programmed with the following parameters: carrier frequency = 868 MHz, SF = 7, BW = 125 kHz, CR = 4/5, and TX power = 14 dBm.

The dual antenna receiver was mounted on a tripod near the Numerica Femto-st research laboratory in the city of Montbeliard. The LoRa transmitter has a specific position and it is located at an altitude of 497 meters on top of the fort of Mount-Bart in the city of Bavans. This distance between the LoRa transmitter and the receiver was approximately 3.48 km in the LOS condition as shown in Figure 5.9.

Figure 5.9: Google Maps image of our direction finding system in an outdoor environment with a distance of 3.8 km.

The Mount-Bar transmitter was configured to be in sleep mode to save battery power. Thus, to wake up the Mont-Bart transmitter, a second LoRa transmitter was used, located at the Numerica laboratory, to communicate with the Mount Bart. The second transmitter send a LoRa signal to the Mount-Bart transmitter, which wakes it up from sleep mode. Once the Mount-Bart transmitter receives the signal, it transmits LoRa signal reply. Both signals were detected by the USRP B210 dual antenna receiver, which calculates the AoA of the signal.

This setup allows for efficient use of battery power while still enabling communication over long distance. By using a wake-up signal, the Mount-Bart transmitter can conserve energy when it is not actively transmitting signals. The setup is illustrated in Figure 5.10.

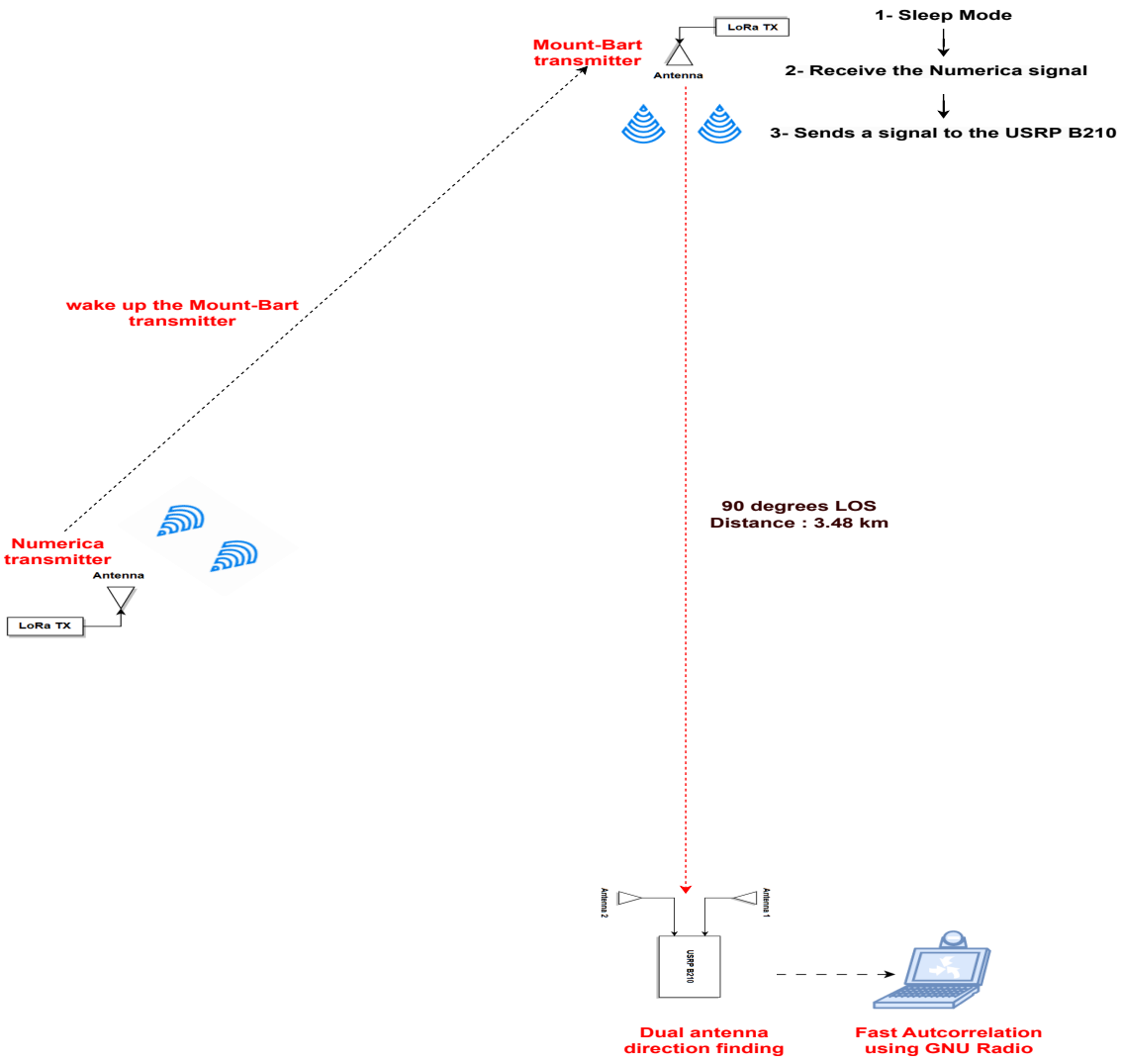

Figure 5.10: Setup of the direction finding system in an outdoor environment.

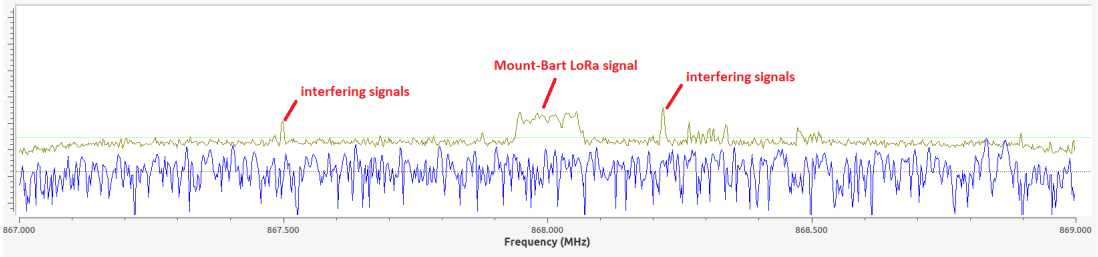

Figure 5.11: FFT of the Mount-Bart Signal with low SNR.

Figure 5.10 shows that the Mount-Bart transmitter is located at 90 degrees from our direction finding receiver. It should be noted that this orientation was chosen for experimental purposes.

Before investigating the AoA estimation accuracy of the direction finding system, we analysed the frequency content of the received signal using the FFT transform, which can help us to identify the presence of unwanted frequencies in the outdoor environment and to reduce the possibility of false AoA estimations.

Figure 5.11 illustrates the frequency components of the received signal. We can clearly see that the Mount-Bart signal is received at a low SNR level. Furthermore, There are interfering signals near the LoRa carrier frequency (868 MHz), which indicates the presence of interference that is affecting the signal.

The Mount-Bart transmitter operates at the 868 MHz carrier frequency over a bandwidth equals to 125 kHz. Thus, any other frequencies operating outside the range of [-62.5, +62.5] kHz should be considered as interfering frequencies. Our goal is to eliminate all frequencies operating outside this range. This can be resolved using a band pass filter.

Using a band pass filter, unwanted frequencies outside the frequency range of interest can be removed. In this way, interference outside of the LoRa's frequency band can be removed. We can implement a Band pass filter in GNU Radio using the *Frequency Xlating FIR Filter* block as shown in Figure 5.12. The *Frequency Xlating FIR Filter* known as Frequency Translating Finite Impulse Response Filter block performs a frequency translating and Band pass filtering on the LoRa signal. It will select the 125 kHz narrow bandwidth of the LoRa signal from the whole bandwidth of the USRP B210 receiver.

As shown in Figure 5.12, the LoRa signals received by the two antennas are passed through the *Frequency Xlating FIR Filter*. After this, the algorithm compute the Fast autocorrelation and the phase difference method.

The *Frequency Xlating FIR Filter* block for Band pass filtering has the following parameters:

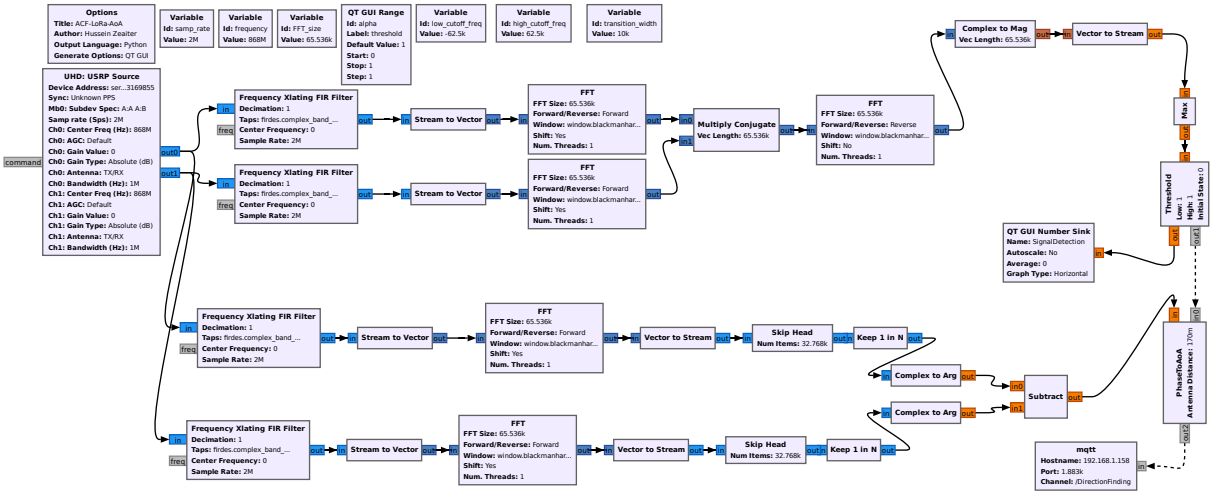

Figure 5.12: A GRC flow graph for the USRP B210 to compute the fast autocorrelation and AoA using a Frequency translating band pass filter.

- **Decimation:** The decimation parameter can be used to reduce the signal sampling rate. In our case, we set the decimation to 1, so that the sample rate is maintained at 2 MHz. For example, for a decimation equals to 2, the sample rate will be equal to 2 MHz / 2 = 1 MHz.

- **Taps:** This parameter is used to define the type of the FIR filter (Band Pass, Low Pass, or a High Pass filter). In our case, we set the type of a Band Pass filter.

- **Low Cutoff Freq:** In our case, the LoRa signal is occupying a bandwidth of 125 kHz. The low cutoff frequency of the Band pass filter must be equal to: 0 - 62.5 kHz = -62.5 kHz.

- **High Cutoff Freq:** The high cutoff frequency of the Band pass filter must be equal to : 0 + 62.5 kHz = +62.5 kHz.

- **Center Frequency:** This parameter allows to define the frequency translation offset. In our case, our LoRa center frequency is 868 MHz (0 Hz in the Base Band). Therefore, the frequency translation offset will be 0 Hz. For example, if we want to identify a LoRa signal with a center frequency of 868.1 MHz or 868.3 MHz, the frequency translation offset will be 100 kHz and 300 kHz.

In this manner, frequencies within the 125 kHz bandwidth of LoRa signals will pass through the filter while frequencies outside of it will be rejected. The frequency content of the received filtered signal using FFT will be as shown in Figure 5.13.

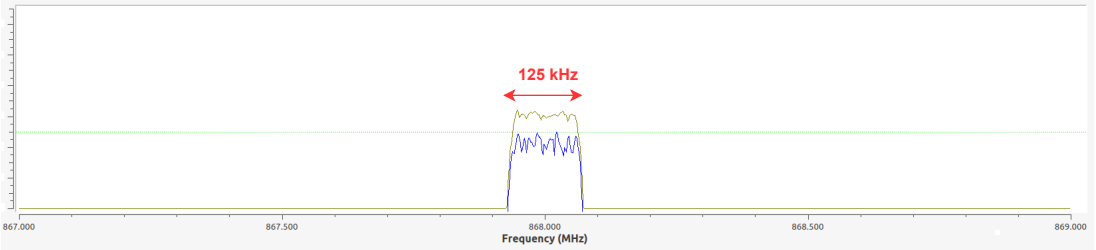

Figure 5.13: FFT of the filtered Mount-Bart Signal.

5.4.4.2/ MEASUREMENT DATA

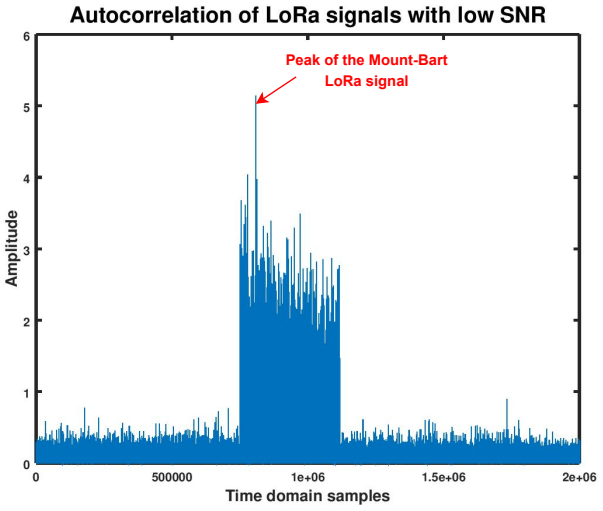

Figure 5.14: Autocorrelation graph of the Mount-bart LoRa signal.

For the measurement data, we investigated the AoA estimation using the developed Fast autocorrelation method. Figure 5.14 shows the autocorrelation plot of a LoRa signal with low SNR level. Within the LOS condition and within 3.48 km away from the receiver, the autocorrelation graph indicates that the LoRa signal can be accurately received from the Mount-bart transmitter.

The autcorrelation plot also reveals mini peaks and a main maximum peak, which corresponds to the subcarrier frequencies and the center frequency of the LoRa signal, respectively. To extract the exact AoA, the maximum peak was detected using the algorithm presented in Figure 5.12.

AoAs were measured for two angular rotations of the dual antenna receiver: 90 degrees and 135 degrees. For each angle rotation, 20 LoRa signals and AoAs were detected. The estimated AoA and deviation error of the Mount-bart transmitter are shown in Figure 5.15.

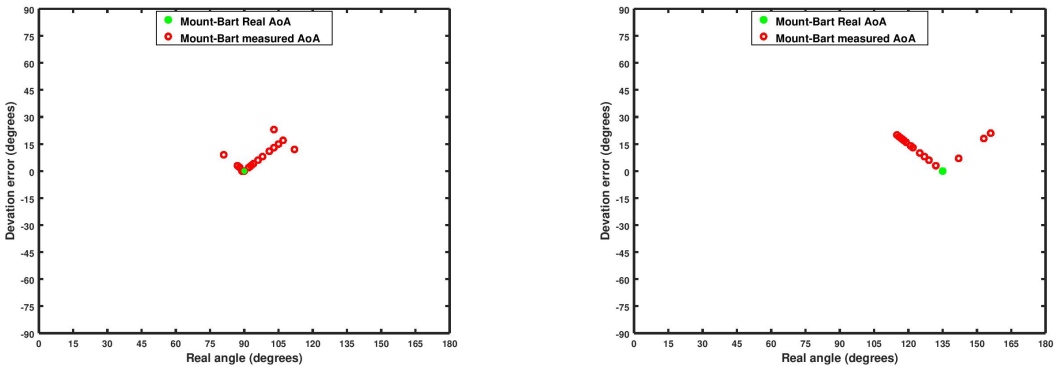

(a) Angle deviation error for 90 degrees

(b) Angle deviation error for 135 degrees

Figure 5.15: Angle deviation error for the Mount-Bart transmitter for both 90 and 135 degrees.

Figure 5.15 (a) and 5.15 (b) show measurements of AoAs versus angular deviation errors of the Mount-Bart transmitter. Among the 20 detected LoRa signals, the measured AoAs range from 80 to 110 degrees with a mean absolute error of 8 degrees when the true angle is 90 degrees, which indicates that, on average, the measured AoAs differ from the true angle by 8 degrees.

When the real angle is 135 degrees, the measured AoAs range from 117 to 156 degrees, with a mean absolute error of 14 degrees for the 20 detected LoRa signals, which indicates that, on average, the measured AoAs differ from the true angle by 14 degrees.

5.4.5/ Experimental and results in outdoor environment (Distance 20 km)

In the previous section, we measured the AoA of LoRa signals in an outdoor environment with a distance between the LoRa transmitter and the B210 dual antenna receiver equals to 3.8 km. In this section, our objective is to increase the distance between the transmitter and the receiver in order to study the performance of our algorithm over very long distances. To benefit from sites favorable to the transmission and reception of radio signals to perform our measurements, we chose to take inspiration from the French military defensive network set up after the defeat of 1870 and the loss of Alsace and Lorraine. At that time, the engineer and General Raymond Adolphe Séré de Rivières chose to build the defensive forts on hills and in line of sight to allow the installation of optical communication systems such as heliographs/heliostats for daytime transmissions and a version integrating a light source for the night. Between these 2 sites, the Fresnel ellipsoid is unobstructed from end to end for the 868 MHz frequency.

5.4.5.1/ EXPERIMENTAL SETUP

In this experiment, the position of the transmitter is always the same at the top of Mount Bart. The position of the receiver was changed and fixed at the top of Mount Salbert located in the city of Belfort at an altitude of 650 m. The distance between the transmitter and the receiver was approximately 20.2 km in LOS condition as shown in Figure 5.17.

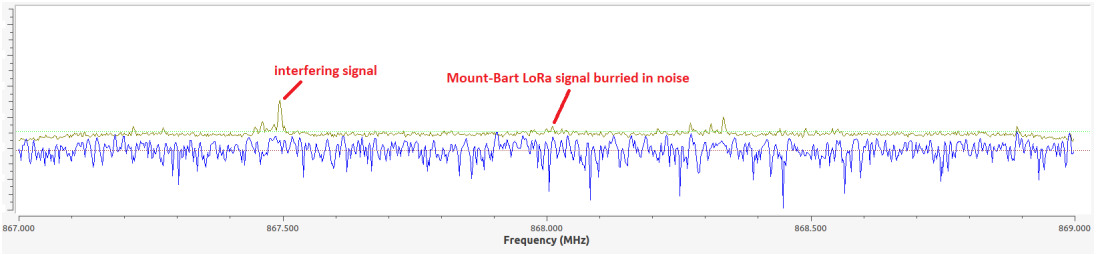

Figure 5.16: FFT of the Mount-Bart Signal with negative SNR.

The frequency content of the received signals in this experiment is illustrated in Figure 5.16. The FFT plot reveals that the Mount-Bart LoRa signal is buried in noise and can not be identified and detected. Thus, the Fast autocorrelation will be used to identify the signal from the noisy environment when it is difficult to detect.

5.4.5.2/ MEASUREMENT DATA

Figure 5.18 shows the amplified Mount-Bart LoRa signal after applying the Fast autcorrelation algorithm. It can be seen that the autocorrelation peaks can be easily to detect from the noise. Furthermore, the results reveal that 9 LoRa signals were transmitted and received every 5 seconds.

Figure 5.19 illustrates the zoomed in autocorrelation result of the first Mount-Bart LoRa detected signal. It is clearly that the result exhibit a first maximum peak and a second maximum peak.

The first maximum peak was identified at an index equals to 6062081, and the second maximum peak was identified at an index equals to 6062057. Therefore, the difference between the two values will indicate the period in samples of the signal. The period in samples for the detected LoRa signal can be calculated by the following equation:

$$T_{samples} = Index_{FirstPeak} - Index_{SecondPeak} \tag{5.6}$$

Equation 5.6, represents the period in samples for the detected LoRa signal. The following equation is used to obtain the period in seconds:

Figure 5.17: Google Maps image of our direction finding system in an outdoor environment with a distance of 20.2 km.

$$T_{seconds} = \frac{T_{samples}}{SampleRate} \tag{5.7}$$

Thus, the period in seconds for the first detected LoRa signal is equal to:

$$T_{seconds} = \frac{6062081 - 6062057}{2MHz} = 12 \times 10^{-6} s \tag{5.8}$$

The frequency of the detected LoRa signal can be calculated as follows:

$$freq = \frac{1}{T_{seconds}} Hz \tag{5.9}$$

Given a period equals to $12 \times 10^{-6} s$, the frequency of the detected signal will be equal

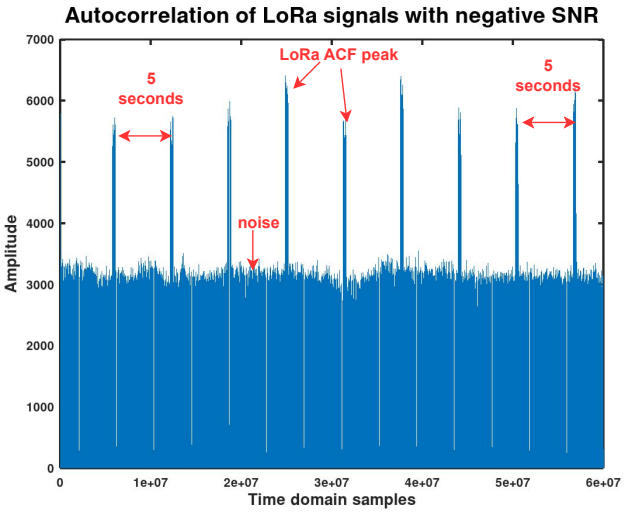

Figure 5.18: Autocorrelation graph of the Mount-bart LoRa signals with negative SNR.

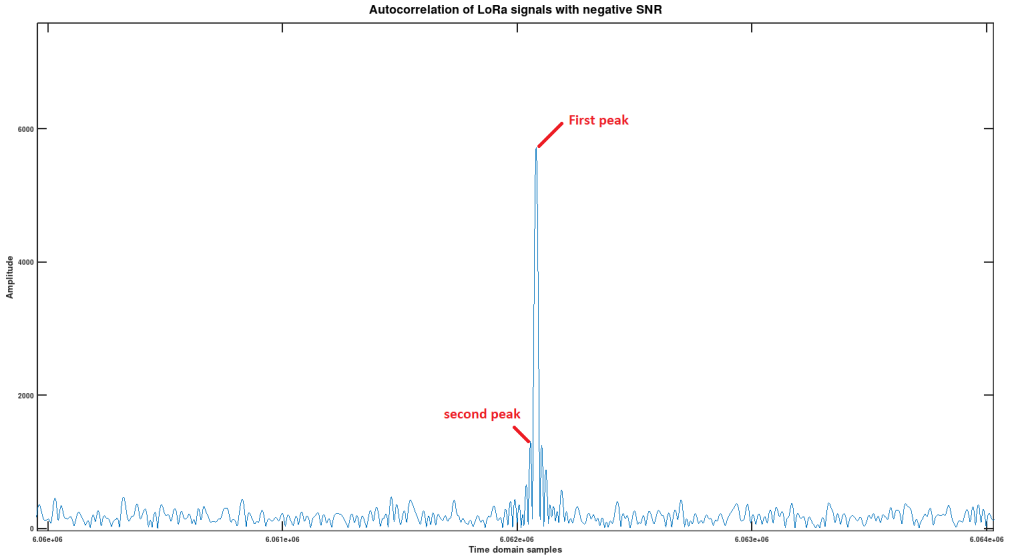

Figure 5.19: Autocorrelation graph of the Mount-bart First detected signal with negative SNR.

to 83.3 kHz. Since our Lora signal is operating at a carrier frequency of 868 MHz, the detected signal has a frequency of 868 MHz + 83.3 kHz = 868.083 MHz.

The Mount-Bart transmitter operates with a carrier frequency equals to 868 MHz and a channel bandwidth of 125 kHz. Thus, its center frequency would be: 868 MHz + (125 kHz / 2) = 868.0625 MHz. According to our algorithm, the measured center frequency is 868.083 MHz. The frequency shift (21 kHz) between the transmitted center frequency and the center frequency calculated by our algorithm is relatively small and could be the temperature difference, which results that the crystal oscillator in the transmitter may shift in frequency. This could result in a frequency shift in the transmitted LoRa signal.

In this experiment AoAs were measured for a rotation of the dual antenna receiver equals to 100 degrees. The AoAs of the 9 detected signals were measured and represented in Figure 5.20.

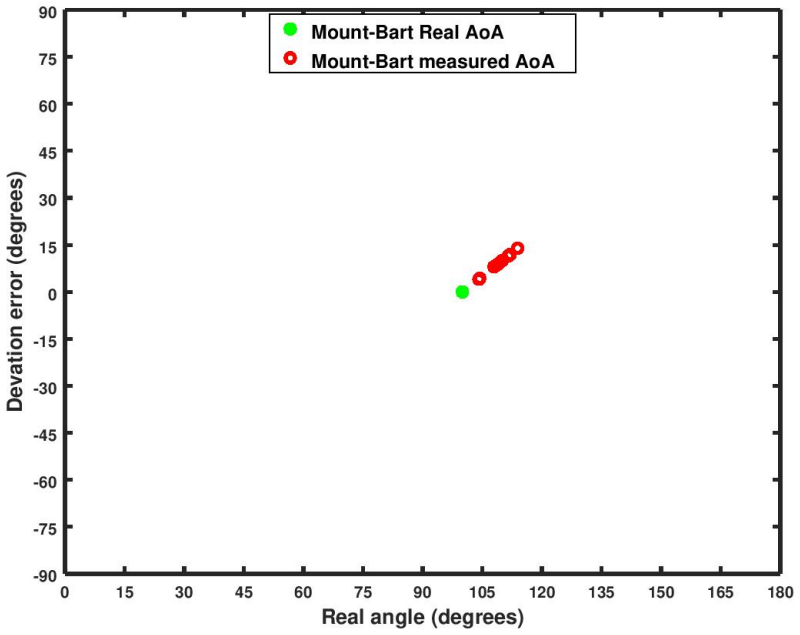

Figure 5.20: Angle deviation error for the Mount-Bart transmitter for 100 degrees true angle.

5.5/ MEASURING AOA OF LORA SIGNAL UNDER INTERFERENCE

LoRa technology encodes its signals using CSS. Therefore, LoRa introduces several SFs (from 7 to 12), which allow orthogonal transmissions to avoid interference and signal collisions. Interference occurs in the case of simultaneous receipt of two or more LoRa signals on the same channel and with the same SF.

When two or more LoRa signals are received simultaneously on the same channel and with the same SF, one packet will be lost if one signal is stronger than the other, and all packets will be lost if the two signals have the same power strength.

The *gr-lora* decoder used in Chapter 4 is able to decode only one signal from concurrent LoRa signals as long as they are on different SF and cannot manage two signals being received simultaneously on the same channel and with the same SF. Improving the decoding step is not in our contribution scope. To our knowledge, there is no previous work on receiving two LoRa signals simultaneously with the same modulation parameters.

This section concerns detecting and measuring AoAs of two concurrent LoRa signals with

the same received power, on the same channel and with the same SF.

5.5.1/ MEASURING AOA OF TWO CONCURRENT LORA SIGNALS USING FAST AUTOCORRELATION

Detecting and measuring the AoAs of two interfering LoRa can be a challenging task, however using the FFT and the autocorrelation function described in Figure 5.12, it will be possible to measure the AoA of both signals. The following are the steps of the proposed algorithm:

- **Band pass filter:** To compute the Fast autocorrelation function, the received signals should be passed through a band pass filter to isolate the frequency band of interest, which in this case is the frequency band used by the two interfering signals.
- **Fast autocorrelation:** Apply the FFT to compute the autocorrelation function of the received signals. The result of the fast autocorrelation will exhibit a maximum peak at zero time lag, which corresponds to the stronger frequency of the two signals, and many sub-peaks or mini-peaks that correspond to the weaker frequencies.
- **Identifying the peaks:** Utilize a threshold detecting mechanism to identify the maximum peak and sub-peaks of the autocorrelation function.
- **Measuring the AoA:** Utilizing the developed phase difference mechanism, the algorithm will measure the AoA of each peak once the maximum peak and sub-peaks have been detected.

5.5.2/ EXPERIMENTAL AND RESULTS

5.5.2.1/ EXPERIMENTAL SETUP

Our goal in this experiment is to validate our contribution for identifying two AoAs received simultaneously by the dual antenna receiver.

To achieve this, two LoRa RFM95 transceivers were configured to transmit the same packet simultaneously on the same SF (7) and channel bandwidth (125 kHz). Both transceivers transmit data at a 868 MHz carrier frequency with a transmit power of +14 dBm. Each transceiver was placed 45 degrees and 135 degrees away from the dual antenna receiver as shown in Figure 5.21.

To allow the two LoRa transmitters to transmit at the same time, we used a third transmitter. The third transmitter acts as a conductor and its role is to ensure the synchronization

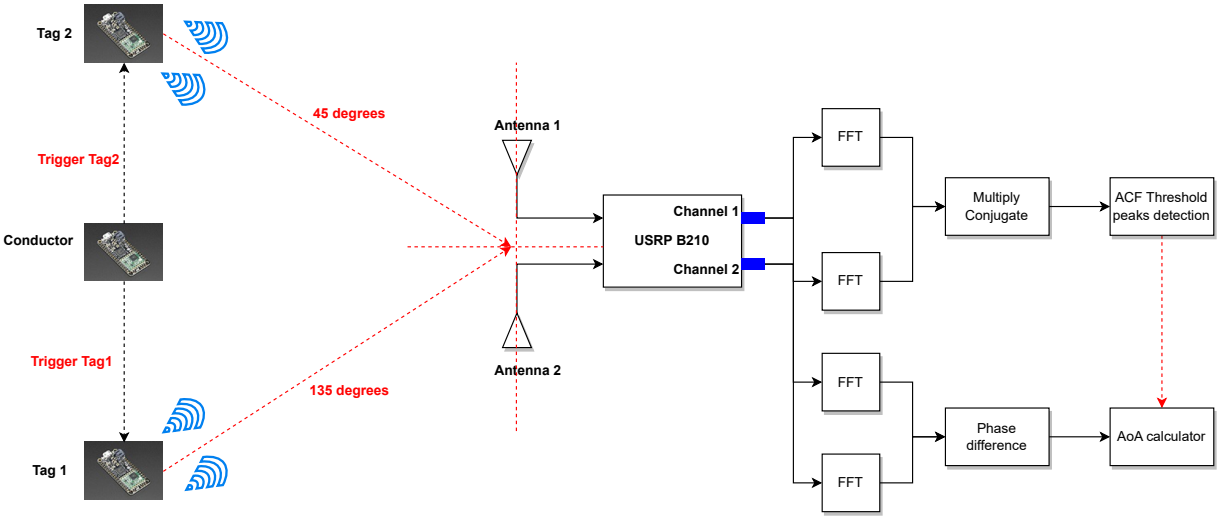

Figure 5.21: A GRC flow graph for the USRP B210 to compute the fast autocorrelation and AoA using a band pass filter.

of signal transmission by transmitters 1 and 2. Transmitters 1 and 2 are continuously listening for incoming signals from the conductor, and when a signal is received, each device open its transmit window immediately to send a response signal.

When the two LoRa signals are transmitted simultaneously, they will propagate through the air and reach the dual antenna receiver at slightly different times. The dual antenna receiver can then use the two received signals to compute the Fast autocorrelation function.

5.5.2.2/ MEASUREMENT DATA

On the USRP B210 side, the sampling frequency is equal to 2 MHz, and the FFT length is equal to 2048 bins. The result of the fast autocorrelation is shown in Figure 5.22 which consists of a maximum peak at the lag=0, and a number of sub-peaks around the lag=0 which reveals two different periodic LoRa signals. Thanks to the LoRa up chirp modulation, it is possible to distinguish the two simultaneous transmissions.

Our solution is to detect the maximum peak frequency and the sub-peaks frequencies and measuring the AoA of each detection. The results of this measurement is Figure 5.23.

Figure 5.23 shows the values of the AoAs of two simultaneous receptions (45 and 135 degrees). The x-axis shows the measured AoAs values, and the y-axis represents the deviation error of the measured AoAs from the two transmitters.

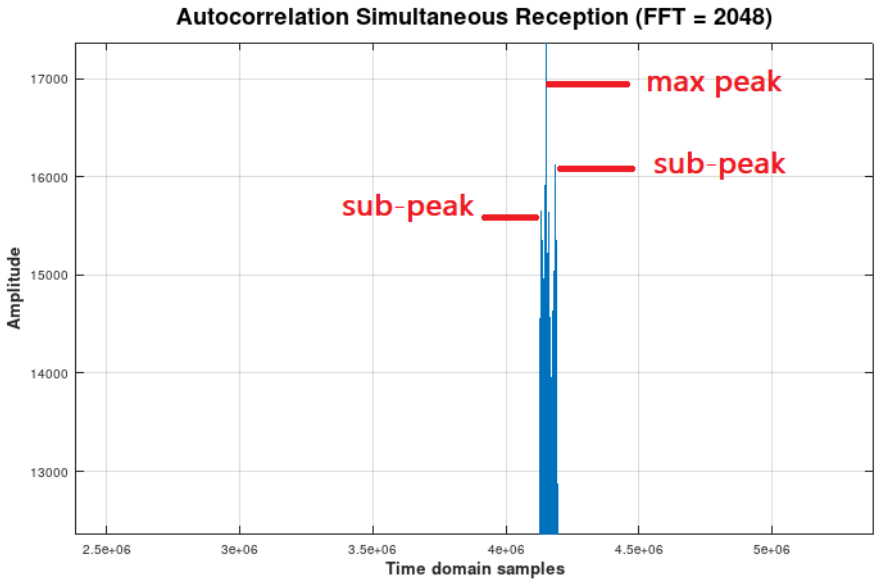

Figure 5.22: Autocorrelation peaks detection.

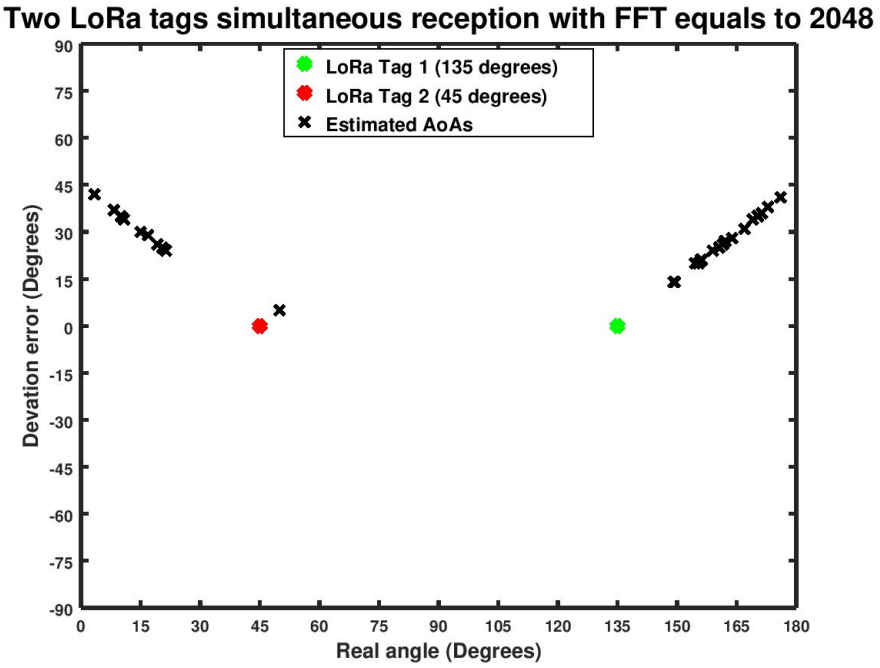

Figure 5.23: AoAs for two simultaneous receptions with FFT size equals to 2048.

In this measurement, we detected 30 peaks, including a maximum peak at the lag=0 and 29 sub-peaks frequencies around the lag=0. The algorithm used in the measurement was able to distinguish two distinct areas of AoAs, one corresponding to the AoAs related to transmitter 1 and the other corresponding to the AoAs related to transmitter 2. Despite this, The measured AoAs are not very close to the real AoA of the two transmitter.

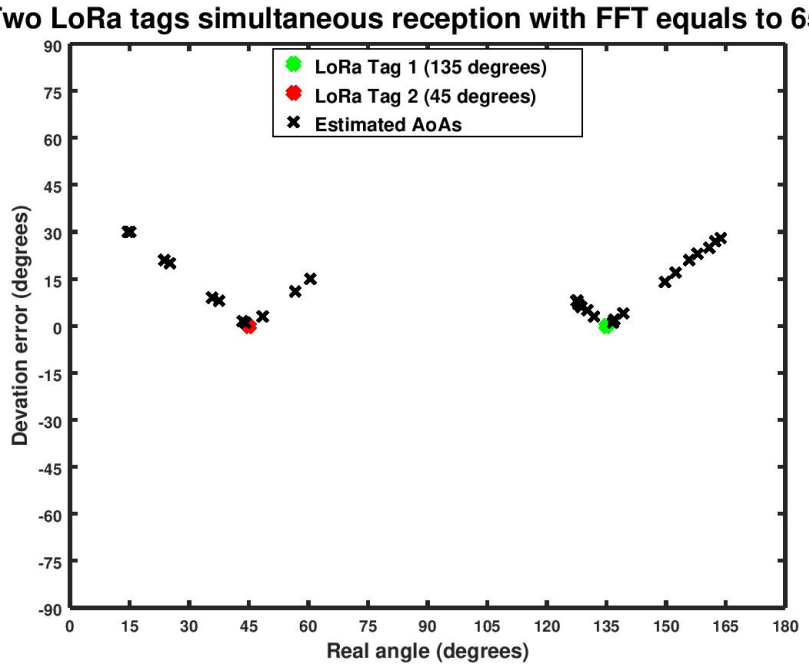

Figure 5.24: AoAs for two simultaneous receptions with FFT size equals to 65536.

To improve the accuracy, we performed the same measurement but with a maximum FFT size equals to 65536. Increasing the size of the FFT typically improves the frequency resolution of this measurement. In fact, for an FFT equal to 65536, the frequency resolution would be (2 MHz / 65536 = 30.5 Hz). This would allow us more accurate detection of peaks and sub-peaks in the frequency domain and could potentially help us to improve the distinction between two simultaneous receptions. The result of this improvement is illustrated in Figure 5.24.

Figure 5.24 reveals that when the FFT is equal to 65536, the AoAs measurements are more accurate and close to the true angle of transmitters 1 and 2 with a mean absolute error of 12 and 13 respectively.

5.6/ SUMMARY AND CONCLUSION

In this chapter, we have presented a new methodology for detecting and measuring the angle of arrival (AoA) of weak LoRa signals utilizing a Software Defined Radio platform. Our innovative solution named *Fast autocorrelation signal detection and AoA measurement* can detect LoRa signals and measure their AoAs at extremely low Signal-to-Noise ratio (SNR) levels. Moreover, our method has effectively detected and measured the AoAs of two interfering LoRa signals that were transmitted simultaneously with identical packet and configuration parameters. Through the analysis of the Fast autocorrelation

function of the received signals, we were able to differentiate and identify the maximum peak and sub-peaks corresponding to the two distinct transmissions.

Our proposed approach utilized a dual antenna USRP B210 based SDR receiver which exploits the Fast Fourier Transform (FFT) and autocorrelation function (ACF) of the signal received by the antennas. We demonstrated that by using a dual antenna SDR receiver, it is possible to receive two replicas of the same user signal, which can be used for both signal detection and AoA calculation. Moreover, the Fast autocorrelation approach is used to determine the existence of LoRa signals in the channel. Accordingly, the following approaches were proposed for detecting and measuring AoAs of weak LoRa signals using a dual antenna USRP B210 SDR receiver.

- **FFT Autocorrelation:** Applying the Fast Fourier transform (FFT) to the received signals by the two antennas to obtain the frequency domain representation of the data. Once the data are in the frequency domain, we applied autocorrelation function to study the similarity between the received LoRa signal and its delayed version.
- **Detecting the signal peak:** The result of the autocorrelation will served as a signal detector. The technique involved finding the maximum peak of the ACF and comparing it to a predefined threshold value. If the maximum value exceeds the threshold, then a signal is detected.
- **Phase difference and AoA calculations:** Once the peak of the ACF was detected, the AoA will be calculated using our phase difference developed algorithm.

To Evaluate the feasibility of our approach, a series of experiments were carried out in both indoor and outdoor environments.

In indoor, our results showed that our approach was able to detect LoRa signals at -20 dB below the noise floor when the LoRa tag was operating at low power transmission (TX), while maintaining excellent accuracy at the AoA. Thus, we have presented an efficient technique for deploying LoRa SDR gateways that leverage low signals and AoAs in indoor infrastructures. Our approach recommends that the dual antennas of the SDR must be oriented towards angles within the range of 45 to 135 degrees, with a maximum deviation error of 9 degrees.

In outdoor, we have been able to evaluate our approach over very long distances. The results showed that our approach was able to detect and measure AoA of LoRa signal with a negative SNR and with a distance separating the LoRa transmitter and the SDR receiver equals to 20 km.

IV

CONCLUSIONS AND PERSPECTIVES

6

GENERAL CONCLUSION

6.1/ SUMMARY OF THE PHD THESIS

Nowadays, the scientific and industrial communities are working on a solution that can complete The Global Navigation Satellite System (GNSS) for indoor environments. While GNSS systems are highly effective and accurate for outdoor tracking, their performance can suffer in indoor environments where GNSS signals are attenuated and reflected by walls and other obstacles. As a result, alternative indoor tracking systems have been developed for emergency applications. One such system is Radio direction finding using radio frequency (RF) angle of arrival (AoA). RF direction finding has been used in different fields including navigation of ships and aircraft, tracking humans and objects, and locate illegal or interfering targets. There are several methods for calculating the direction of arrival of the radio signal. However, providing accurate solution using RF AoA is still a challenge.

In recent years, radio frequency engineering has gained significant attention from both the scientific and industrial communities, and Software Defined Radio (SDR) has become an important concept in this field. SDR enables the use of programmable radio platforms that can be reconfigured to support different radio technologies and protocols, making it a versatile and adaptable tool for studying and investigating existing radio frequency technologies such as the Long-Range (LoRa) radio frequency technology. The objective of this thesis is to provide an indoor tracking solution exploiting the AoA of the LoRa technology in indoor environment using Software Defined Radio platform.

The main objective of this thesis is to design, develop and validate an accurate and low-cost indoor tracking system that exploits the AoAs of LoRa radio signals in indoor environments. Therefore, it is necessary to establish an infrastructure of LoRa radio frequency communication consisting of Anchor nodes whose coordinates are known and target nodes whose coordinates are to be determined. In this thesis, we propose the following contributions and perspectives.

Main Contributions

1. As a first step in the first contribution, an embedded software platform was developed to organize radio frequency communication between LoRa sensor nodes. The second step involved studying and investigating LoRa's physical layer in real-time using a Software Defined Radio platform. Through the SDR, we processed, demodulated, and decoded LoRa signals using the *gr-lora* library in GNU radio. It provides a set of signal processing blocks that can demodulate and decode LoRa signals using different configuration parameters.

2. In the second contribution, we proposed an indoor tracking system based on the AoA of a LoRa signal. We performed three steps to calculate the AoA: detecting the presence of a signal in the channel; measuring the phase of the received signal by each antenna of the SDR receiver, and calculate the phase difference among the antennas, as well as the AoA.

3. The third contribution involved the development of signal processing solution for detecting and measuring the AoA of LoRa signals operating below the noise level. We developed an innovative approach for detecting weak LoRa signals we called Fast autocorrelation. Our approach is based on Fast Fourier Transform (FFT) and autocorrelation function (ACF) to measure the autcorrelation of LoRa signal in the frequency domain. We demonstrated that the combination of FFT and ACF improves the detection accuracy and the signal-to-noise ratio level, and allows the detection of a weak LoRa signal while maintaining good angle of arrival accuracy.

4. Our approach was also successful in detecting and measuring the AoAs of two interfering LoRa signals with the same packet and same configuration parameters transmitting simultaneously. By analyzing the Fast autocorrelation function of the received signals, we identified the maximum peak and the sub-peaks, which corresponded to the two different transmissions. In situations where interference and multiple transmissions may occur, our approach is an efficient and accurate method of finding and measuring AoAs.

Feasibility Study: we conducted a feasibility study of our direction finding system with real LoRa transceivers. The direction finding system consisted of Adafruit Feather M0 modules containing a RFM95 LoRa transceiver, and the USRP B210 dual antenna based SDR receiver. The dual antenna USRP B210 was connected to a personal computer that runs the direction finding software. The software was implemented in GNU Radio, and the phase difference received by the antennas of the receiver, and thus the AoAs, were measured in real-time.

The experiments were done in both indoor and outdoor environments. In indoor, we conducted an experiment for two types of LoRa signals: strong signals with a positive signal-to-noise ratio, and weak signals with a negative signal-to-noise ratio (up to -20dB). We have shown that our system can measure the AoA with a maximum deviation error of 5 degrees for strong LoRa signals, and with a maximum deviation error of 12 degrees for weak LoRa signals.

In outdoor environment, we conducted an experiment to validate the performance of our system over long distances, which we believe that can be a challenge due to various factors that can affect the quality of our LoRa signal, and thus the measured AoA.

Notwithstanding the challenges, we were able to successfully detect and measure the AoA of a very weak LoRa signal over a distance equals to 20 km. This was achieved using our dual antenna B210 SDR receiver and the Fast autocorrelation signal detection and AoA measurement approach.

In conclusion, this dissertation involved creating an indoor tracking system that relies on the AoA of LoRa signals, utilizing a Software Defined Ratio. The findings from this research will be implemented in the *SYLOIN* project, with the plan to incorporate our AoA-based direction system into a customized embedded board.

6.2/ PERSPECTIVES AND FUTURE WORKS

In this thesis, we provided a low-cost and accurate direction of arrival system for LoRa signals using Software Defined Radio platform. We suggest possible directions for future studies including.

- **Three antennas array direction finding system:** In this thesis, our direction finding system can estimate the AoA of a LoRa signal on one dimension (azimuth or elevation). We suggest to use an array of three antennas, and thus, the AoA can be estimated in three dimensions (both azimuth and elevation dimensions), which can provide more accurate localization of the signal source. By comparing the phase differences of the received signal between the three antennas, triangulation can be performed to determine the location of the signal in three dimensional space.
- **Four antennas array direction finding system:** To perform an AoA estimation in a fully spherical coverage (0 to 360 degrees), at least four antennas are required. As we mentioned before, with three antennas, the AoA can be determined in a 3D space, but not with full coverage on the range of [0, 360] degrees. Thus, we suggest four or more antennas distributed uniformly on the surface of a sphere, the AoA can be estimated in any direction in 3D space with full coverage.

- **Improving the LoRa physical layer to decode very weak LoRa signals:** as described in this thesis, improving the decoding step of weak LoRa signals is not in our contribution scope. However, our developed Fast autocorrelation detection method can be used to improve the demodulating and decoding of weak LoRa signal. Moreover, we suggest to utilize an FFT threshold denoising approach to enhance the weak LoRa signal before it is passed through the *gr-lora* library for decoding. This approach is expected to improve the decoding of weak LoRa signals by enhancing the signal quality and reducing the impact of noise.

- **Interference of more than two LoRa transmitters:** In this thesis, we showed that the Fast autocorrelation method has proven to be an effective approach for detecting and measuring the AoA of two LoRa signals received simultaneously at the dual antenna receiver. In future studies, this method could be extended to detect and measure the AoA of more than two LoRa signals, which can be useful for tracking multiple LoRa devices. We suggest to use more than two antenna elements or multiple antenna elements along with the Fast autocorrelation approach to improve the accuracy of the AoA estimation.

- **Beamforming approach:** In this thesis, we have developed a Fast autocorrelation approach using a dual antenna USRP B210 SDR receiver to detect and measure the AoA of weak LoRa signals. This approach help us to save the battery life of the LoRa tag, while still allowing us to track its location. As mentioned in this thesis, demodulating and decoding weak LoRa signal was outside the scope of our contribution. Therefore, we suggest the following approach to overcome this problem.

  We propose to use a beamforming approach with the dual antenna of the SDR gateway to steer the signal towards the desired tag, in order to request an increase in its transmission power. This should help increase the SNR value and allow us to use the *gr-lora* library to decode the message.

  It is important to highlight that this scenario would only be necessary if the gateway requested a full power transmission from the tag. In most cases, the tag would transmit at low power to save energy, and the autocorrelation function we developed would be sufficient to detect and measure the AoA.

- **Multi-channel through autocorrelation:** Our Fast autocorrelation can detect and measure the AoA of weak LoRa signals operating in the same channel. Our approach can be extended to work with LoRa signals from multiple channels. Thus, we propose the following approach for multi-channel weak signals and AoA measurements.

  We suggest using multiple FIR bandpass filters to separate the signals in their specific channels, allowing us to measure the AoA of each signal within its specific

channel. This approach is effective because it allows us to focus on the signals within the frequency bands and help reduce interference from other signals.

- **Selection of the best gateways for localization:** The selection of the best gateways for localization could be done by combining the Received Signal Strength Indicator (RSSI) measurements to the Angle of Arrival (AoA).

  The objective will be to estimate the position of a LoRa tag in a building based on the measurements received by multiple gateways (typically 6 gateways). The two best gateways are selected based on their AoA measurements, which should be close to 90 degrees (where the angle deviation error is minimum), and the highest RSSI values. Thus, the selection of the best two gateways is based on the two criteria: the highest RSSI value and an AoA close to 90 degrees. To estimate the measurement error, we suggest using the following formula:

$$error = |Friis(RSSI) \times sin(Ferr(AoA)| \tag{6.1}$$

  Where *Friis(RSSI)* is the received signal strength indicator measured by the SDR gateway using the Friis free space equation, and *sin(Ferr(AoA))* is the sinus of the angle deviation error which converts the angle deviation error into distance error.

  Multiplying the *Friis(RSSI)* by the *sin(Ferr(AoA))* give us the error estimated in meters for each gateway. Therefore, the two gateways with the lowest errors will be selected.

BIBLIOGRAPHY

[1] Statista. Internet of Things (IoT) connected devices. URL: https://www.statista.com/statistics/471264/iot-number-of-connected-devices-worldwide/.

[2] Roberto Minerva, Abyi Biru, and Domenico Rotondi. "Towards a definition of the Internet of Things (IoT)". In: IEEE Internet Initiative 1.1 (2015), pp. 1–86.

[3] Da Zhang et al. "Localization technologies for indoor human tracking". In: 2010 5th international conference on future information technology. IEEE. 2010, pp. 1–6.

[4] Alan Bensky. Wireless positioning technologies and applications. Artech House, 2016.

[5] Feng Hu, Zhigang Zhu, and Jianting Zhang. "Mobile panoramic vision for assisting the blind via indexing and localization". In: European Conference on Computer Vision. Springer. 2014, pp. 600–614.

[6] Cole Gleason et al. "VizMap: Accessible visual information through crowdsourced map reconstruction". In: Proceedings of the 18th International ACM SIGACCESS Conference on Computers and Accessibility. 2016, pp. 273–274.

[7] Rainer Mautz and Sebastian Tilch. "Survey of optical indoor positioning systems". In: 2011 international conference on indoor positioning and indoor navigation. IEEE. 2011, pp. 1–7.

[8] Byung Hwa Kim et al. "Localization of a mobile robot using images of a moving target". In: Proceedings 2001 ICRA. IEEE International Conference on Robotics and Automation (Cat. No. 01CH37164). Vol. 1. IEEE. 2001, pp. 253–258.

[9] Brett Ausmeier, Thomas Campbell, and Sonia Berman. "Indoor Navigation Using a Mobile Phone". In: 2012 African Conference for Sofware Engineering and Applied Computing. 2012, pp. 109–115. DOI: 10.1109/ACSEAC.2012.26.

[10] Nishkam Ravi et al. "Indoor Localization Using Camera Phones". In: Seventh IEEE Workshop on Mobile Computing Systems & Applications (WMCSA'06 Supplement). Vol. Supplement. 2007, pp. 1–7. DOI: 10.1109/WMCSA.2006.4625206.

[11] Martin Werner, Moritz Kessel, and Chadly Marouane. "Indoor positioning using smartphone camera". In: 2011 International Conference on Indoor Positioning and Indoor Navigation. 2011, pp. 1–6. DOI: 10.1109/IPIN.2011.6071954.

[12] Ernesto Martin Gorostiza et al. "Infrared sensor system for mobile-robot positioning in intelligent spaces". In: Sensors 11.5 (2011), pp. 5416–5438.

[13] Ke Wang et al. “Indoor infrared optical wireless localization system with background light power estimation capability”. In: Optics Express 25.19 (2017), pp. 22923–22931.

[14] Mike Hazas and Andy Hopper. “Broadband ultrasonic location systems for improved indoor positioning”. In: IEEE Transactions on mobile Computing 5.5 (2006), pp. 536–547.

[15] Faheem Ijaz et al. “Indoor positioning: A review of indoor ultrasonic positioning systems”. In: 2013 15th International Conference on Advanced Communications Technology (ICACT). IEEE. 2013, pp. 1146–1150.

[16] Kaikai Liu, Xinxin Liu, and Xiaolin Li. “Guoguo: Enabling fine-grained indoor localization via smartphone”. In: Proceeding of the 11th annual international conference on Mobile systems, applications, and services. 2013, pp. 235–248.

[17] Kaikai Liu, Xinxin Liu, and Xiaolin Li. “Guoguo: Enabling Fine-Grained Smartphone Localization via Acoustic Anchors”. In: IEEE Transactions on Mobile Computing 15.5 (2016), pp. 1144–1156. DOI: 10.1109/TMC.2015.2451628.

[18] Toshihiko Komine and Masao Nakagawa. “Fundamental analysis for visible-light communication system using LED lights”. In: IEEE transactions on Consumer Electronics 50.1 (2004), pp. 100–107.

[19] Ye-Sheng Kuo et al. “Luxapose: Indoor positioning with mobile phones and visible light”. In: Proceedings of the 20th annual international conference on Mobile computing and networking. 2014, pp. 447–458.

[20] Toni Adame et al. “IEEE 802.11 AH: the WiFi approach for M2M communications”. In: IEEE Wireless Communications 21.6 (2014), pp. 144–152.

[21] Deepak Vasisht, Swarun Kumar, and Dina Katabi. “{Decimeter-Level} Localization with a Single {WiFi} Access Point”. In: 13th USENIX Symposium on Networked Systems Design and Implementation (NSDI 16). 2016, pp. 165–178.

[22] Manikanta Kotaru et al. “Spotfi: Decimeter level localization using wifi”. In: Proceedings of the 2015 ACM Conference on Special Interest Group on Data Communication. 2015, pp. 269–282.

[23] Alessandro Cidronali et al. “Analysis and performance of a smart antenna for 2.45-GHz single-anchor indoor positioning”. In: IEEE Transactions on Microwave Theory and Techniques 58.1 (2009), pp. 21–31.

[24] Shuyu Shi et al. “Accurate location tracking from CSI-based passive device-free probabilistic fingerprinting”. In: IEEE Transactions on Vehicular Technology 67.6 (2018), pp. 5217–5230.

[25] Jin Ren et al. “A novel high precision and low consumption indoor positioning algorithm for internet of things”. In: IEEE Access 7 (2019), pp. 86874–86883.

[26] K Myungchul, L Jeongkeun, T Kwon, et al. “A multi-pronged approach for indoor positioning with WiFi magnetic and cellular signals”. In: 2014 International Conference on Indoor Positioning and Indoor Navigation, IPIN 2014-Conference Proceedings. 2014, pp. 27–30.

[27] Tan Kim Geok et al. “Review of indoor positioning: Radio wave technology”. In: Applied Sciences 11.1 (2020), p. 279.

[28] Faheem Zafari, Athanasios Gkelias, and Kin K Leung. “A survey of indoor localization systems and technologies”. In: IEEE Communications Surveys & Tutorials 21.3 (2019), pp. 2568–2599.

[29] Romeo Giuliano et al. “Indoor localization system based on bluetooth low energy for museum applications”. In: Electronics 9.6 (2020), p. 1055.

[30] Fei Liu et al. “An indoor localization method for pedestrians base on combined UWB/PDR/Floor map”. In: Sensors 19.11 (2019), p. 2578.

[31] Abdulrahman Alarifi et al. “Ultra wideband indoor positioning technologies: Analysis and recent advances”. In: Sensors 16.5 (2016), p. 707.

[32] Stefania Monica and Federico Bergenti. “Hybrid indoor localization using WiFi and UWB technologies”. In: Electronics 8.3 (2019), p. 334.

[33] Anahid Basiri et al. “Indoor location based services challenges, requirements and usability of current solutions”. In: Computer Science Review 24 (2017), pp. 1–12.

[34] Gabriel Deak, Kevin Curran, and Joan Condell. “A survey of active and passive indoor localisation systems”. In: Computer Communications 35.16 (2012), pp. 1939–1954.

[35] Abdul Alif Wafi Ab Razak and Fahmi Samsuri. “Active RFID-based Indoor Positioning System (IPS) for industrial environment”. In: 2015 IEEE International RF and Microwave Conference (RFM). IEEE. 2015, pp. 89–91.

[36] SIGFOX. Available online: URL: https://www.sigfox.com/.

[37] Bharat S Chaudhari, Marco Zennaro, and Suresh Borkar. “LPWAN technologies: Emerging application characteristics, requirements, and design considerations”. In: Future Internet 12.3 (2020), p. 46.

[38] Michiel Aernouts et al. “Sigfox and LoRaWAN datasets for fingerprint localization in large urban and rural areas”. In: Data 3.2 (2018), p. 13.

[39] Hazem Sallouha, Alessandro Chiumento, and Sofie Pollin. “Localization in long-range ultra narrow band IoT networks using RSSI”. In: 2017 IEEE International Conference on Communications (ICC). IEEE. 2017, pp. 1–6.

[40] LoRa. Available online: URL: https://www.semtech.com/lora.

[41] Lorenzo Vangelista. “Frequency shift chirp modulation: The LoRa modulation”. In: IEEE Signal Processing Letters 24.12 (2017), pp. 1818–1821.

[42] Umber Noreen, Ahcène Bounceur, and Laurent Clavier. “A study of LoRa low power and wide area network technology”. In: 2017 International Conference on Advanced Technologies for Signal and Image Processing (ATSIP). IEEE. 2017, pp. 1–6.

[43] Shilpa Devalal and A Karthikeyan. “LoRa technology-an overview”. In: 2018 second international conference on electronics, communication and aerospace technology (ICECA). IEEE. 2018, pp. 284–290.

[44] Martin Bor and Utz Roedig. “LoRa transmission parameter selection”. In: 2017 13th International Conference on Distributed Computing in Sensor Systems (DCOSS). IEEE. 2017, pp. 27–34.

[45] Nicolas Sornin. “M. Luis (Semtech), T. Eirich (IBM), T. Kramp (IBM), and O. Hersent (Actility)”. In: LoRaWAN Specification V1 (2015).

[46] Yi Yu et al. “Adaptive multi-channels allocation in LoRa networks”. In: IEEE Access 8 (2020), pp. 214177–214189.

[47] L’houssaine Aarif, Mohamed Tabaa, and Hanaa Hachimi. “Experimental test and performance of RSSI-based indoor localization in LoRa Networks”. In: (2022).

[48] Mahnoor Anjum et al. “RSSI fingerprinting-based localization using machine learning in LoRa networks”. In: IEEE Internet of Things Magazine 3.4 (2020), pp. 53–59.

[49] Bashima Islam et al. “Lorain: Making a case for lora in indoor localization”. In: 2019 IEEE International Conference on Pervasive Computing and Communications Workshops (PerCom Workshops). IEEE. 2019, pp. 423–426.

[50] Sebastian Sadowski and Petros Spachos. “Rssi-based indoor localization with the internet of things”. In: IEEE Access 6 (2018), pp. 30149–30161.

[51] Nico Podevijn et al. “Performance comparison of rss algorithms for indoor localization in large open environments”. In: 2018 International Conference on Indoor Positioning and Indoor Navigation (IPIN). IEEE. 2018, pp. 1–6.

[52] Kyungki Kim et al. “Feasibility of LoRa for smart home indoor localization”. In: Applied Sciences 11.1 (2021), p. 415.

[53] Nico Podevijn et al. “TDoA-based outdoor positioning in a public LoRa network”. In: 12th European Conference on Antennas and Propagation (EuCAP 2018). IET. 2018, pp. 1–4.

[54] David Plets et al. “Experimental performance evaluation of outdoor tdoa and rss positioning in a public lora network”. In: 2018 International Conference on Indoor Positioning and Indoor Navigation (IPIN). IEEE. 2018, pp. 1–8.

[55] Michiel Aernouts et al. “TDAoA: A combination of TDoA and AoA localization with LoRaWAN”. In: Internet of Things 11 (2020), p. 100236.

[56] Michiel Aernouts et al. “Combining TDoA and AoA with a particle filter in an outdoor LoRaWAN network”. In: 2020 IEEE/ION Position, Location and Navigation Symposium (PLANS). IEEE. 2020, pp. 1060–1069.

[57] Kyung-Jin Baik, Sangjoon Lee, and Byung-Jun Jang. “Hybrid RSSI-AoA positioning system with single time-modulated array receiver for LoRa IoT”. In: 2018 48th European Microwave Conference (EuMC). IEEE. 2018, pp. 1133–1136.

[58] Hussein Kwasme and Sabit Ekin. “RSSI-based localization using LoRaWAN technology”. In: IEEE Access 7 (2019), pp. 99856–99866.

[59] Andrew Mackey and Petros Spachos. “LoRa-based localization system for emergency services in GPS-less environments”. In: IEEE INFOCOM 2019-IEEE Conference on Computer Communications Workshops (INFOCOM WKSHPS). IEEE. 2019, pp. 939–944.

[60] Mohamed Tabaa, Hanaa Hachimi, et al. “Experimental test and performance of RSSI-based indoor localization in LoRa Networks”. In: Procedia Computer Science 203 (2022), pp. 420–425.

[61] Richa Bharadwaj, Clive Parini, and Akram Alomainy. “Experimental investigation of 3-D human body localization using wearable ultra-wideband antennas”. In: IEEE Transactions on Antennas and Propagation 63.11 (2015), pp. 5035–5044.

[62] Dong-Ho Shin and Tae-Kyung Sung. “Comparisons of error characteristics between TOA and TDOA positioning”. In: IEEE Transactions on Aerospace and Electronic Systems 38.1 (2002), pp. 307–311.

[63] Henk Wymeersch, Jaime Lien, and Moe Z Win. “Cooperative localization in wireless networks”. In: Proceedings of the IEEE 97.2 (2009), pp. 427–450.

[64] Swen Leugner, Mathias Pelka, and Horst Hellbrück. “Comparison of wired and wireless synchronization with clock drift compensation suited for U-TDoA localization”. In: 2016 13th workshop on positioning, navigation and communications (WPNC). IEEE. 2016, pp. 1–4.

[65] Vitomir Djaja-Josko, Jerzy Kolakowski, and Jozef Modelski. “TDOA estimation using a pair of synchronized DW1000 based anchor nodes”. In: 2018 22nd International Microwave and Radar Conference (MIKON). IEEE. 2018, pp. 57–60.

[66] Huthaifa Obeidat et al. “A review of indoor localization techniques and wireless technologies”. In: Wireless Personal Communications 119.1 (2021), pp. 289–327.

[67] Jie Xiong and Kyle Jamieson. “{ArrayTrack}: A {Fine-Grained} Indoor Location System”. In: 10th USENIX Symposium on Networked Systems Design and Implementation (NSDI 13). 2013, pp. 71–84.

[68] Ahmed Badawy et al. “A simple aoa estimation scheme”. In: arXiv preprint arXiv:1409.5744 (2014).

[69] Hsieh-Chung Chen et al. “Determining RF angle of arrival using COTS antenna arrays: A field evaluation”. In: MILCOM 2012-2012 IEEE Military Communications Conference. IEEE. 2012, pp. 1–6.

[70] Shun Kawakami, Shohei Ikeda, and Tomoaki Ohtsuki. “Localization using iterative angle of arrival method sharing snapshots of coherent subarrays”. In: Proceedings: APSIPA ASC 2009: Asia-Pacific Signal and Information Processing Association, 2009 Annual Summit and Conference. Asia-Pacific Signal and Information Processing Association, 2009 Annual . . . 2009, pp. 883–886.

[71] Zheng Yang, Zimu Zhou, and Yunhao Liu. “From RSSI to CSI: Indoor localization via channel response”. In: ACM Computing Surveys (CSUR) 46.2 (2013), pp. 1–32.

[72] Di He et al. “3-D spatial spectrum fusion indoor localization algorithm based on CSI-UCA smoothing technique”. In: IEEE Access 6 (2018), pp. 59575–59588.

[73] Xuyu Wang et al. “CSI-based fingerprinting for indoor localization: A deep learning approach”. In: IEEE Transactions on Vehicular Technology 66.1 (2016), pp. 763–776.

[74] Apurv Bhartia et al. “Harnessing frequency diversity in wi-fi networks”. In: Proceedings of the 17th annual international conference on Mobile computing and networking. 2011, pp. 253–264.

[75] Blossom Eric. Exploring Gnu Radio. URL: http://www.gnu.org/software/gnuradio/doc/exploring-gnuradio.html.

[76] Ettus. Ettus Research, The leader in Software Defined Radio (SDR). URL: https://www.ettus.com/.

[77] Ettus. Ettus Research, The leader in Software Defined Radio (SDR). URL: https://www.ettus.com/wp-content/uploads/2019/01/b200-b210_spec_sheet.pdf.

[78] AD9361 RF Agile Transceiver. URL: https://www.analog.com/en/products/ad9361.html#product-overview.

[79] GNU Radio. The free & Open Software Radio System. URL: https://www.gnuradio.org/.

[80] GNU Operating System. URL: https://www.gnu.org/software/software.en.html.

[81] C.E. Shannon. “Communication in the Presence of Noise”. In: Proceedings of the IRE 37.1 (1949), pp. 10–21. DOI: 10.1109/JRPROC.1949.232969.

[82] Matthew Knight and Balint Seeber. “Decoding LoRa: Realizing a modern LPWAN with SDR”. In: Proceedings of the GNU Radio Conference. Vol. 1. 1. 2016.

[83] Pieter Robyns et al. “A Multi-Channel Software Decoder for the LoRa Modulation Scheme.” In: IoTBDS. 2018, pp. 41–51.

[84] Eryk Schiller, Silas Weber, and Burkhard Stiller. “Design and evaluation of an SDR-based LoRA cloud radio access network”. In: 2020 16th International Conference on Wireless and Mobile Computing, Networking and Communications (WiMob). IEEE. 2020, pp. 1–7.

[85] MyriadRF. MyriadRF-LoRa-SDR. URL: https://github.com/myriadrf/LoRa-SDR.

[86] Jack Capon. “High-resolution frequency-wavenumber spectrum analysis”. In: Proceedings of the IEEE 57.8 (1969), pp. 1408–1418.

[87] Minghui Li, Yilong Lu, and Bo He. “Array signal processing for maximum likelihood direction-of-arrival estimation”. In: Journal of Electrical and Electronic Systems 3.1 (2013), p. 117.

[88] Wang Tao et al. “A modified MUSIC to estimate DOA of the coherent narrowband sources based on UCA”. In: 2006 International Conference on Communication Technology. IEEE. 2006, pp. 1–4.

[89] Roald Goossens and Hendrik Rogier. “Closed-form 2D angle estimation with a spherical array via spherical phase mode excitation and ESPRIT”. In: 2008 IEEE International Conference on Acoustics, Speech and Signal Processing. IEEE. 2008, pp. 2321–2324.

[90] Meng-Chang Hua, Cheng-Han Hsu, and Hsin-Chin Liu. “Implementation of direction-of-arrival estimator on software defined radio platform”. In: 2012 8th International Symposium on Communication Systems, Networks & Digital Signal Processing (CSNDSP). IEEE. 2012, pp. 1–4.

[91] Akinbiyi Akindoyin, Marc Willerton, and Athanassios Manikas. “Localization and array shape estimation using software defined radio array testbed”. In: 2014 IEEE 8th Sensor Array and Multichannel Signal Processing Workshop (SAM). IEEE. 2014, pp. 189–192.

[92] Mirel PĂUN, Răzvan TAMAS, and Ion Marghescu. “A Software-Defined Radio Approach for Direction Finding”. In: UPB Sci. Bull., Series C 77.4 (2015).

[93] Noori BniLam et al. “LoRay: AoA estimation system for long range communication networks”. In: IEEE Transactions on Wireless Communications 20.3 (2020), pp. 2005–2018.

[94] Miklós Maróti et al. “Radio interferometric geolocation”. In: Proceedings of the 3rd international conference on Embedded networked sensor systems. 2005, pp. 1–12.

[95] GNU Radio. Polymorphic Types (PMTs). URL: https://wiki.gnuradio.org/index.php?title=Polymorphic_Types_(PMTs).

[96] Li-Jen Shang and Kuo-Kai Shyu. “A method for extracting chaotic signal from noisy environment”. In: Chaos, Solitons & Fractals 42.2 (2009), pp. 1120–1125.

[97] Robert Vautard, Pascal Yiou, and Michael Ghil. “Singular-spectrum analysis: A toolkit for short, noisy chaotic signals”. In: Physica D: Nonlinear Phenomena 58.1-4 (1992), pp. 95–126.

[98] Mengjiao Wang, Weiyu Yu, and Jiuchao Feng. “An adaptive denoising algorithm for chaotic signals based on complete ensemble empirical mode decomposition”. In: International Journal of Information and Communication Technology 11.4 (2017), pp. 564–575.

[99] Ji Shu-Yao et al. “Application of stochastic resonance technology in underwater acoustic weak signal detection”. In: OCEANS 2016-Shanghai. IEEE. 2016, pp. 1–5.

[100] Thomas Kokumo Yesufu and Abimbola Oyewole Atijosan. “Weak Amplitude Modulated (AM) Signal Detection Algorithm for Software-Defined Radio Receivers”. In: International Journal of Intelligent Information Systems 4.4 (2015), p. 79.

[101] Ivan V Malygin et al. “Radio signal detection using machine-learning approach”. In: Proc. CEUR Workshop. 2017, pp. 57–61.

[102] Xuanchao Liu and Xiaoli Feng. “Research on weak signal detection for downhole acoustic telemetry system”. In: 2010 3rd International Congress on Image and Signal Processing. Vol. 9. IEEE. 2010, pp. 4432–4435.

[103] Wang Xiao-Fei et al. “A chaotic signal denoising method developed on the basis of noise-assisted nonuniformly sampled bivariate empirical mode decomposition”. In: Acta Physica Sinica 63.17 (2014).

[104] Jie Wang et al. “Current progress on weak signal detection”. In: 2013 International Conference on Quality, Reliability, Risk, Maintenance, and Safety Engineering (QR2MSE). IEEE. 2013, pp. 1812–1818.

[105] SJ Thiruvengadam et al. “Signal detection algorithm using discrete wavelet transform and radon transform”. In: IETE journal of research 50.5 (2004), pp. 353–360.

[106] Z Do et al. “Detection method of weak low-frequency electromagnetic signal based on multi-layer autocorrelation”. In: Int. J. Signal Process., Image Process. Pattern Recognit. 9.4 (2016), pp. 27–36.

[107] Shin So et al. “A Study of Peak Finding Algorithms for the Autocorrelation Function of Speech Signal”. In: Journal of The Korea Society of Computer and Information 21.12 (2016), pp. 131–137.

[108] Wei-Lung Mao et al. “Design of peak-finding algorithm on acquisition of weak GPS Signals”. In: 2006 IEEE International Conference on Systems, Man and Cybernetics. Vol. 3. IEEE. 2006, pp. 1820–1825.

List of Figures

List of Tables

List of Definitions

- **ACF**: Autocorrelation function
- **ADC**: Analog to Digital Converter
- **AM**: Amplitude Modulation
- **ANN**: Artificial Neural Network
- **AoA**: Angle of Arrival
- **AP**: Access Point
- **BLE**: Bluetooth Low Energy
- **BPSK**: Binary Phase Shift Keying
- **BW**: Bandwidth
- **C/A**: Coarse/Acquisition code
- **CF**: Carrier Frequency
- **CR**: Coding Rate
- **CRC**: Cyclic Redundancy Check
- **CSI**: Channel State Information
- **CSS**: Chirp Spread Spectrum
- **DAC**: Digital to Analog Converter
- **DFT**: Discrete Fourier Transform
- **DoA**: Direction of Arrival
- **DSP**: Digital Signal Processing
- **DWT**: Discrete Wavelet Transform
- **ESPIRIT**: Estimation of Signal Parameters via Rotational Invariance Technique

- **Femto-st**: Franche-Comté Électronique Mécanique Thermique et Optique - Sciences et Technologies
- **FFT**: Fast Fourier Transform
- **FM**: Frequency Modulation
- **FPGA**: Field Programmable Gate Array
- **FSK**: Frequency Shift Keying
- **GFSK**: Gaussian Frequency Shift Keying
- **GPP**: General Purpose Processor
- **GRC**: GNU Radio Companion
- **HF**: High Frequency
- **ID**: Unique Identifier code
- **IF**: Intermediate Frequency
- **IoT**: Internet of Things
- **ISM**: Industrial, Scientific and Medical
- **LED**: Light Emitting Diode
- **LoRa**: Long-Range
- **LOS**: Line Of Sight
- **ML**: Machine Learning
- **ML**: Maximum Likelihood
- **MQTT**: Message Queuing Telemetry Transport
- **MUSIC**: Multiple Signal Classification
- **NIC**: Network Interface Controller
- **NLOS**: Non Line Of Sight
- **PCB**: Print Circuit Board
- **PMT**: Polymorphic Types Messaging
- **PSD**: Power Spectral Density
- **PSK**: Phase Shift Keying

- **RF**: Radio Frequency
- **RFID**: Radio Frequency Identification
- **RSSI**: Received Signal Strength Indicator
- **SDR**: Software Defined Radio
- **SF**: Spreading Factor
- **SNR**: Signal-to-noise ratio
- **SURF**: Speeded Up Robust Features
- **SWIG**: Simplified Wrapper and Interface Generator
- **SYLOIN**: Système de Localisation en Intérieure
- **TDoA**: Time Differential of Arrival
- **TMA**: Time Modulated Array
- **ToA**: Time of Arrival
- **TP**: Transmission Power
- **UHD**: USRP Hardware Driver
- **UHF**: Ultra High Frequency
- **ULA**: Uniform Linear Array
- **UNB**: Ultra Narrow Band
- **USRP**: Universal Software Radio Peripheral
- **UUID**: Universally Unique Identifier
- **UWB**: Ultra-Wideband
- **VLC**: Visible Light communication
- **WLAN**: Wireless Local Area Network
- **WPAN**: Wireless Personal Area Network
- **WT**: Wavelet Transform
- **GFSK**: Gaussian Frequency Shift Keying
- **GPS**: Global Positioning System
- **GRC**: GNU Radio Companion

V

Appendix

A

LoRa Transceiver code

```
1 /*
2  * Author: Zeaiter Hussein
3  * Date:   8 march, 2023
4  */
5 #include <SPI.h>
6 #include <RH_RF95.h>
7
8
9
10 #define RFM95_CS 8 // Specific to the feather 32u4 and m0
11 #define RFM95_RST 4 // Specific to the feather 32u4 and m0
12 #define RFM95_INT 3 // Specific to the feather m0
13 //#define RFM95_INT 7 // Specific to the feather 32u4
14 #define RF95_FREQ 868 //acceptable values are 868 or 915 MHz
15 #define RF95_PWR 14 //acceptable range includes all integers
     between 5 and 23 dBm
16 String OPERATOR = "Feather:ID1"; //name of the user sending from
     this console
17
18 RH_RF95 rf95(RFM95_CS, RFM95_INT);
19
20 String message="Operator:FeatherM0:ID1";
21 //char * MACADD = "00C";
22
23 long lastSendTime = 0; //last send time
24 int interval = 3000;   // interval between sends
25 int send_counter = 0;
26
```

```
27  char reg0x1D;
28
29
30 void setup() {
31
32   // pinMode(RFM95_RST, OUTPUT);
33    //digitalWrite(RFM95_RST, HIGH);
34
35    pinMode(4, OUTPUT);
36    digitalWrite(4, HIGH);
37
38    while (!Serial);
39    Serial.begin(9600);
40    //delay(100);
41
42    Serial.println("Booting LoRa Radio");
43
44    // manual reset
45    digitalWrite(RFM95_RST, LOW);
46    delay(10);
47    digitalWrite(RFM95_RST, HIGH);
48    delay(10);
49
50    while (!rf95.init()) {
51      Serial.println("LoRa Radio Init Failed");
52      while (1);
53    }
54    Serial.println("LoRa Radio OK!");
55
56
57
58    // If you are using RFM95/96/97/98 modules which uses the
      PA_BOOST transmitter pin, then
59    // you can set transmitter powers from 5 to 23 dBm:
60
61     // Defaults after init are 434.0MHz, 13dBm, Bw = 125 kHz, Cr
      = 4/5, Sf = 128chips/symbol, CRC on
62    // rf95.setModemConfig(RH_RF95::Bw125Cr45Sf128);// bandwith =
      125KHz, Code Rate = 4/5, Spreading Factor = 2pow7
```

```
63    // config(13, 868.1, 250, 8, 8);
64
65    // Defaults after init are 434.0MHz, modulation
      GFSK_Rb250Fd250, +13dbM
66    if (!rf95.setFrequency(RF95_FREQ)) {
67      Serial.println("setFrequency failed");
68      while (1);
69    }
70    Serial.print("Freq set to: "); Serial.print(RF95_FREQ); Serial
      .println("MHz");
71
72    // Setup Spreading Factor (6 ~ 12)
73    rf95.setSpreadingFactor(7); //spreading factor = 6 ===>
      implicit header on
74
75   // Setup BandWidth, option:
      7800,10400,15600,20800,31250,41700,62500,125000,250000,500000
76   //Lower BandWidth for longer distance.
77   rf95.setSignalBandwidth(125000);
78
79   // Setup Coding Rate:5-->(4/5),6-->(4/6),7-->(4/7),8-->(4/8)
80   rf95.setCodingRate4(8);
81
82    // The default transmitter power is 13dBm, using PA_BOOST.
83    rf95.setTxPower(RF95_PWR,false);//False: we active PA_BOOST ,
      and TRUE: we disable the PA_BOOST
84    Serial.print("TXPower set to: "); Serial.print(RF95_PWR);
      Serial.println("dBm");
85
86   //rf95.setPayloadCRC(false);
87
88   // rf95.setLowDatarate();
89
90   //rf95.setImplicitHeader();
91
92   //rf95.setSyncword();
93   //rf95.setPreambleLength(8);
94
95   // rf95.setLNAGain();
```

```
96
97    Serial.println("Ready!");
98
99 }
100
101 void loop()
102
103 {
104
105     //Avoid collisions between LoRa transmissions, each tag has
      its own sending interval
106     if (millis() - lastSendTime > interval) {
107
108       message = OPERATOR;
109
110
111     //explode string to char array for sending
112     int messageSize = message.length()+1;
113     //int messageSize = OPERATOR.length()+1;
114     char radiopacket[messageSize];
115     message.toCharArray(radiopacket, messageSize);
116
117     //send the message OTA
118     //Serial.print(message);
119     delay(10);
120     rf95.send((uint8_t *)radiopacket, messageSize);
121     delay(10);
122     rf95.waitPacketSent();
123     Serial.print("Message sent : ");
124     send_counter = send_counter + 1;
125     Serial.println(send_counter);
126
127
128     //report and clean up
129     //Serial.println(OPERATOR);
130     //message="MacAddress:00";
131
132     lastSendTime = millis();
133     interval = 5000;
```

```
134       }
135
136       message = "OPERATOR : " + OPERATOR;
137       uint8_t messageSize = message.length()+1;
138       uint8_t buf[RH_RF95_MAX_MESSAGE_LEN];
139       uint8_t len = sizeof(buf);
140
141
142       //receiving messages from other LoRa transceivers
143       if (rf95.recv(buf, &messageSize))
144       {
145         RH_RF95::printBuffer("Received: ", buf, messageSize);
146         Serial.print("Receiving from..."); delay(10);
147         Serial.println((char*)buf);
148         //Serial.print("Message Size is:");Serial.println((sizeof(
      buf))/(sizeof(uint8_t)));
149         //Serial.print("RSSI: "); Serial.println(rf95.lastRssi(),
      DEC);
150
151       }
152
153 }
```

B

GNU Radio: Phase and AoA Calculator

```
1  /* -*- c++ -*- */
2  /*
3   * Copyright 2021 gr-LoRaATC Hussein Zeaiter.
4   *
5   * This is free software; you can redistribute it and/or modify
6   * it under the terms of the GNU General Public License as published by
7   * the Free Software Foundation; either version 3, or (at your option)
8   * any later version.
9   *
10  * This software is distributed in the hope that it will be useful,
11  * but WITHOUT ANY WARRANTY; without even the implied warranty of
12  * MERCHANTABILITY or FITNESS FOR A PARTICULAR PURPOSE.  See the
13  * GNU General Public License for more details.
14  *
15  * You should have received a copy of the GNU General Public License
16  * along with this software; see the file COPYING.  If not, write to
17  * the Free Software Foundation, Inc., 51 Franklin Street,
18  * Boston, MA 02110-1301, USA.
19  */
20
21 #ifdef HAVE_CONFIG_H
22 #include "config.h"
23 #endif
24
25 #include <gnuradio/io_signature.h>
26 #include "PhaseToAoA_impl.h"
27 #include <iostream>
28 #include <cstdio>
29 #include <ctime>
30 #include <cstdlib>
31 #include <cstring>
32 #include <unistd.h>
```

```
33
34 #include <float.h>
35 using namespace std;
36
37 namespace gr {
38   namespace LoRaATC {
39
40     PhaseToAoA::sptr
41     PhaseToAoA::make(float alpha)
42     {
43       return gnuradio::get_initial_sptr
44         (new PhaseToAoA_impl(alpha));
45     }
46
47 void
48 PhaseToAoA_impl::message_port_sub(pmt::pmt_t msg)
49 {
50     reception = 1;
51     return;
52 }
53
54     /*
55      * The private constructor
56      */
57 PhaseToAoA_impl::PhaseToAoA_impl(float alpha)
58     : gr::sync_block("PhaseToAoA",
59       gr::io_signature::make(1, 1, sizeof(float)),
60       gr::io_signature::make(1, 1, sizeof(float)))
61 {
62   //alpha is the separation distance between the 2 antennas. alpa is 1/2
       wavelength
63   d_alpha = alpha;
64   message_port_register_in(pmt::mp("in0"));
65   message_port_register_out(pmt::mp("out2"));
66   set_msg_handler(pmt::mp("in0"), boost::bind(&PhaseToAoA_impl::
       message_port_sub, this, _1));
67 }
68
69 /*
70 * Our virtual destructor.
71 */
72 PhaseToAoA_impl::~PhaseToAoA_impl()
73 {
74 }
75
76 int
77 PhaseToAoA_impl::work(int noutput_items,
78 gr_vector_const_void_star &input_items,
79 gr_vector_void_star &output_items)
```

```
80  {
81   if(reception == 1)
82   {
83   reception = 0;
84   const float *in = (const float *) input_items[0];
85   float *out = (float *) output_items[0];
86   float arg = 0;
87   float avg = 0;
88   float avg1 = 0;
89   int j = 0;
90
91   // Do <+signal processing+>
92   for(int i = 0; i<noutput_items;i++)
93   {
94    arg = ((in[i] * longeur_donde) / (2 * M_PI * d_alpha));
95    out[i] = (acos(arg) * 180) / M_PI;
96    j = i;
97    if(i == noutput_items-1) avg =  out[i];
98    }
99    //save data into a file for post processing
100   std::ofstream out1;
101   out1.open( "/home/doctorant/Documents/bin.dat", std::ios::app | std::ios::
        binary);
102   out1.write( reinterpret_cast<const char*>( &arg ), sizeof( float ));
103   out1.close();
104   //publish the data on the output port
105   std::string s = std::to_string( avg);
106   string fullstring = "Direction Of Arrival: " + s;
107   pmt::pmt_t str0 = pmt::string_to_symbol(std::string(fullstring));
108   message_port_pub(pmt::mp("out2"),str0);
109   //print the AoAs values in real time
110   std::cout<< "********** AoA ="; std::cout<<avg; std::cout<< "Degrees
        **********\n";
111   // Tell runtime system how many output items we produced.
112   return noutput_items;
113 }
114 else if (reception == 0)
115 {
116  //std::cout<< "********** No LoRa signal was detected";std::cout<<
       "**********\n";
117   return 0;
118 }
119 }
120 } /* namespace LoRaATC */
121 } /* namespace gr */
```

PhaseToAoA_impl.cc

C

GNU Radio: MQTT PUBLISH

```
1
2
3  #!/usr/bin/env python
4  # -*- coding: utf-8 -*-
5  #
6  # Copyright 2022 gr-MQTT Hussein Zeaiter.
7  #
8  # This is free software; you can redistribute it and/or modify
9  # it under the terms of the GNU General Public License as published by
10 # the Free Software Foundation; either version 3, or (at your option)
11 # any later version.
12 #
13 # This software is distributed in the hope that it will be useful,
14 # but WITHOUT ANY WARRANTY; without even the implied warranty of
15 # MERCHANTABILITY or FITNESS FOR A PARTICULAR PURPOSE.  See the
16 # GNU General Public License for more details.
17 #
18 # You should have received a copy of the GNU General Public License
19 # along with this software; see the file COPYING.  If not, write to
20 # the Free Software Foundation, Inc., 51 Franklin Street,
21 # Boston, MA 02110-1301, USA.
22 #
23
24
25 import pmt
26 import paho.mqtt.client as pmqtt
27 import numpy
28 import json
29 from datetime import datetime
30 from gnuradio import gr
31
32
33
34 class mqtt(gr.basic_block):
35     """
```

```
36      docstring for block mqtt
37      """
38
39
40      msg_to_sent_all_data = {}
41
42      def __init__(self, hostname = "127.0.0.1", port = 1883, channel = "/
        DirectionFinding"):
43          gr.basic_block.__init__(self,
44              name="mqtt",
45             # in_sig=[<+numpy.float32+>, ],
46             #out_sig=[<+numpy.float32+>, ])
47             in_sig=None,
48             out_sig=None)
49
50          self.channel = channel
51          self.message_port_register_in(pmt.intern('in'))
52          self.message_port_register_in(pmt.intern('in0'))
53          self.set_msg_handler(pmt.intern('in'), self.handle_msg)
54          self.set_msg_handler(pmt.intern('in0'), self.handle_msg_new)
55          self.client = pmqtt.Client()
56          print("Connecting to hostname: " + hostname)
57          self.client.connect(hostname, port, 60)
58          self.client.loop_start()
59
60
61
62      def handle_msg(self, msg):
63          msg = pmt.to_python(msg)
64          msg_str = {
65              "Direction" : str(msg),
66              "time": datetime.strftime(datetime.utcnow(), "%y-%m-%dT%H:%M:%SZ")
67          }
68
69          global msg_to_sent_all_data
70          msg_to_sent_all_data = json.dumps(msg_str)
71          #self.client.publish(self.channel, msg_to_sent_all_data)
72
73      def handle_msg_new(self, msg):
74          msg = pmt.to_python(msg)
75          msg_str = {
76              "Data" : str(msg),
77              "time1": datetime.strftime(datetime.utcnow(), "%y-%m-%dT%H:%M:%SZ")
78          }
79          msg_to_sent = json.dumps(msg_str)
80
81          a = json.loads(msg_to_sent)
82          b = json.loads(msg_to_sent_all_data)
83          merged = {**a, **b}
```

```
84          merged_dict = {key: value for (key, value) in (list(b.items()) + list(a
        .items()))}
85          #c = dict(list(a.items()) + list(b.items()))
86          jsonString_merged = json.dumps(merged_dict)
87          #print(a)
88          #print(b)
89          #print(merged)
90
91          self.client.publish(self.channel, jsonString_merged)
92
93
94
95      def forecast(self, noutput_items, ninput_items_required):
96          #setup size of input_items[i] for work call
97          for i in range(len(ninput_items_required)):
98              ninput_items_required[i] = noutput_items
99
100     def general_work(self, input_items, output_items):
101         output_items[0][:] = input_items[0]
102         consume(0, len(input_items[0]))        #self.consume_each(len(
        input_items[0]))
103         return len(output_items[0])
```

Document generated with LaTeX and:
the LaTeX style for PhD Thesis created by S. Galland — https://github.com/gallandarakhneorg/tex-templates
the tex-upmethodology package suite — http://www.arakhne.org/tex-upmethodology/

SPIM

école doctorale **sciences pour l'ingénieur et microtechniques**

UBFC UNIVERSITÉ BOURGOGNE-FRANCHE-COMTÉ

Université Bourgogne-Franche-Comté
32, avenue de l'Observatoire
25000 Besançon, France